UNIVERSITY OF KWAZULU-NATAL

CHARACTERIZATION AND MODELING OF THE CHANNEL AND NOISE FOR BROADBAND INDOOR POWERLINE COMMUNICATION (PLC) NETWORKS

MODISA MOSALAOSI

NOVEMBER 2016

CHARACTERIZATION AND MODELING OF THE CHANNEL AND NOISE FOR BROADBAND INDOOR POWERLINE COMMUNICATION (PLC) NETWORKS

MODISA MOSALAOSI

In fulfilment of the Degree of
Doctor of Philosophy in Electronic Engineering.
College of Agriculture, Engineering and Science,
University of KwaZulu-Natal, Durban

NOVEMBER 2016

Supervisor:

Professor Thomas J. O. Afullo

EXAMINER'S COPY

Declaration 1 - Plagiarism

I, Modisa Mosalaosi, declare that

1. The research reported in this thesis, except where otherwise indicated, is my original research.

2. This thesis has not been submitted for any degree or examination at any other university.

3. This thesis does not contain other persons' data, pictures, graphs or other information, unless specifically acknowledged as being sourced from other persons.

4. This thesis does not contain other persons' writing, unless specifically acknowledged as being sourced from other researchers. Where other written sources have been quoted, then:

   (a) Their words have been re-written but the general information attributed to them has been referenced

   (b) Where their exact words have been used, then their writing has been placed in italics and inside quotation marks, and referenced.

5. This thesis does not contain text, graphics or tables copied and pasted from the Internet, unless specifically acknowledged, and the source being detailed in the thesis and in the References sections.

Signed..... Date.....

Declaration 2 - Publications

[Overlapping Chapter 3]

M. Mosalaosi, T. J. O. Afullo, "Broadband Characteristics for Multi-Path Power Line Communication Channels: Indoor Environments", *International Journal on Communications Antenna and Propagation* (IRECAP), vol. 6, no. 4, pp. 244 - 254, 2016.

M. Mosalaosi, T. J. O. Afullo, "A Deterministic Channel Model for Multi-Access Broadband Powerline Communication", in *IEEE AFRICON conference*, Addis Ababa, Ethiopia, 14-17, September, 2015.

[Overlapping Chapter 4]

M. Mosalaosi, T. J. O. Afullo, "Channel Modeling for High Speed Indoor Powerline Communication Systems: The Lattice Approach", (Accepted in) *Annals of Telecommunications.*

[Overlapping Chapter 5]

M. Mosalaosi, T. J. O. Afullo, "Analysis of Broadband Power Line Communications Noise for Indoor Environments", in *Southern Africa Telecommunication Networks and Applications Conference* (SATNAC), Kogelberg, South Africa, September 6-9, 2015.

M. Mosalaosi, T. J. O. Afullo, "Prediction of Asynchronous Impulsive Noise Volatility for Indoor Powerline Communication Systems using GARCH Models", in *Progress In Electromagnetics Research Symposium Proceedings* (PIERS), Shanghai, China, August 8-11, pp. 4876-4880, 2016.

[Overlapping Chapter 6]

M. Mosalaosi, T. J. O. Afullo, "Cyclostationary Spectral Identification and Analysis of Broadband Power-Line Communication Impulsive Noise", in *Southern Africa Telecommunication Networks and Applications Conference* (SATNAC), George, South Africa, 4-7, September, 2016.

M. Mosalaosi, T. J. O. Afullo, "Parameter Estimation for Linear Regression Models in Powerline Communication Systems Noise Using Generalized Method of Moments (GMM)",

in *Progress In Electromagnetics Research Symposium Proceedings* (PIERS), Shanghai, China, 8-11, August, pp. 4858-4862, 2016.

Acknowledgements

First and foremost I have to thank my parents, Mr and Mrs Thokweng, for their love and support throughout my life. Thank you both for giving me strength to reach for the stars and chase my dreams, even when it had to be so far from you. I extend my gratitude to my siblings who supported my adventures and stood by me in many ways to mention.

I would like to sincerely express my deepest appreciation to my supervisor, Professor T. J. O. Afullo for his guidance and support throughout this study, and especially his confidence in me. With his attitude and substance of intellect, he continually and persuasively conveyed the spirit of adventure and excitement in this research. Without his contribution in stimulating suggestions and encouragement, this dissertation would not have been possible.

Furthermore, I would also like to acknowledge with much appreciation the crucial role of the technical staff for making it possible to gather all the necessary material required to build our test bed. I extend my acknowledgements to Mr Mike Asiyo, Mr Feyisa Dhiba, Mr Ebenezer Esenogho and Dr Alonge Akintunde for the discussions and knowledge sharing, thank you for making the time. Finally, all the contributions towards this work were made possible by the lord God and may all the glory be his.

Abstract

Power Line Communication (PLC) is an interesting approach in establishing last mile broadband access especially in rural areas. PLC provides an already existing medium for broadband internet connectivity as well as monitoring and control functions for both industrial and indoor usage. PLC network is the most ubiquitous network in the world reaching every home. However, it presents a channel that is inherently hostile in nature when used for communication purposes. This hostility is due to the many problematic characteristics of the PLC from a data communications' perspective. They include multipath propagation due to multiple reflections resulting from impedance mismatches and cable joints, as well as the various types of noise inherent in the channel. Apart from wireless technologies, current high data rate services such as high speed internet are provided through optical fibre links, Ethernet, and VDSL (very-high-bit-rate digital subscriber line) technology. The deployment of a wired network is costly and demands physical effort. The transmission of high frequency signals over power lines, known as power line communications (PLC), plays an important role in contributing towards global goals for broadband services inside the home and office. In this thesis we aim to contribute to this ideal by presenting a powerline channel modeling approach which describes a powerline network as a lattice structure. In a lattice structure, a signal propagates from one end into a network of boundaries (branches) through numerous paths characterized by different reflection/transmission properties. Due to theoretically infinite number of reflections likely to be experienced by a propagating wave, we determine the optimum number of paths required for meaningful contribution towards the overall signal level at the receiver. The propagation parameters are obtained through measurements and other model parameters are derived from deterministic power system. It is observed that the notch positions in the transfer characteristics are associated with the branch lengths in the network. Short branches will result in fewer notches in a fixed bandwidth as compared to longer branches. Generally, the channel attenuation increase with network size in terms of number of branches. The proposed model compares well with experimental data. This work presents another alternative approach to model the transfer characteristics of power lines for broadband power line communication. The model is developed by considering the power line to be a two-wire transmission line and the theory of transverse electromagnetic (TEM) wave propagation. The characteristic impedance and attenuation constant of the power line

are determined through measurements. These parameters are used in model simplification and determination of other model parameters for typical indoor multi-tapped transmission line system. The transfer function of the PLC channel is determined by considering the branching sections as parallel resonant circuits (PRC) attached to the main line. The model is evaluated through comparison with measured transfer characteristics of known topologies and it is in good agreement with measurements. Apart from the harsh topology of power line networks, the presence of electrical appliances further aggravates the channel conditions by injecting various types of noises into the system. This thesis also discusses the process of estimating powerline communication (PLC) asynchronous impulsive noise volatility by studying the conditional variance of the noise time series residuals. In our approach, we use the Generalized Autoregressive Conditional Heteroskedastic (GARCH) models on the basis that in our observations, the noise time series residuals indicate heteroskedasticity. By performing an ordinary least squares (OLS) regression of the noise data, the empirical results show that the conditional variance process is highly persistent in the residuals. The variance of the error terms are not uniform, in fact, the error terms are larger at some portions of the data than at other time instances. Thus, PLC impulsive noise often exhibit volatility clustering where the noise time series is comprised of periods of high volatility followed by periods of high volatility and periods of low volatility followed by periods of low volatility. The burstiness of PLC impulsive noise is therefore not spread randomly across the time period, but instead has a degree of autocorrelation. This provides evidence of time-varying conditional second order moment of the noise time series. Based on these properties, the noise time series data is said to suffer from heteroskedasticity. GARCH models addresses the deficiencies of common regression models such as Autoregressive Moving Average (ARMA) which models the conditional expectation of a process given the past, but regards the past conditional variances to be constant. In our approach, we predict the time-varying volatility by using past time-varying variances in the error terms of the noise data series. Subsequent variances are predicted as a weighted average of past squared residuals with declining weights that never completely diminish. The parameter estimates of the model indicates a high degree of persistence in conditional volatility of impulsive noise which is a strong evidence of explosive volatility. Parameter estimation of linear regression models usually employs least squares (LS) and maximum likelihood (ML) estimators. While maximum likelihood remains one of the best estimators within the classical statistics paradigm to date, it is highly reliant

on the assumption about the joint probability distribution of the data for optimal results. In our work, we use the Generalized Method of Moments (GMM) to address the deficiencies of LS/ML in order to estimate the underlying data generating process (DGP). We use GMM as a statistical technique that incorporate observed noise data with the information in population moment conditions to determine estimates of unknown parameters of the underlying model. Periodic impulsive noise (short-term) has been measured, deseasonalized and modeled using GMM. The numerical results show that the model captures the noise process accurately. Usually, the impulsive signals originates from connected loads in an electrical power network can often be characterized as cyclostationary processes. A cyclostationary process is described as a non-stationary process whose statistics exhibit periodic time variation, and therefore can be described by virtue of its periodic order. The focus of this chapter centres on the utilization of cyclic spectral analysis technique for identification and analysis of the second-order periodicity (SOP) of time sequences like those which are generated by electrical loads connected in the vicinity of a power line communications receiver. Analysis of cyclic spectrum generally incorporates determining the random features besides the periodicity of impulsive noise, through the determination of the spectral correlation density (SCD). Its effectiveness on identifying and analysing cyclostationary noise is substantiated in this work by processing data collected at indoor low voltage sites.

Contents

List of Figures

List of Tables

CHAPTER 1

Introduction

In recent times, the telecommunications industry has gone through a massive evolution which resulted in the advent of mobile phones, digital subscriber line (DSL) technology, IP services etc. The demand for high data rates, services and of guaranteed Quality of Service (QoS) is rapidly increasing. The telecom service providers are confronted with a challenge to satisfy the requirements of their customers. The mobility needs of the customers are generally fulfilled through the cellular networks. Nevertheless, the data throughput of mobile networks is limited. Another prevalent wireless solution for access to provision of data services is the Wireless Fidelity (Wi-Fi). The Wi-Fi has capability to provide data rates in the order of tens of megabits per second (Mbps), though it facilitates limited mobility. Wireless networks, however, suffers a great deal from variable link reliability. Furthermore, the presence of electromagnetic interference (EMI) affects the network's performance. In consequence, high speed data services are predominantly rolled out on the wired networks. The provision of high data rate services like the high speed internet are currently delivered over optical fibre links, Ethernet and very-high-bit-rate digital subscriber line (VDSL) technology. The substantial physical effort and cost required for the deployment of a wired network is prohibitive. In general, optical fibre cables serve as backbone access networks and are deployed underground with the objective for long term planning. Technologies such as the fibre to the home (FTTH) extends the optical fibre network to the customer premises, although additional infrastructure should be installed within the house to successfully exploit the benefits of the high throughput of the fibre link supports. The same applies to the case with VDSL technology. Majority of telecom and entertainment services such as the internet, voice, television and live video streams are provided through IP technology. In numerous households multiple rooms are furnished with several terminals like a computer, a television set and play station providing access to such services. Nonetheless, it is unlikely that there is availability of high data rate terminals in every room. In terms of ADSL technology, the telephone line already in place is used to provide the high bit rate services. Internet connectivity based on VDSL is generally not pervasive in the home since a house is normally

equipped with one or two telephone connection points. Likewise, it is not common to find pre-installed Ethernet cables in an ordinary home. Furthermore, the necessary installation of the new cables to expand the network in the home may be restrictive in the customers' view for aesthetic reasons. Customers need an expansive, high speed and reliable data network within the home. Power line communication (PLC) technology on the other hand delivers ubiquitous high speed data services with no further installation of infrastructure necessary. The prevalent in-home electrical wiring which is primarily deployed to provide the electrical energy to the home is exploited by the PLC technology to further serve as a data communication channel. In general, every room in the house has an electrical wiring and several power points of connection. Accordingly, PLC technology can deliver the maximum reach of the high speed telecom services everywhere in the house. This technology is capable of realizing data rates in the order of several hundreds of Mbps. The inhome electrical wiring network is typically a single phase power supply network delivering 230 volts of alternating current (AC) mains at 50 Hz (60 Hz in some parts of the world). Accordingly, the network cabling design is suitable to transport electrical energy at low frequencies. Thus, they may not guarantee fidelity when deployed to transport high frequency communication signals. On that basis, the inhome electrical network presents a hostile environment for communication signals. Moreover, the numerous types of noise injected into the channel generated by electrical appliances connected to the inhome electrical network further aggravates the channel conditions. The success of PLC technology towards reliable and guaranteed provision of high speed services therefore necessitates service providers not only to study the PLC channel and noise but also to explore new data communication strategies over this channel.

Power line communication (PLC) is a technology where information is carried by the conductor that is normally deployed for electrical power distribution. Electrical energy is transmitted over high voltage transmission lines, distributed over medium voltage lines and used inside premises at lower voltages. Each stage of the electrical power system is capable of hosting various PLC applications. The evolution of PLC stretches over one hundred years. Initially, the transfer of information over power lines was merely used for exchange of telemetry and telecommand of the electrical distribution system power. In recent years, there has been an emergence of numerous inhome applications such as the automation of household appliances and security of premises, homes etc. As is common with any technology, PLC technology has come through several phases to accomplish its current mould. Although,

in its introduction, it started by providing very low data rate services, PLC technology is currently promising to deliver broadband applications at customer buildings. Early in 1838, there was a proposal for remote electricity supply metering in order to monitor battery voltage levels at unstaffed sites. A power line signalling electricity meter was then patented in 1897. Due to the substantial evolution of electronics, in the period 1900's to 1970's, numerous developments were made towards the reading of electricity meters remotely [1].

The first main real application pertaining to transmission of information over power cables was for the electrical distribution grid protection in the event of fault. In fact, telemetry or telecommand for electrical distribution network on high voltage power lines remains one of the principal applications of PLC [2]. In order to circumvent or curb damage during faults, it is necessary for information to be exchanged between power plants, substations and distribution centres. Due to their robustness, availability and readiness for connectivity, electrical networks make the PLC technology a viable solution. shortly after the commencement of widespread electrical power supply, narrowband power line communication followed. The first carrier-frequency systems started to function around the year 1922 utilizing the high voltage lines in the frequency range from 15 to 500 kHz for telemetry purposes, and this application has continued to date [3]. Load management of the electrical power system was the principal motivation for the development and deployment of PLC technology. One might wonder why this technology has stimulated renewed attention in recent times, taking into account that data transmission over power lines has been around for a reasonably long time. This is especially the case considering that the data rate required for protection and telemetry is hardly more than few kbps and thus not proportional to the Mbps data rate required to be sustained for multimedia services. This can be explained by a combination of effects that transpired during the 1990's, namely, the dramatic development of the internet as well as the enormous strides in very large scale integration (VLSI) and digital signal processing (DSP) techniques. Moreover, the deregulation of the telecommunication market, initially in the US and eventually in Europe and Asia. These circumstances enabled power line communications to position itself as a realistic technology for various applications requiring high data rates spanning up to 100 Mbps.

1.1 PLC Ecosystem

The field of PLC has various manufacturers, operators and standardization associations. The focus of some of the groups, for instance, Gigle and Spidcom, is solely in chip manufacturing. Other groups involved include large telecom operators such as France Telecom and British Telecom. HomePlug Powerline Alliance and Home Grid Forum remains the major consortiums.

1.2 Standards

The anticipated evolution of PLC technology involves numerous discussions with standardization bodies for telecommunications. The objective of the proposed standards is to satisfy the following principal targets:

- General Requirements.
- Safety.
- Electromagnetic Compatibility.
- Performance & Interoperability.

Numerous Standard Definition Organizations (SDO) like ETSI PLT, IEEE 1901, and ITU G.hn perform the standardization for PLC technologies. Moreover, different industrial consortiums are involved in the development towards the evolution of PLC technology, such as the HomePlug powerline Alliance and the Home Grid Forum.

1.2.1 European Telecommunication Standards Institute (ETSI)

Concerning the overall interoperability of PLC systems and the electricity standards in Europe, ETSI standards plays a significant role. High quality standards and specifications to deliver telecommunication services through the pervasive public and private electrical power grids is the core objective of the ETSI TC (Technical Committee) PLC. To facilitate interoperability between products from different manufacturers and co-existence of numerous PLC systems within the same framework, standards are developed with sufficient details [4]. Moreover, ETSI TC PLT has published and developed the required standards to ensure that

PLC thrives in coexistence with other technologies and services [5]. The ETSI requirements are provided in:

- TR 102049 "Quality of service (QoS) requirements for in-house systems": this document stipulates the classification of home applications, home devices, service categories, traffic categories and QoS demands.
- TR 102494 "Technical requirements for in-house PLC modems": Currently, there is nearly no technical specification provided on physical (PHY) and medium access control (MAC) layers.

1.2.2 IEEE 1901

In January 2011, the IEEE P1901 standard was officially published. This standard is developed by the IEEE working group and its objective is to deliver high data rate PLC technology with PHY (physical layer) data rates in excess of 100 Mbps. The standard covers the frequency range up to 100 MHz and it includes the access part (up to 1.5 km from the user) as well as the local network part (up to 100 m from the terminals) [6]. Qualcomm Atheros have already proposed the chipsets AR7400 which is compatible with the IEEE P1901 standard [7].

1.2.3 International Telecommunications Union (ITU) G.hn

The G.hn working group is committed to an alternative recommendation characterizing transceivers for in-building networking over metallic conductors like telephone loops, coaxial, data and power cables. The ITU G.9960 standard was released in 2009. It was anticipated that the first chipsets to implement this standard would be available at the beginning of 2012. Indeed by the end of that year a few participants announced compliance of their silicon with the standard, with only interoperability tests remaining. The maximum data rate and the quality of service (QoS) are stipulated to undertake the triple play (Internet, video over IP, voice over IP) solutions. Even though the expected data rate is projected up to 1 Gbps, however, this is perhaps only possible for the coaxial cables. The original proposition of the G.hn working group was to confront numerous classes of existing wires in the home environment as a collective. In this viewpoint, the development of a unique solution employing any wired medium accessible in the customer premises should be enabled.

In September 2011, ITU has released the G.9963 standard, with the multiple input multiple output (MIMO) communication functionalities for powerline communication included [8].

1.3 Major Players

Owing to the prospective benefits associated with PLC technology, various enterprises and research groups in the telecom community have taken recognition. The description here includes some of the major players.

1.3.1 HomePlug Power Alliance (HPA)

The HomePlug Power Alliance Inc. is an industry-led initiative. In its establishment, the mandate was to create specifications for inhome high speed powerline networking products and control and command among platforms. The Alliance stimulates demand for HomePlug-enabled products and services globally through the sponsorship of market and customer education programs. The growth of membership in the Alliance includes in excess of 75 industry-leading companies. France Telecom, as a telecom operator, is also a member participant. HomePlug Powerline Alliance developed numerous specifications for PLC standards including HomePlug 1.0, HomePlug AV, HomePlug BPL, HomePlug Green PHY and HomePlug command and control. The latest HPAV 2.0 incorporates the MIMO communication functionalities [9].

1.3.2 Universal Powerline Association (UPA)

UPA is an international organization. The organization advances DS2 chipsets developing the Digital Home Standard (DHS) in the process, which is dedicated to create a comprehensive specification required by the silicon vendors for the design of integrated circuits for voice, video and data communication through electric power grids [4], [10].

1.3.3 Consumers Electronics Powerline Communication Alliance (CEPCA)

CEPCA as an alliance also seeks to advance power line communication. It has fourteen participants comprising largely of Japanese manufacturers (Sony, Mitsubishi, Panasonic etc.). The goal of CEPCA is to make it possible for the numerous power line communication systems to co-operate. Panasonic (i.e Matsushita Electric Industrial) advances the High defini-

tion Powerline Communication (HD-PLC) chipsets, that employs an efficient high frequency Wavelet OFDM modulation technique, with a programmable notch filter that prevents interference with other radio frequency broadcasts like amateur radio. In theory, the expected peak data transmission rate is up to 190 Mbps [4], [11].

1.4 Power line Communication Projects

To date, there are numerous applications that can be realised through the use of PLC technology. In order to develop a reliable technology, performance metrics such as latency, bandwidth and availability are key to its growth and survival. To this end, some well-funded mega projects were put in place with specific objectives and time lines. Such projects include, but not limited to; development of a high bandwidth access network, affirmation of cognitive broadband over power lines, standardization and technology development.

1.4.1 OMEGA

The OMEGA project is dedicated to the development of a comprehensible indoor access network capable of providing high bandwidth services and content at a transmission rate of one Gbps. The interdisciplinary project consortium comprise of twenty European associates from industry as well as the academic community. The project was introduced at the beginning of 2008 and completed by the end of 2010. OMEGA is an integrated project in the information and communication technology (ICT) domain supported financially by the European Commission under EU Framework Program 7 (FP7). Considering that the fibre to the home (FTTH) access has potential to deliver symmetric data at a minimum rate of 100 Mbps, it is then conceivable that a home network would support Gbps data transmission and a latency time in the order of milliseconds. Therefore it is expected that the performance of the home network must be high enough to sustain numerous services concurrently, even when they individually have different demands. Moreover, it must be cheaper and less complicated to manufacture at an industrial scale. The OMEGA home network seeks to provide Gbps capacity with low latency within the home as well as the access network, through either the wireless communication or communication the existing wired home infrastructure, thus facilitating access to and the advancement of alternative and innovative services [12].

1.4.2 Powernet

The Powernet project was completed in 2008. Its objective was to demonstrate and affirm the new cognitive broadband over power lines (CBPL) under actual world scenarios in field experiments using a large number of CBPL apparatus. The project derives its motivation from the big market potential for PLC technology. The major advantage of broadband over power line (BPL) over its counterparts is that the power cables which are already in place necessitates no further deployment of extra cables. The new cognitive BPL technology has been developed recently based on the substantial knowledge of the shortcomings experienced in the prior field trials conducted. A MATLAB simulation of the CBPL technology had been successfully implemented; the results were encouraging: high data rates attainable (reaching 300 Mbps) at lower transmit power spectral density (PSD), for example, lower electromagnetic radiations. The leakage energy in the frequency bands allocated to other users measures as low as -100 dBm/Hz implying that CBPL does not interfere with other users [13].

1.4.3 OPERA

The strategic purpose of the OPERA project was to drive PLC technology in the entirety of relevant aspects (standardization, technology development, installation aids and procedures, telecom services, smart grid services, distribution) in order to enhance it as an alternative that provides broadband access to all European residents using the most pervasive infrastructure. This development of the PLC technology will promote the development of the European Information Society in line with the proposed objectives in the eEurope 2005 plan by the means of:

- Improved competition in the broadband access: PLC networks can be rapidly and seamlessly deployed with minimum investments by exploiting the existing power networks. PLC is a ubiquitous solution for access and inhome distribution that will provide a real alternative last mile access network.

- Encouraging widespread services availability: PLC attributes such as the transparent integration with numerous communication technologies (Wi-Fi etc.) and the complete end-user coverage will contribute to the deployment of value-added-services over broadband such as smart home, video streaming, e-health, VoIP, etc.

- European industry leadership: PLC technology expertise and technical prowess are presently based in Europe. This represents a remarkable opportunity for the development, competitiveness and authority of European broadband industry that will stimulate the creation of employment, to the enhancement of the information society technologies in Europe and also the socio-economic prosperity in EU [14].

1.5 Electromagnetic Compatibility

From the electromagnetic compatibility (EMC) perspective, an equipment or system must neither be the source nor the victim of unwanted electromagnetic noise in its frequency band of operation. The transmission of the perturbations between a transmitter and a receiver is either through conduction or through radiation. In Europe, the PLC system must adhere to the CISPR22 standard which deals with the radio electric perturbations [15].

1.6 Research Objectives

In line with the general perspective that power lines could become more desirable in their deployment as media for data communication purpose, the principal objective of this work is to explore the indoor powerline network as a communication channel and its associated noise. As the most ubiquitous wired network, PLC has a huge potential to meet the alarming demand of high-speed broadband services in the home/office environment. However, its structure and topology is rather hostile to high frequency signals as it was only intended for low frequency power signals. The heavy presence of impulsive noise generated by normal operation of household appliances also contributes adversely to the propagation of communication signals. To that effect, this thesis focuses on PLC channel and noise characterization and modeling in low voltage indoor scenarios. The main objectives of this thesis are outlined as follows:

- Model practical power line communication channels in the frequency domain by considering their frequency-selective nature. A multipath approach has been adopted.
- Study the dispersive properties of indoor PLC channels through their impulse responses. The time-delay spread parameters are derived and represented by their cumulative distributions. The PLC channels are then characterized by their coherence

bandwidth.

- Develop a deterministic PLC channel model based on the two-wire transmission line and theory of transverse electromagnetic (TEM) wave propagation. The branching elements of the multi-tapped transmission line system are considered to be parallel resonant circuits attached to the working line (bus topology).

- Analysis of the overall impulsive noise captured at a wall plug in an office environment. The impulsive noise is described by its peak-to-average value and its probability distribution (PDF) is determined and presented alongside a typical band-limited Gaussian reference for comparison purpose.

- Estimation of PLC asynchronous impulsive noise volatility in indoor PLC environments using Generalized Autoregressive Conditional Heteroskedastic processes. The basis of this approach stems from the fact that, after performing an ordinary least square regression on the noise register, the noise time series residuals indicates heteroskedasticity. The modeling is outlined and applied to a measured noise data.

- A channel model is developed and presented which describes the power network as a lattice structure. In its derivation, transmission/reflection paths between network nodes are easily traceable and characterized. Thus the model can be regarded as a Deterministic-Multipath (DM) approach. The simplicity of the lattice structure enables us to determine the optimum number of paths to be considered meaningful.

- Spectral identification and analysis of impulsive cyclostationary additive noise. Cyclic spectral analysis is employed to identify and analyse the second-order periodicity (SOP) of the measured noise time sequences. The cyclostationarity analysis comprise mainly of estimating random aspects and periodic behaviour of the impulsive noise through the spectral correlation density.

- Introduced Generalized Method of Moments for parameter estimation for Linear Regression models. Linear regression models usually employs least squares and maximum likelihood estimators for parameter estimation. While effective, these estimators are over reliant on the assumption about the joint probability distribution of the data for optimal results. This shortcoming is, however, addressed by the use of GMM. An au-

toregressive GMM driven model is finally used to model a short-term cyclostationary impulsive noise.

1.7 Thesis organisation

This thesis comprises of seven chapters. The individual chapters presents insight into the work in the form of introduction, objective or summary. The organisation is as follows:

Chapter 1 presents the general introduction of the subject matter pertaining to the concepts. The evolution of PLC technology is discussed as well as its general framework.

Chapter 2 provides a brief review on the structure and characteristics of power lines as well as prior work in the field of power line communication related to the work presented in this thesis. Prominent approaches towards modeling of both PLC channel and impulsive noise are discussed.

Chapter 3 presents a frequency domain channel model for practical power line communication scenarios. A multipath approach has been adopted. Study the dispersive properties of indoor PLC channels through their impulse responses. These parameters are valuable in wideband antenna design. We also developed a deterministic PLC channel model based on the two-wire transmission line and theory of transverse electromagnetic (TEM) wave propagation. The branching elements of the multi-tapped transmission line system are considered to be parallel resonant circuits attached to the working line (bus topology).

Chapter 4: A channel model is developed and presented which describes the electrical power network as a lattice structure. In its derivation, transmission/reflection paths between network nodes are easily traceable and characterized. Thus the model can be regarded as a Deterministic-Multipath (DM) approach. The simplicity of the lattice structure enables us to determine the optimum number of paths to be considered meaningful.

Chapter 5: The overall impulsive noise captured at a wall plug in an office environment is analysed. The impulsive noise is described by its peak-to-average value and its probability distribution (PDF) is determined and presented alongside a typical band-limited Gaussian

reference for comparison purpose. Furthermore, PLC asynchronous impulsive noise volatility in indoor PLC environments is estimated using GARCH processes. The basis of this approach stems from the fact that, after performing an OLS regression on the noise register, the noise time series residuals indicates heteroskedasticity. The modeling is outlined and applied to a measured noise data.

Chapter 6 presents the spectral identification and analysis of impulsive cyclostationary PLC noise. Cyclic spectral analysis is employed to identify and analyse the second-order periodicity (SOP) of the measured noise time sequences. The cyclostationarity analysis comprise mainly of estimating random aspects and periodic behaviour of the impulsive noise through the spectral correlation density. Moreover, the Generalized Method of Moments is introduced for parameter estimation for Linear Regression models. Linear regression models usually employ least squares and maximum likelihood estimators for parameter estimation. While effective, these estimators are over reliant on the assumption about the joint probability distribution of the data for optimal results. To circumvent this shortcoming, GMM is used. An autoregressive GMM driven model is finally used to model a short-term cyclostationary impulsive noise.

Chapter 7 provides the summary conclusions drawn from the study undertaken. It provides a detailed insight into the research contributions of this thesis with possible future endeavours highlighted. It further outlines the thesis contributions as summarized under section 1.6 and also reflected under declaration of publications.

1.8 Contributions in terms of Journals and Conference Proceedings

The listed publications below are materials forming part of this thesis with appearance in peer-reviewed and accredited journals as well as conference proceedings.

1. **M. Mosalaosi, T. J. O. Afullo**, "Broadband Characteristics for Multi-Path Power Line Communication Channels: Indoor Environments", *International Journal on Communications Antenna and Propagation* (Accepted in)(IRECAP)

2. **M. Mosalaosi, T. J. O. Afullo**, "Channel Modeling for High Speed Indoor Pow-

erline Communication Systems: The Lattice Approach", (To appear in) *Annals of Telecommunications*.

3. **M. Mosalaosi, T. J. O. Afullo**, "A Deterministic Channel Model for Multi-Access Broadband Powerline Communication", presented in *IEEE AFRICON conference*, Addis Ababa, Ethiopia, 14-17, September, 2015.

4. **M. Mosalaosi, T. J. O. Afullo**, "Analysis of Broadband Power Line Communications Noise for Indoor Environments", presented in *Southern Africa Telecommunication Networks and Applications Conference* (SATNAC), Kogelberg, South Africa, September 6-9, 2015.

5. **M. Mosalaosi, T. J. O. Afullo**, "Prediction of Asynchronous Impulsive Noise Volatility for Indoor Powerline Communication Systems using GARCH Models", presented in *Progress In Electromagnetics Research Symposium Proceedings* (PIERS), Shanghai, China, August 8-11, 2016.

6. **M. Mosalaosi, T. J. O. Afullo**, "Cyclostationary Spectral Identification and Analysis of Broadband Power-Line Communication Impulsive Noise", presented in *Southern Africa Telecommunication Networks and Applications Conference* (SATNAC), George, South Africa, 4-7, September, 2016.

7. **M. Mosalaosi, T. J. O. Afullo**, "Parameter Estimation for Linear Regression Models in Powerline Communication Systems Noise Using Generalized Method of Moments (GMM)", presented in *Progress In Electromagnetics Research Symposium Proceedings* (PIERS), Shanghai, China, 8-11, August, 2016.

CHAPTER 2

Literature Review

2.1 Introduction

The fundamental principle of power line communication is utilizing the existing electrical power networks for data communications purposes. For a greater period of their existence, power line have fulfilled its duties as a medium for transmission and distribution of low frequency electrical signals. Primitive power line communication was restricted to low speed applications such as remote metering and operations management services that serve the needs of utility companies. This narrow scope of PLC usage has improved a great deal recently, owing to the tremendous increase in demand for high speed broadband multimedia communication services.

This chapter aims to provide insight into some of the contributions in literature with regards to power line communication. The development of new PLC technology and systems requires extensive knowledge of the structure and properties of the electrical power network for its consideration as a viable data communication channel. In this regard, the historical development and current advances in the PLC technology are outlined. Channel and noise modelling approaches and developments are also outlined. This chapter serves as a knowledge basis that will be used in later sections of the dissertation to investigate existing techniques and develop approaches to serve the aim of enhancing the performance of PLC systems.

2.2 Properties of Electrical Power Networks

Power line communication systems exploit the existing electrical power grid infrastructure to transport communication signals aimed at delivering narrowband and broadband data services to the consumer. The primary purpose of the electrical power system is, nonetheless, the transmission and distribution of mains signal at 50 or 60 Hz (50 Hz in Africa and other parts of the world, 60 Hz in North America) from the power generating plants to the customers. Accordingly, electrical power networks differ significantly in topology, structure

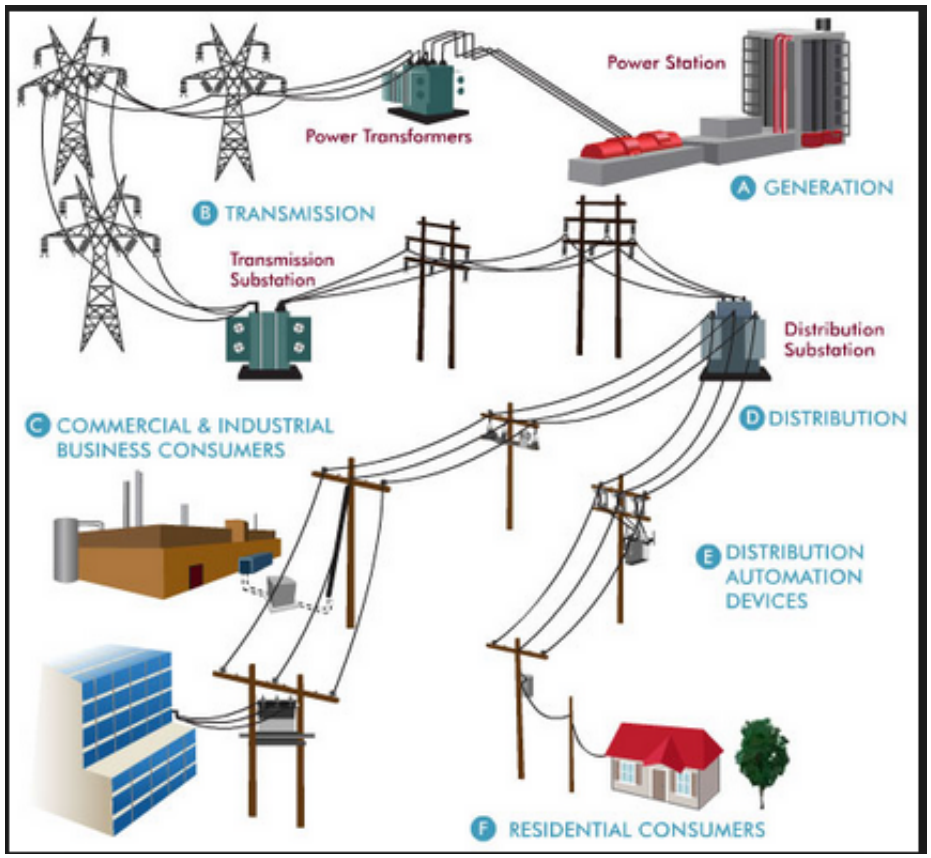

Figure 2-1: Typical Electrical Power System

and physical characteristics from conventional data communication media constituted by twisted pair, Ethernet cables, coaxial cables, and optical fibres. The viability of the electrical power grids for high speed data transfer requires a comprehensive understanding of their structure and underlying properties. Electrical power networks are classified based on their voltage levels into three classes [16]: the high voltage (HV) level (110 - 330 kV), the medium voltage (MV) level (10 - 30 kV) and the low voltage (LV) level (0.4 kV). These three segments of the electrical power network are interconnected by transformers. The transformer present a data transmission blockage at high frequencies as it will only allow low frequency electrical signals to pass because it is modeled as an open circuit for PLC signals with spectral content related to broadband technology. Figure 2-1 shows a typical structure of an electric power system. The indoor PLC scenario is described by points C and F in Figure 2-1.

2.2.1 High Voltage Networks

High voltage power lines are used for the transmission of electrical power generated at the power plant to multiple substations, traversing long geographical distances of up to several hundred kilometres. High voltage power networks form the electric power backbone for the utility company. HV power transmission is usually carried out through overhead three phase conductors. This level of voltage is more suitable for transportation over long distances essentially to reduce the energy losses. The main losses present in high voltage lines are the heat loss caused by the resistance of the power line material and leakage losses [16]. A convenient selection of the wire material and appropriate dimensioning of electrical cables can restrict heat losses to acceptable levels. Corona losses are likely to occur due to the discharge activities in the vicinity of the conductors caused by high electric field strengths at high voltages. Thinner conductors are more prone to these discharge effects when employed to transport high voltage signals. Moreover, corona discharge can produce concentrated high frequency impulses which may cause interference with radio broadcasting utilizing the low and medium frequency bands. Data Communication over high voltage lines at high frequencies is also subject to interference, reducing system reliability. Two dominant types of high frequency interferences in high-voltage overhead lines [16]: the first is the periodic short-duration impulsive interference generated by switching events and atmospheric discharges. It tends to have broadband spectra in the frequency domain. Since the conductors are carrying high voltages, the resulting impulses are characterized by very high magnitudes which may lead to dangerous peaks arriving at the receiver. The second type of interference prevalent in HV lines is a persistent broadband interference having a fairly high power spectral density (PSD). This interference is brought about by discharge activities and can be modelled as white Gaussian noise (WGN) with its PSD strongly dependent on weather conditions, increasing drastically in the presence of rain, frost and fog. Due to severe interference and attenuation at high voltages, HV power lines are not suitable for data transmission [17]. Alternatively, fibre optic cables are generally installed along high voltage routes for control and monitoring purposes as well as for data transmission exploiting their high capacity.

2.2.2 Medium Voltage Networks

Medium voltage networks are typically employed to supply electricity to rural areas, small towns and independent industrial companies. Generally, MV electrical power lines carry voltage levels ranging between 10 kV and 30 kV and have typical lengths of about 5 - 25 km [16]. Overhead lines and underground cables are both used in the medium voltage range for the transmission and distribution of electrical power. However, in densely-populated urban areas, underground cables are normally preferred. Unlike overhead high voltage lines, medium voltage overhead lines tends to require relatively smaller poles and smaller wire cross-sections because of the lower voltage they carry. With regards to the physical structure, MV lines are mainly made of copper and aluminium with various cross-section shapes including round, sector-shaped and oval [16]. The preferred insulation for medium voltage power line networks is usually Polyvinyl chloride (PVC) or vulcanized polyethylene (VPE). Regarding data transmission, medium voltage lines form the backbone of the electric utility data communications over power lines [17].

2.2.3 Low Voltage Networks

The low voltage network is the last portion of the electrical power network supplying electrical energy to the consumers at 100 - 400 volts. In Europe underground cables are mainly used in this voltage level [16], [18]. However, in South Africa, low voltage overhead lines are still visible in urban areas. In terms of the physical structure, low voltage lines are similar to medium voltage lines and are composed of copper or aluminium with PVC or VPE insulation. The length of LV electrical power lines normally extends up to 500 m from the MV/LV transformer station to the consumer's premises. Power line communication technologies utilize the low voltage electrical wiring to deliver data communications services to the home or office. Furthermore, in-building networking solutions can be established through the power line network.

2.3 Characteristics of Power Lines

Power lines form the medium of transmission in PLC systems. Since the primary purpose of these lines is the transmission of mains signals at 50 or 60 Hz, their design did not take into consideration the possibility for data transport at higher frequencies. This section serves to

provide an overview of the technical characteristics of electrical wiring pertaining to their usability and/or suitability for data transmission.

2.3.1 Capacitance and Inductance

The power line network distributes electrical energy to various devices connected to the grid. Appliances connected to the electric power grid are characterized by a certain inductance (L) and capacitance (C) each of which depends on the amount of current flowing through the device's circuit. The inductance of an electrical circuit defines the amount of magnetic flux due to the current running in the circuit. Depending on the amount of inductance (amount of flux), it may cause interference with neighbouring circuits if it is not restricted within the generating loop. Consider a current (I) inducing a magnetic flux (ϕ), then the inductance (L) is given [19] as:

$$L = \frac{\phi}{I} \tag{2.1}$$

In the event that the circuit is driven by an alternating current (AC) of voltage (V) and frequency *(f)*, the inductance is calculated as follows:

$$L = \frac{V}{j2\pi fI} \tag{2.2}$$

The capacitance of an electric circuit represents a measure of the amount of electrical energy stored for a given potential created between two adjacent conductive surfaces with opposite charges [19]. The capacitance is defined in terms of the electric charge (Q) and the voltage (V) between two planes according to

$$C = \frac{Q}{V}. \tag{2.3}$$

For the AC voltage supplied by the electrical grid, capacitance (C) can be represented as follows:

$$C = \frac{I}{j2\pi fV} \tag{2.4}$$

2.3.2 Impedance

The overall opposition to the flow of current in alternating current (AC) circuits is measured by impedance. The impedance (Z) of a cable is made of resistive, capacitive and inductive components and can be represented by a complex form [19]:

$$Z = R + jL2\pi f + \frac{1}{jC2\pi f} \tag{2.5}$$

For circuits only operated by a direct current (DC), the impedance will be equivalent to a pure resistance. Normal operation in electrical networks entails continuous connection to or disconnection of appliances from the power network. Accordingly, the input impedance seen by a PLC device connected to the network in the vicinity of such loads may be variable and unpredictable. This inconsistency makes it difficult to model the power line channel to determine its suitability for simultaneous transmission of data communication signals. Poor or lack of matching of the loads in the electrical network to the cable's characteristic impedance leads to reflections from the loads back along the cable towards the source. The severity of the reflections depends on the output impedances of the loads, with significant reflections able to deter the communication signal from reaching the receiver with sufficient energy. This channel variation caused by plugging and/or unplugging of electrical appliances makes for a difficult prospect in modelling PLC channels. Section 2.5 presents some of the attempts in literature towards modelling of power line channels.

2.4 PLC Noise

One of the significant features of electrical networks, particularly in the "last mile" area and in-building wiring, is the susceptibility to a variety of signals. Understanding of the different interference sources in the electrical power network is key to establishing reliable high speed PLC data systems. Generally, the electrical devices connected to the network or its proximity are the main sources of interference. This is, however, not always a result of any kind of malfunction in the power network as some of the electrical machinery and devices can cause interference even during their normal operation. In addition, switching electrical appliances (ON and OFF) causes impulsive current and voltage peaks propagating along the electrical wiring. Typical noise-generating electrical devices include light dimmers, fluorescent and

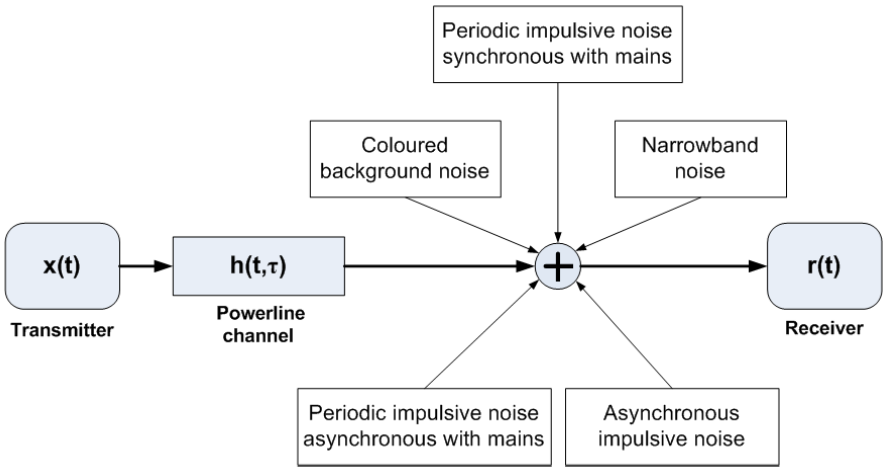

Figure 2-2: The components of the additive noise model for PLC channels

halogen lamps, universal motors and so forth [3, 20]. Another kind of impairment affecting broadband power line communications is with regards to electromagnetic interference (EMI) and electromagnetic compatibility of power lines. The unshielded electrical wiring is susceptible to radiation effects from radio services operating in the same radio frequency (RF) band. Broadband power line devices typically operate in the frequency range 2 - 68 MHz. Radio services operating within this frequency range such as amateur radio have been using parts of the medium frequency (MF) and high frequency (HF) bands for decades. Accordingly, contrary to conventional data communication channels, noise in electric power grids cannot be described by the classical approach of additive white Gaussian noise (AWGN). The noise present in power lines is often categorized into classes. As reported in [16], noise at a wall power outlet is summarized into three main categories: coloured background noise, narrowband interference and impulsive noise. According to [21], there are five types of noise: coloured background noise, narrowband noise, periodic impulsive noise synchronous to the mains frequency, periodic impulsive noise asynchronous to the mains and asynchronous impulsive noise. Figure 2-2 depicts a PLC scenario under a noisy conditions encountered during data transmission. The transmitted signal $x(t)$ passes through a PLC channel represented by its time-varying channel impulse response (CIR), $h(t, \tau)$. Various types of noise are added to $\hat{n}(t)$, channel output free of noise, before its arrival at the receiver. The different types of noise scenarios that are depicted in Figure 2-2 are described with more details as follows:

- **Coloured Background Noise**: this type of noise is usually assumed to be the aggregate

result of various sources of white noise characterized by different noise amplitudes at different portions of the frequency band [22]. Coloured background noise is typically characterized by a fairly low power spectral density (PSD). This PSD tends to decrease with an increase in frequency. Its highest value is in the frequency band closest to the mains signal frequency (50 Hz or 60 Hz) up to about 20 kHz [16].

- **Narrowband Noise**: this type of noise occurs at narrow portions of the frequency band with a relatively high PSD. Narrowband interference appears in the form of sharp peaks of noise amplitudes in the frequency domain. It is generally caused by the radio stations (amateur radio, AM radio, FM radio, etc.) broadcasting their signals in the frequencies typically within the 1 - 68 MHz range. Nonetheless, narrowband interference may occur at lower frequency bands. Its occurrence at such low frequencies is due to the switching of electrical appliances such as television sets, power supplies, fluorescent lamps or computer screens [16].

- **Periodic Impulsive Noise Synchronous to the Mains Frequency**: the main cause of periodic impulsive noise is the switching of rectifiers in AC/DC power converters [22] and phase control in electric devices such as light dimmers, which takes effect synchronously with the power signal frequency. Cyclic voltage peaks of impulsive nature are generated at every zero-crossing of the mains signal leading to repetition rates of the multiples of the mains frequency (i.e. 50 or 100 Hz for 50 Hz power grids). These type of impulses are generally characterized by short durations and a PSD that decreases with frequency.

- **Periodic Impulsive Noise Asynchronous to the Mains Frequency**: this periodic interference occurs with repetition rates in the range of 50 - 200 kHz. Impulses of this type are generated as a result of switched capacitor based AC/DC converters.

- **Asynchronous Impulsive Noise**: the main cause of asynchronous impulsive noise is switching transients that occur in various parts of the electric network. Measurements in [21] show that typical impulses of this type have durations ranging from some microseconds to a few milliseconds. The threat posed by this random noise occurring in bursts on high speed PLC data communication is quite significant. Effectively, it imposes the use of robust modulation techniques and powerful channel coding schemes.

The first three noise types described above generally remain stationary over long periods of time (i.e. seconds, minutes or hours) and can be summarized as background noise [16, 21, 23]. The last two types have a random time-varying nature and can be described as impulsive noise. A review of some of the prevalent approaches to modelling impulsive noise will be given in Section 2.6.

2.5 PLC Channel Modelling

The emergence of new communication systems demands an extensive knowledge and understanding of the characteristics of the transmission medium for effective data communication. The choice of the transmission technique and other design parameters is based on the channel transfer properties, noise characteristics and as a consequence, the offered capacity. Therefore, suitable models that can describe the data transmission behaviour over a medium with sufficient precision are required. As mentioned before, the electrical power grid is not designed for high speed data transmission, hence modelling this medium is a very difficult task and forms one of the major technical challenges [18, 22, 24, 25]. In addition to the impulsive noise dilemma that was discussed in the previous section, electrical networks exhibit strong branching topologies due to their intricate distribution structures, which gives rise to significant degradation of transmission quality. Signal propagation along power lines does not only take a single path from the transmitter to the receiver. Multiple paths are possible due to the numerous routes created by the numerous branches. Furthermore, reflections from the loads connected at the branch end points lead to the reception of delayed copies (echoes) of the transmitted signal. Several attempts to model the electric power grid as a communication medium can be found in the literature, for example [26–29]. The existing models for the transfer function of power line channels are based on two fundamental approaches: time domain and frequency domain [18]. Time domain models are typically based on averaged measurement trials of obtained results. On the other hand, frequency domain models, are based on a deterministic approach. These two approaches are briefly reviewed in the following two sub-sections.

2.5.1 Time Domain Approach: The Multipath Model

The topology and structure of electric power networks differs from those of conventional telecommunication networks. In electric grids, the connection of customer premises to substations is not of point-to-point type as in the case of communication networks such as telephone local loops. As shown previously in Figure 2-1, the link from a transformer substation consists of a distribution link forming a bus topology and house connections with variable lengths representing branches from the distributed cable. The house connection is terminated at a house connection box, which is then succeeded by numerous branches in the in-building wiring. Due to the heavy presence of branching and impedance mismatches in the power line network, multiple reflections occur, giving rise to a multipath propagation scenario (frequency) selectivity. Furthermore, this frequency selectivity causes frequency-dependent attenuation and thus should be considered in the modelling process. Generally, signal attenuation in power lines is the result of coupling losses which depends on the PLC transceiver design and line losses depending on the length of the cable [24]. In addition to the frequency-dependent attenuation, the channel transfer characteristic is also time-varying and depends on the location of the receiver since different appliances are constantly been plugged in and out of the electrical network causing changes in the transfer function. Models of the power line channel transfer function that describe the multipath propagation effects have been proposed by Phillips [27] and Zimmermann and Dostert [26,30]. According to [26], the channel transfer function $H(f)$ that describes the signal transmission in PLC channels in the 500 kHz to 20 MHz band is given as follows:

$$H(f) = \sum_{i=1}^{N_p} c_i e^{-(a_0 + a_1 f^k) d_i} e^{-j2\pi f \tau_i} \tag{2.6}$$

where $N_p \in \mathbb{N}$ is the number of meaningful propagation paths, $c_i \in \mathbb{R}$ and $d_i \in \mathbb{R}$ denotes the weighting factor and the ith path length, respectively. Accordingly, the multipath scenario is represented by a superposition of signals arriving from N_p different paths. Frequency-dependent attenuation is described by the parameters $a_0 \in \mathbb{R}$, $a_1 \in \mathbb{R}$ and the exponent $k \in \mathbb{R}$. In this model, the first exponential represents the attenuation factor, whereas the second exponential describes the echo scenario where $\tau_i \in \mathbb{R}$ is the path delay and is given by the following:

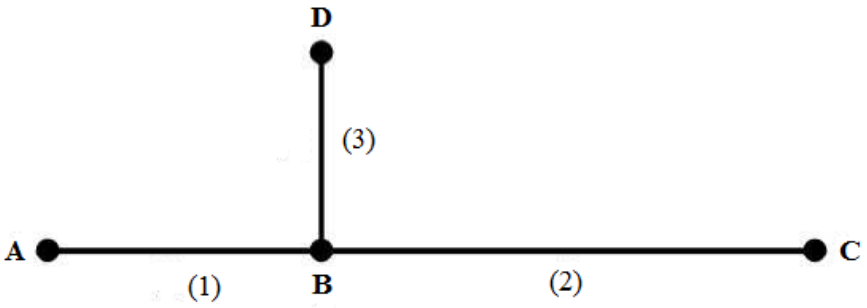

Figure 2-3: Single branch PLC channel

$$\tau_i = \frac{d_i\sqrt{\varepsilon_r}}{c_0} = \frac{d_i}{v_p}, \tag{2.7}$$

where ε_r is the dielectric constant of the insulating material, c_0 is the speed of light and v_p is the propagation velocity. To demonstrate the multipath signal propagation in electric power grids, a simple example extracted from [26] is illustrated in Figure 2-3. This simple topology, commonly known as the T-network, consists of a power line with a single branch represented by the line segment from point B to point D in the figure. The three segments of the link (i.e. (1), (2) and (3)) are assumed to have different lengths and different characteristic impedances. Consider that points A and C (transmitter and receiver respectively) are matched to their line characteristic impedances, then it follows that only points B and D can cause reflections in the link. These reflections occurring at terminals B and D will lead to infinitely many routes from terminal A to terminal C (e.g. A-B-C or A-B-D-B-D-...C). The transmission and reflection factors in each branch determines the weighting factor each propagation path will have, which is denoted by g_i in the transfer function given in (2.6). Generally, the parameters of the model in (2.6) can be obtained from measurements of the PLC channel transfer function. The magnitude of the channel frequency response can be used in the determination of the attenuation parameters (i.e. a_0, a_1 and k). The path parameters (g_i, d_i and τ_i) can be obtained from the channel impulse response of the channel. The number of paths is typically in the range 5 - 50 paths [22].

2.5.2 Frequency Domain Approach: Transmission Line Theory Models

The power line channel can be modelled using deterministic approaches provided a detailed knowledge of the electrical power grid between the transmitter and the receiver is

available. Thus, knowledge of the network topology, physical properties of the cable, and load impedances should be available. Two models based on a two-conductor and a multi-conductor transmission line (MTL) theory are briefly reviewed.

2.5.2.1 Two-Conductor Transmission Line Models

Various researchers have utilized the two-conductor transmission line theory to model the power line channel can be found in [28] and [29]. Typically, these models use either scattering or transmission matrix approach [18]. A two-conductor transmission line, with ground being the second conductor supports four modes of signal propagation. The signal travels along the line in two spatial modes each having two directions of propagation [18]. The two spatial modes are the differential and common modes. The dominant mode that carries the data signal in the desired direction along the transmission line is the differential mode. Differential signalling can be used to excite the propagation in the differential mode only, and reduce the propagation in the common mode which is normally induced by external noise. To achieve good rejection of unwanted external signals, the two conductors must be well balanced as any imbalance between them promotes common mode propagation. The two-conductor model does not address the effects of wiring and grounding practices in the transmission behaviour. In addition, the model neglected the effect of electromagnetic compatibility issues in the estimation of the common mode currents. Additionally, the two-conductor model does not explain the propagation in the presence of a third conductor present in single-phase power lines leading to a MTL situation. Consequently, the attempts to model the power line channel based on a two-conductor transmission line approach does not fully explain the propagation behaviour along power lines [18].

2.5.2.2 Multi-Conductor Transmission Line Models

Power cables used in single-phase connections normally consist of three or four conductors, which limits the applicability of the two-conductor transmission line model in explaining the propagation behaviour. Therefore, the modelling of the power line channel in the presence of a third or fourth conductor should rather consider multiple-conductor transmission line theory. In MTL, a transmission line consisting of N conductors and ground is partitioned into N simple TL's, each representing a single propagation mode [30]. Accordingly, the signal at the input of an MTL is broken into N modal components, each of which tra-

verses the corresponding modal TL. Recombination of the modal components of the signal takes place at the output ports. The coupling between each port and each modal TL is obtained using the weighting factors in the voltage and current transformation matrices. If a three-conductor power cable is used, then six propagation modes exist in the line resulting from three spatial modes (i.e. differential, pair and common). Each of the three spatial modes has two directions of propagation. The desired signal current generally travels in the differential mode. The signal in the pair-mode corresponds to the current flowing from the ground wire and the other two wires, whereas the signal in the common mode of operation corresponds to the overall imbalance between the modes and is directly related to the cable installation practices [25]. In indoor electric power grid, there is usually an imbalance between the propagation modes which results in coupling between the propagation modes [25]. Frequency-domain channel models based on TL theory offer the advantage of low computational complexity that is almost independent of the electric power grid topology [18]. Nevertheless, a comprehensive knowledge of the transmission link must be available *a priori*. The model requires details about the topology, properties of the cables used and impedance values at the end of every branch involved. The validity of the model can easily be nullified if an appreciable amount of knowledge of such parameters is not available. In a practical scenario, such knowledge of the power line network is nearly impossible, which makes modelling the power line using the frequency-domain models based on TL theory unrealistic. The time-domain approach described in Section 2.5.1, however, does not require such details about the network.

2.6 Impulsive Noise Modelling

High-speed data communications over power lines is confronted with a significant challenge due to the asynchronous impulsive noise presence. Practical measurements show that this type of noise can have large energy leading to a significant degradation in the performance of PLC systems [22,31]. Its ability to frequently sweep complete data symbols is a cause for concern in the research community as well as designers of PLC devices and systems. In [32], it is reported through practical measurements in power lines that the typical strength of a single impulse is more than 10 dB above the background noise level and can exceed 40 dB. Measurements in [21] indicate that the power spectral density of impulsive noise generally

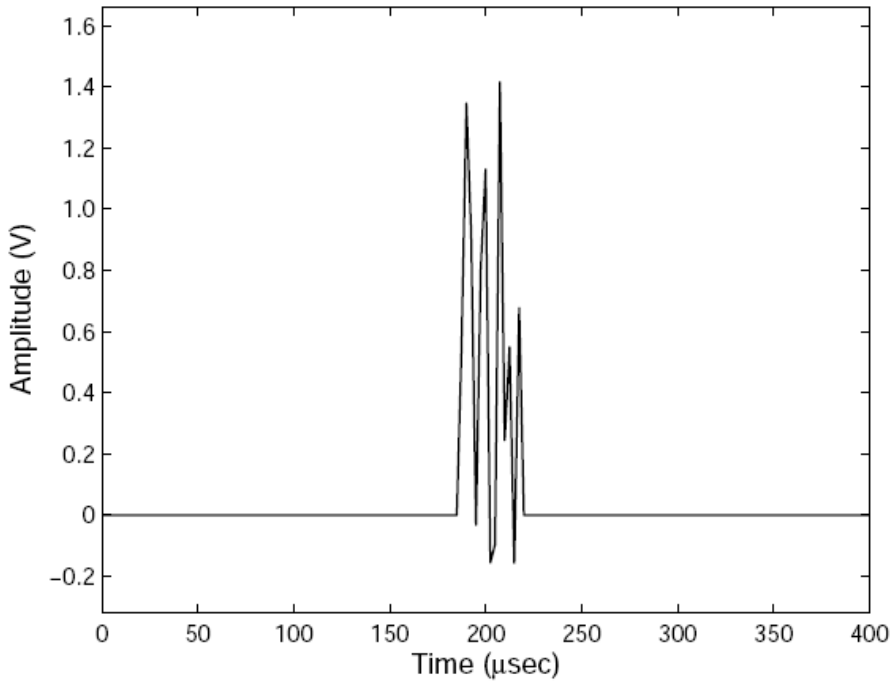

Figure 2-4: Sample of an Impulsive Noise

exceed that of background noise by 10 - 15 dB in most parts of the 0.2 - 20 MHz band. Furthermore, this difference may even rise to more than 50 dB at certain parts of the band. Figure 2-4 shows a sample impulse having a duration of approximately 50 μs. In the time-domain, three random variables characterize the impulsive noise that occurs in power lines and other data communication mediums. These are: impulse width, amplitude and inter-arrival time (IAT). Several attempts to derive the probability distribution statistics of these three parameters based on practical measurements in power line networks can be found in [32] and [33]. The impulse width and amplitude both represents the energy carried by a single impulse. The frequency of the impulses (the reciprocal of IAT) along with the impulse energy describe the power of the impulsive noise. Numerous statistical approaches have been put forward in literature in an attempt to model impulsive noise as described in the following sub-sections. Background noise on the other hand is usually modelled as white Gaussian random process (WGN) [32].

2.6.1 Middleton Class A Noise Model

Middleton in [34–36] classifies the electromagnetic (EM) noise or interference into three main classes: Class A, Class B and Class C (the sum of Class A and Class B). Various

researchers concede that the Middleton Class A noise model satisfactorily describes the statistical characteristics of the impulsive noise in PLC environments as in [33,37–39] as well as in other communication environments [40]. This model integrates both background and impulsive noises. Following the Middleton Class A model, the overall noise is a sequence of independent and identically distributed (i.i.d.) random variables with the probability density function (PDF):

$$p(z) = \sum_{m=0}^{\infty} e^{-A} \frac{A^m}{m!} \frac{1}{2\pi\sigma_m^2} exp\left(-\frac{z^2}{2\sigma_m^2}\right), \tag{2.8}$$

where the variance σ_m^2 is defined as:

$$\sigma_m^2 = (\sigma_g^2 + \sigma_i^2)\frac{\left(\frac{m}{A}\right) + \Gamma}{1+\Gamma}, \tag{2.9}$$

where the parameter A is called the impulsive index and is determined as the product of the average rate of impulses per unit time and average impulse duration. The variances σ_g^2 and σ_i^2 denote the power of background noise and impulsive noise respectively. The ratio between background noise and impulsive noise is given by

$$\Gamma = \frac{\sigma_g^2}{\sigma_i^2}. \tag{2.10}$$

It can be deduced from (2.8) that the PDF of the Middleton Class A noise is actually a weighted sum of Gaussian PDFs with mean equal to zero. Accordingly, the mean and variance of this process can be obtained by the following [31]:

$$\mu_z = E\{z\} = \int z.p(z)dz = \sum_{m=0}^{\infty} e^{-A} \frac{A^m}{m!} \frac{1}{2\pi\sigma_m^2} \int z.exp\left(-\frac{z^2}{2\sigma_m^2}\right) = 0 \tag{2.11}$$

$$\sigma_m^2 = E\{z^2\} = \sum_{m=0}^{\infty} e^{-A} \frac{A^m}{m!} \frac{1}{2\pi\sigma_m^2} \int z^2.exp\left(-\frac{z^2}{2\sigma_m^2}\right) = \frac{e^{-A}\sigma_g}{\Gamma} \sum_{m=0}^{\infty} \frac{A^m}{m!}\left(\frac{m}{A} + \Gamma\right) \tag{2.12}$$

The Middleton Class A model was originally developed to describe the man-made EM interference with impulsive behaviour. Despite the fact that this model has been considered by many researchers to describe impulsive noise, its applicability to model impulsive noise in power line networks remains inconclusive.

2.6.2 Bernoulli-Gaussian Model

Owing to its simplicity, the Bernoulli-Gaussian model is frequently used to model impulsive noise in electrical power grids and other data communication media [29, 41–44]. In a Bernoulli-Gaussian model of impulsive noise, the occurrence of impulsive noise is modelled according to the Bernoulli process $b(m)$, whereas the amplitude of the impulses is modelled according to the Gaussian distribution $n(m)$ [45]. A Bernoulli process is an i.i.d. sequence of ones and zeros with a probability that the process takes a value of '1' ($p(b(m) = 1) = \alpha$); therefore, the process takes a value of '0' with a probability of $1 - \alpha$. The probability mass function (pmf) of a Bernoulli process is defined by:

$$f(x) = \begin{cases} \alpha, & \text{for } b(m) = 1 \\ 1 - \alpha, & \text{for } b(m) = 0 \end{cases} \tag{2.13}$$

The mean and variance of the Bernoulli process are given by:

$$\mu_b = E[b(m)] = \alpha \tag{2.14}$$

and

$$\sigma_b^2 = E\left\{[b(m) - \mu_b]^2\right\} = \alpha(1 - \alpha), \tag{2.15}$$

respectively. The amplitudes of impulses are obtained from a Gaussian distribution with zero mean and variance σ_n^2, which has the following probability density function (pdf):

$$G[n(m)] = \frac{1}{\sigma_n\sqrt{2\pi}} \exp\left(-\frac{n^2(m)}{2\sigma_n^2}\right). \tag{2.16}$$

2.6.3 Poisson-Gaussian Model

A simple and efficient way that is often used to model impulse noise is the Poisson-Gaussian model [39, 41, 42]. In [42], it has been determined through measurements in residential power line networks, that the arrival of impulsive noise resembles a Poisson distribution. In the Poisson-Gaussian model, the impulse arrival time is modelled according to the Poisson process and the impulsive noise amplitudes are modelled as a Gaussian process of zero mean and variance σ_n^2. Thus, the occurrence of impulsive noise is governed by a Poisson

distribution of rate λ units per second, therefore the probability of m arrivals of a process per unit time is

$$P_p(m) = P_p(M = m) = e^{-\lambda}\frac{\lambda^m}{m!}, \qquad m = 0, 1, 2, \cdots \tag{2.17}$$

However, the amplitude of impulsive noise is modelled as a Gaussian process with a mean of zero and variance σ_n^2 as described in the previous section. To model the overall noise experienced during PLC transmission in the discrete time domain, the background noise w_k is usually assumed to be an additive white Gaussian random process (AWGN) [28, 41]. The k^{th} sample of the impulsive noise can be obtained using the Poisson-Gaussian model as:

$$i_k = b_k g_k, \tag{2.18}$$

where b_k denotes the arrival of impulses according to the Poisson process and g_k is a white Gaussian process characterizing the impulse amplitudes. This model can be thought of as each transmitted symbol being independently struck by an impulse with a probability of b_k having a random Gaussian amplitude of g_k [40]. If the signal a_k is transmitted over power lines impaired by impulsive noise, the received signal can be represented by

$$r_k = a_k + n_k. \tag{2.19}$$

The probability density function of the total noise n_k is given by [40]

$$p(n_k, n_k) = (1 - \alpha)G(n_k, 0, \sigma_w^2) + \alpha G(n_k, 0, \sigma_w^2 + \sigma_i^2)G(n_{kI}, 0, \sigma_w^2 + \sigma_i^2), \tag{2.20}$$

where α denotes the probability of occurrence of impulsive noise and $G(x, \mu, \sigma^2)$ represents the Gaussian probability distribution function of mean μ and variance σ^2 as shown in (2.16).

2.6.4 Autoregressive Moving Average (ARMA) Models

This model presents a statistical approach to model periodic impulsive noise generated by appliances connected to the electrical power network in indoor environments. The derivation of the models is based on collected data from a measurement campaign. The models also leverage on the deseasonalization of measured data and applying autoregressive moving

average modeling of cyclostationary random processes. Noise generated by power loads has a dominant effect on the overall noise measured in indoor scenarios. This noise, periodic in nature, usually emanates from power suppliers connected to the electrical power grid. Owing to this, significant efforts have been made towards modeling the periodic impulsive component of the aggregate noise. Notably, the power spectral density of this noise and its short-term cyclic variations have been studied in [23] and [46] respectively; with the findings of [46] progressively been utilized to develop a complete channel simulator for PLC [47]. Key features of the periodic impulsive noise such as properties of the impulses (impulse shape, repetition rate, impulse duration and magnitude) as well as the power spectral density have been presented in [48–51] following further experiments. The associated models capturing these results have thus been determined. It should be noted, however, that only in [50] has a fully statistical model been developed to represent the periodic impulsive noise. Therein, this noise is characterized as a sequence of impulses whose duration, amplitude, and inter-arrival time follows specific statistical laws. Further statistical representations of the periodic impulsive noise are presented in [37] and [52] on the basis of a Poisson process, unfortunately, they do not rely on experimental data. In [53], statistical models for periodic impulsive noise are developed. The key features of the models are such that:

- They are based on experimental data acquired from indoor environments.
- Simplicity in implementation since they are based on ARMA modeling of time series.

Considering the many variants of the ARMA family, only the deseasonalized autoregressive moving average (DARMA) model enables the development of accurate statistical representation with low implementation complexity [53]. In general, the DARMA modeling technique of a time series follows the following steps:

- Determine a suitable one-to-one mathematical transformation capable of removing the cyclostationarity of the process under analysis.
- Utilize this transformation to generate a stationary time series.
- Fit the stationary series to an ARMA model.
- The cyclostationarity is then restored by applying an inverse transformation to generate a data sequence with statistical properties similar to the original time series.

Given a measured cyclostationary time series data sequence w_n, it can be transformed to a new stationary sequence z_n ($z_n = G(w_n)$, with the deseasonalization technique detailed in [54]. An ARMA(p, q) model for a random process z_n can be expressed as [54, 55]

$$(z_n - \mu) - \phi_1(z_{n-1} - \mu) - \cdots - \phi_p(z_{n-p} - \mu) = a_n - \theta_1 a_{n-1} - \cdots - \theta_q a_{n-q}, \tag{2.21}$$

where μ represents the expected value of z_n and ϕ_i ($i = 1, 2, \cdots, p$) and θ_j ($j = 1, 2, \cdots, q$) are the pth and qth order parameters of the autoregressive (AR) and moving average (MA) parts, respectively. On the other hand, a_n denotes a real white Gaussian process with zero mean and variance σ^2. The ARMA(p, q) model of (2.21), having an expected value of a_n equal to zero, can be represented in the form

$$z_n = a_n - \sum_{j=1}^{q} \theta_j a_{n-j} + \sum_{i=1}^{p} \phi_i z_{n-i} \tag{2.22}$$

from which the AR(p) and MA(q) models can be selected by setting $\theta_j = 0$ and $\phi_i = 0$ respectively. In the process of the DARMA modeling, the coefficients of (2.21) need to be computed. The parameters θ_j of the MA(q) model are recursively determined through the *innovations algorithm* [55] by using the recursive form

$$\theta_{q-k} = v_k^{-1} \left[R_z(q-k) - \sum_{j=0}^{k-1} \theta_{q-j} \theta_{k-j} v_j \right] \tag{2.23}$$

for $k = 0, 1, \cdots, q-1$, with $v_0 = R_z(0)$

and

$$v_k = R_z(0) - \sum_{j=0}^{k-1} \theta_{k-j}^2 v_j \tag{2.24}$$

for $k \geq 1$. It should be noted that v_q corresponds to the variance σ^2 of the samples of the process a_n of the MA model. Here,

$$R_z(\tau) \doteq E[z_n z_{n+\tau}] = \frac{1}{N} \sum_{n=1}^{N-\tau} z_n z_{n+\tau} \tag{2.25}$$

denotes the autocorrelation of the stationary data sequence z_n. The operator $\doteq$ denotes isomorphism while $E[.]$ represents the expectation. On the other hand, the parameters ϕ_i of the AR(p) model are determined by using the Yule-Walker equations [54]; that is, the vector of the unknown parameters $\mathbf{\Phi}_p \doteq [\phi_1, \phi_2, \cdots, \phi_p]^T$ is calculated as

$$\mathbf{\Phi}_p = \mathbf{P}_p^{-1}\mathbf{R}_p \tag{2.26}$$

where $\mathbf{R}_p \doteq [R_z(1), R_z(2), \cdots, R_z(p)]^T$ is a p-dimensional vector and

$$\mathbf{P}_p = \begin{bmatrix} 1 & R_z(1) & R_z(2) & \dots & R_z(p-2) & R_z(p-1) \\ R_z(1) & 1 & R_z(1) & \dots & R_z(p-3) & R_z(p-2) \\ \vdots & \vdots & \vdots & \ddots & \vdots & \vdots \\ R_z(p-2) & R_z(p-3) & R_z(p-4) & \dots & 1 & R_z(1) \\ R_z(p-1) & R_z(p-2) & R_z(p-3) & \dots & R_z(1) & 1 \end{bmatrix} \tag{2.27}$$

is a symmetric $p \times p$ matrix.

In the AR model the sample variance of a_n is determined as

$$\sigma^2 = R_z(0) - \sum_{i=1}^{p} \phi_i R_z(i). \tag{2.28}$$

In the case of determining the parameters of the ARMA(p, q) model, the process is not usually as facile as it is with both the AR(p) and MA(q) models due to numerical stability issues [56, 57]. In their efforts to combat this problem, [53] have employed the Matlab function *armax.m* [58] based on an iterative algorithm to estimate the parameters of the ARMA process [59]. The procedures outlined above allows any of the AR(p), MA(q) or ARMA(p, q) models to be employed in the generation of the stationary sequence z_n. The cyclostationarity of the original sequence can be restored via the inverse transformation of the stationary sequence. A new data sequence is thus generated with similar statistical properties to the original sequence. The generated data sequence is thus given by

$$\hat{w}_n \doteq G^{-1}(z_n). \tag{2.29}$$

The challenge of this modeling approach is proper selection of the model order p and q given that they can take any value. The higher their values the higher the statistical accuracy, which also leads to higher computational complexity. Expectedly, the choice of the model order is a compromise between statistical accuracy and computational complexity.

Throughout this study, the focus will be on PLC channel and noise modeling. Powerline channels are known to exhibit multipath propagation which results in notches in the channel transfer function evaluated in the frequency domain. The depth of these notches depends on several topology parameters such as branch lengths and terminating impedance. This study will approach the channel modeling in two ways, depending on information available about the electrical network. One way aims to take advantage of known electrical network parameters and the other considers an unknown realistic channel and estimate its transfer function.

This study will also investigate noise characteristics in electrical power grids. PLC noise differs significantly from popular wireless noise characteristics. Known to be dominated by impulsive components generated by appliances in the electrical network, this noise will be investigated and characterized.

CHAPTER 3

Broadband Characteristics and Modeling of Multi-Path Powerline Communication Channels

3.1 Introduction

In the quest to develop new communication systems, the choice of the transmission technique and other design parameters is reliant on the characteristics of the channel transfer functions, additive noise and as a consequence, possible channel capacity. This consequently places a demand for accurate models that can describe the transmission phenomena over the power line with sufficient precision. Numerous approaches to model the transfer function of electrical power grids have been brought forward in literature. In general, the factors which determine the reliability and accuracy of these models are essentially the modeling algorithms and the model parameters. The modelling approaches are generally classified into two categories depending on how the model parameters are obtained: the top-down strategy and the bottom-up strategy. With regards to the top-down strategy, which is also commonly known as the empirical approach, the model parameters are obtained through measurements. This approach requires minimal computation intensity and has little difficulty in its implementation. Comparatively, the bottom-up technique computed with *a priori* methodology starts off with a theoretical derivation of the parameters, with a clear description on the connection between the parameters and performance metrics. The empirical and deterministic modeling techniques each has advantages and disadvantages. The top-down modelling technique boasts simplicity in its usage as well as implementation. The transfer function parameters are extracted from actual measurements of a PLC network. However, its susceptibility to measurement errors and lack of generality in its application to different PLC networks proves to be a major setback. On the other hand, the bottom-up modeling strategy derives all its transfer function parameters theoretically. It is therefore necessary to acquire a detailed knowledge of all the relevant components' characteristics. Typically these details are the topology (network architecture), cable lengths and proper-

ties, and impedance loadings at every branch termination. The network behaviour relative to the model parameters is thus clearly defined. Alterations in the transfer function are predictable as per changes in the network configuration. The transfer function modeling will however be significantly compromised should some of the parameters be unavailable. The major drawback of this approach lies in its computational efforts. In this chapter, the two approaches are adopted and two models are developed. This is brought about by the realization that the two approaches, regardless of their respective shortcomings, are environment specific in their application. Their specificity in application makes it impossible to combine their advantages for improved determination and implementation.

3.2 Multi-Path PLC Channels

The idea of utilizing electrical power grids as a communication medium dates back to the 1900's [60]. However, until recently, their use has been restricted to narrowband applications. The main reason for dismissing usage of power lines for broadband applications was simply because the channel was considered too noisy and unpredictable [61]. Furthermore, interference with primary users of the spectrum was also a big issue. However, advances in digital transmission techniques have provided a different perspective on the prospect of employing PLC systems for broadband applications. Thus, applications such as PLC local area networks (LAN) would not be restricted to computer connections, but also extended to peripherals and multimedia equipment. PLC has a promising future in developing countries, as opposed to developed countries where there is a strong competition from digital subscriber lines (DSL), wireless networks, fibre optics, and cable services [61]. Telecom operators globally are currently offering triple play solutions (telephony, video, and internet access) and PLC is a viable option to deliver broadband data to the residential gateway, to the television set top box and the computer [61]. Electrical power grids have variable physical characteristics and network topologies vary across countries due to different wiring practices [62]. Another problematic factor is the presence of noise generated by appliances connected to the power network. The noise characteristics experienced in PLC environments are rarely stationary, white and Gaussian [23, 63]. The provision of the service is still deterred by lack of unified standards as well as channel models. Another factor in question is as to whether PLC systems are capable of rivalling their counterparts in terms of bit

rates. The variability of channel characteristics in indoor environments has led to numerous channel modelling approaches and consequently lack of a common agreement on the most suitable channel model. A series of standards such as IEEE P1901-2010 and ITU-T G.hn/G.cx, have been released owing to the increasing market demand for indoor broadband communications, smart grid applications, and in-home energy management [64]. Thus, the quest to develop accurate models to facilitate these technologies remain an on-going process. The existing models proposed in literature can be classified into two main categories [65]: the multipath approach (top-down strategy) [26,66–69] and the transmission line theory approach (bottom-up strategy) [70, 71]. The multipath model takes into account the reflected signals due to impedance discontinuities at branches and other mismatches such as cable heterogeneity. Its accuracy is completely reliant on the proper selection of the parameters of the signal propagation properties [65]. The effective number of paths is derived from the actual measurements of channel transfer functions; thus it is only the dominant paths that are evaluated based on the propagation properties of each individual path. On the other hand, transmission line theory based models consider an electrical power grid as a series of cascaded two port networks and can thus be adapted to different network topologies using popular transmission matrices [65]. This model is rather computation intensive especially when dealing with complex networks. The other drawback is its dependency on the availability of the line parameters to generate matrices, thus its applicability to real networks of unknown cable types and topology is limited. In this section, we consider a top-down multipath approach and treat the networks under consideration as a "black box" of unknown parameters and describe its frequency response in the frequency range 1 - 30 MHz. Though a popular model, its application is usually restricted to theoretical channel generation the results of which are then used to quantify channel metrics such as channel capacity and throughput. Little has been done in its application to real world PLC channel representation. The primary inputs to the model are derived from cable properties typically used by the local electrical utility. Other model parameters are tuned to match the measured data. Due to the vast variability of channels experienced by signal propagation in PLC networks, we also present a time-domain approach which enables a statistical representation of time dispersive nature of parameters of PLC channels. An ensemble of PLC channel measurements are carried out in indoor environments and their impulse responses studied from which the time-domain parameters are derived.

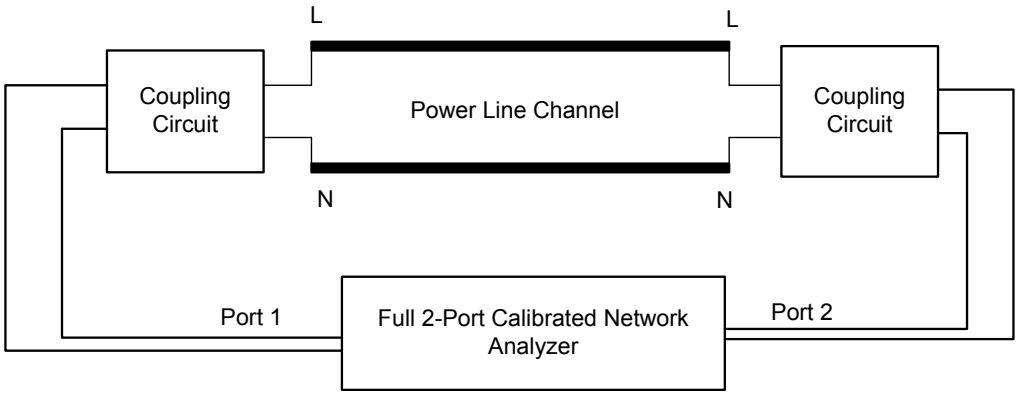

Figure 3-1: Measurement Configuration

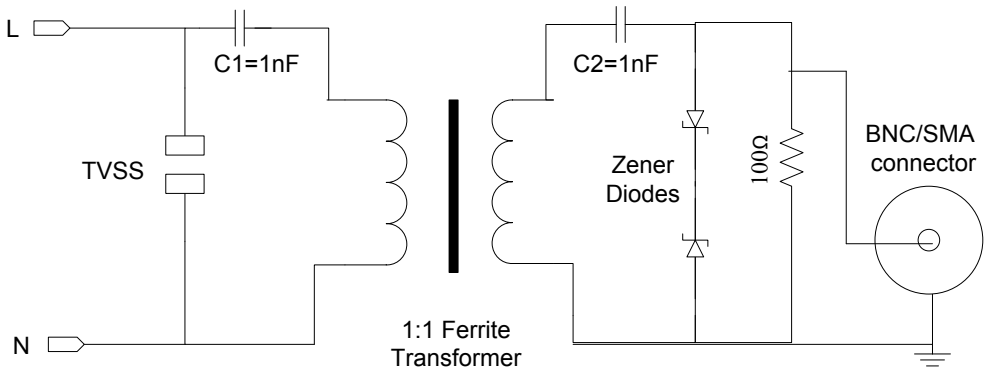

Figure 3-2: Coupling Circuitry

3.2.1 Measurement Description & Instrumentation

The measurements have been performed in three different in-building scenarios in the Electrical Engineering building at the University of KwaZulu-Natal, Durban, South Africa: small office, large office, and a laboratory. The measurement setup is as shown in Figure 3-1 with the coupling circuitry employed shown in Figure 3-2. Frequency domain measurements were performed using the Rhode & Schwartz ZVL13 vector network analyser for channel frequency response (CFR); it has specifications as described in [72].

The measuring instrument was coupled to and from the electrical power grids through broadband PLC couplers to provide the necessary protection and galvanic isolation from the low frequency mains signal. The coupler is designed to have a fairly flat transfer response for frequencies up to 30 MHz, with an average loss of 1.59 dB in this band as shown in Figure 3-3. This response is taken into consideration in all subsequent measurements by offsetting measurements by this value. The coupler presents an attenuation of 46.3 dB at 9

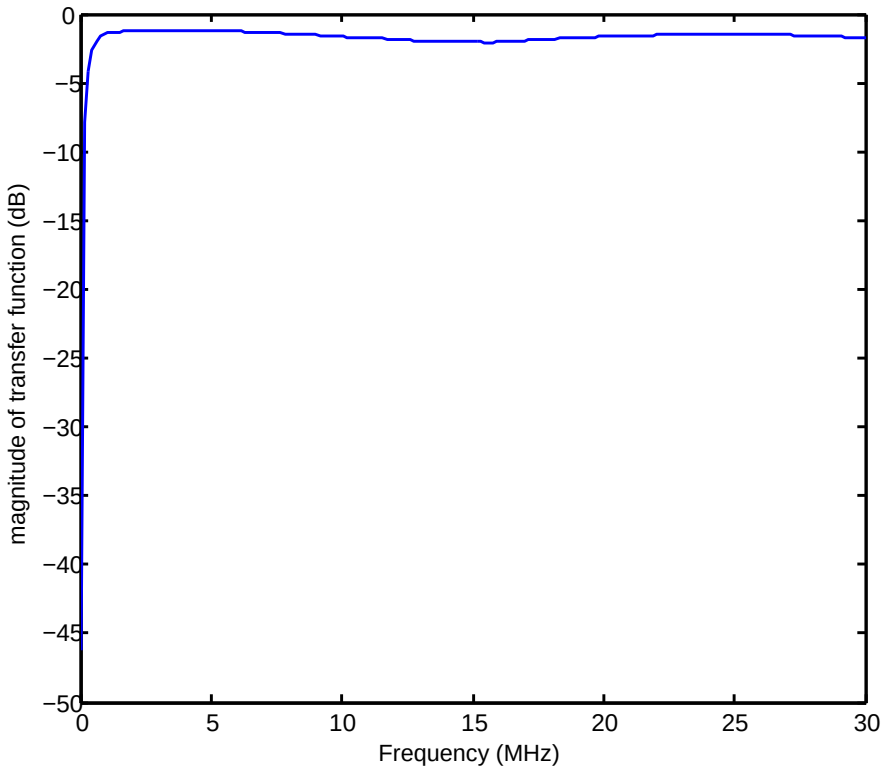

Figure 3-3: Coupling Circuitry

kHz (instrument lower frequency limit, see [72]) - hence the attenuation is expected to be even much higher at the mains frequency (50 Hz), which guarantees adequate mains isolation. Incorporating the coupler characteristics in the measurement post-processing provides necessary measurement integrity and reliability in the band of interest.

3.2.2 Channel frequency Response Measurements

The large post-graduate office houses several computers, a large heavy-duty printer and two medium-sized air conditioning units; the laboratory comprises of 30 - 40 computer working stations and medium-size motors, while a small office has at most three PCs and a single air conditioner. All the loads connected throughout the building were running as usual, and to anticipate worst case scenarios, all measurements were performed during the day time. Three channels were considered in each scenario and presented, with a total of twenty (20) measurement acquisitions taken for each individual circuit. This allows for a fair average characterization of each channel, considering the unpredictable nature of the channel due to

noise and loading. As the signal traverses the electrical power grid, it experiences multiple reflections due to impedance mismatches and branching. Delayed signals thus show up at the receiver as multiple echoes, resulting in notches throughout the frequency band. The concentration of notches translates into the population of branches and loading conditions in a given electrical power grid. The state of the electrical power grid depends not only on its architecture, but also on the load. This characterises a channel as periodically time-variant and unpredictable due to the arbitrary load profile the electrical power grid is subjected to. To accommodate the time-dependence of channel variability, an average channel response is considered in order to capture its behaviour as shown in Figure 3-4(a) through 3-4(c). Channel 1 and 2 (student laboratory and a large post-graduate office, respectively) are characterized by a series of deep notches distributed across the band, while channel 3 (small office) consists of a single deep notch at 10 MHz. In general, we can assume channel 1 and 2 to be heavily branched and loaded and thus expect longer impulse responses as opposed to channel 3 [64].

3.2.3 Practical PLC Channel Modeling

It is common in literature to use PLC channel emulators to generate channel transfer functions and further determine the performance of the link. Other approaches include mimicking the electrical grid scenario in the form of test beds, on which transfer functions can be measured through vectorised network analysers. The aim of this work is to model the measured channel transfer functions from real-world electrical grids.

3.2.3.1 Channel Response Characteristics

The electrical power grid is considered to be a multipath propagation medium hence the PLC channel is frequency selective. This arises from the fact that in power-line communication channels, transmitted signals do not only propagate along a direct "line-of-sight" path between the transmitter and the receiver but also suffers multiple reflections (echoes) due to additional paths [73]. The multipath behaviour is caused by the presence of power cable joints (branches), consumer equipments, connection boxes and in some cases the heterogeneity of the power lines resulting in impedance mismatches. In this work, a top-down approach is employed to model the power line channel as a black box and describe its transfer characteristics within the frequency band of 1 - 30 MHz. We propose the model of Zimmermann

& Dostert [26], structured based on the fundamental physical effects analysed over a great number of measurements. The basis of this model was first brought forward in [30] while a simpler but less precise multipath approach was provided in [27]. As pointed out in [26], only when considering simpler topologies such as single-branched cables, can one easily attribute portions of the observed results to specific physical effects (cable loss, reflection, and transmission factors). Thus, in practical electrical power grids, back-tracing of measurements results to physical effects will prove generally impossible due to the complexity of the network topology. Regardless of this short-coming, the proposed model describes the frequency response of real networks with sufficient precision. The proposed band-pass CFR PLC model takes into account the multipath effects that is inherent with the power line. The channel frequency response can be synthesized as follows [26]:

$$H(f) = \sum_{i=1}^{N_i} g_i(f) e^{-j\frac{2\pi d_i}{v} f} A(f, d_i), \tag{3.1}$$

where N_i is the number of paths, $g_i(f)$ represents the complex and frequency-dependent transmission/reflection factor for path i. The path length is represented by d_i while $v = c/\sqrt{\varepsilon}_r$, with c the speed of light and ε_r the cable's dielectric constant. The lossy cables cause an attenuation given by $A(f, d_i)$ which increases with frequency and distance. In [64], it is suggested that it is possible to simplify the specification of the weighting factors g_i to being complex but not frequency-dependent. Furthermore, considering practical interests, g_i can even be assumed real-valued [26]. Equation (3.1) is therefore simplified by considering the attenuation of a power line cable given by

$$A(f, d_i) = e^{-\alpha(f) d_i} = e^{-(a_0 + a_1 f^K) d_i}. \tag{3.2}$$

So that,

$$H(f) = A \sum_{i=1}^{N_i} g_i e^{-j\frac{2\pi d_i}{v} f} e^{-(a_0 + a_1 f^K) d_i}, \tag{3.3}$$

where the parameters a_0 , a_1 , K, and N_i are chosen to adapt the model to a specific electrical power grid. In this work, the cable attenuation constant $\alpha(f)$ has been measured as a function of frequency and the obtained relationship is used to determine the model parameters in (3.2). Variables a_0 , a_1 , and K are determined through a Least-Absolute

Residual (LAR) robust analysis of the attenuation constant. Parameter A is brought in to adjust the attenuation of the final result. Appropriate parameter fitting enables the model to realistically capture the channel frequency response. The expression in (3.3) covers all the relevant propagation effects of the transfer function of a typical electrical power grid. However, this parametric model should be used to fit measured channel frequency responses [26]. However, it is common practice for researchers to apply the model to generated data. To further enhance the usability of the model, we consider the approach of [4], which evaluates performance with a statistical model that allows for capture of the ensemble of power line channels. Parameters in (3.3) are considered to be random variables. This allows us to model the channel transfer function through a realisation of these parameters [4]. The resultant multiple paths are assumed to be caused by reflectors placed over a finite distance interval with the first reflector placed at distance $d_1(i = 1)$. The remaining reflectors are distributed according to a Poisson arrival process with intensity $\Lambda[m^{-1}]$. As mentioned before, the reflection factors g_i are considered real-valued and are further characterized as independent and uniformly distributed random variable in [-1, +1]. This is due to the fact that reflection/transmission coefficients are never greater than unity in absolute magnitude. The values of a_0 , a_1 and K are then extracted as previously described. The derivation in (3.2) describes the physical effects of a power cable; nonetheless it is not facile to determine the parameters a_0 , a_1 and K from prior knowledge of cable parameters. In practical terms, even so, the usefulness of the model is not restricted due to the fact that it is infeasible to acquire all the necessary cable geometry information for practical electrical networks [26]. To estimate the attenuation parameters, we consider the attenuation profile of a single-path cable link. The attenuation coefficient from (3.2) is given as:

$$\alpha(f) = a_0 + a_1 f^K. \tag{3.4}$$

The plot of $\alpha(f)$ versus frequency is fairly linear in the frequency range 0 - 30 MHz as shown in Figure 4-3(b), as also confirmed by the results of the LAR algorithm, allowing us to estimate the value of K to be ~ 1. The intercept and slope of the graph gives us an estimate of a_0 and a_1 respectively. Initial estimates were obtained through tests of two types of cables commonly used by the local electrical utility. We have used the $2.5\,mm^2$ and $4\,mm^2$ cables of both VVF and NYM types. The parameters do not vary much with cable diameter but

rather significantly with cable type as frequency increases. The value of $a_0 = 1 \times 10^{-3}(m^{-1})$ is recorded for the two cable types while $a_1 = 1.16 \times 10^{-9}(S/m)$ and $6.6 \times 10^{-10}(S/m)$ for NYM and VVF cable types, respectively. An average value of $a_1 = 1 \times 10^{-9}(S/m)$ is then considered since neither the cable diameter nor the cable type is readily known. This does not exclude the fact that the electrical power network could also be heterogeneous. These parameters are the starting point in the parameter estimation technique. They can further be tuned to adapt to the particular network under consideration. The three electrical power networks under study are successfully captured by the model as shown in Figure 3-4(a) through 3-4(c) using (3.3) and the dominant notches are not underestimated or exaggerated in all the cases. It is not realistic to expect a perfect fit since the model is constructed without any knowledge of the actual electrical power network topology and condition. Nonetheless, the ability of the model to capture unknown and uncharacterised practical electrical power network is adequately demonstrated. It is observed that in between the notches, there exist frequency bands with fairly linear phase details, hence such bands could be opportunistically targeted and strategically combined for reliable signal transmission [64].

3.2.3.2 Channel Model Parameters

In Utilizing the model discussed above, PLC channel models are generated based on the parameters in Table 3.1. The fact that indoor propagation involves a significantly high number of short paths is considered, and thus the Poisson arrival process intensity of $\Lambda = 1/3[m^{-1}]$ is chosen. This corresponds to an average of a single reflector every 3 m. This is simply because our measurements were taken in laboratories and fairly populated offices, the environments populated with multiple power outlets (roughly within 3 m of each other) for multiple users. The same goes for a post-graduate office which houses 6-7 post-graduates. The first ray is set at d_1 with exponential distribution and the maximum path length is taken to be 200 m. The frequency band of operation is within 1 - 30 MHz and the final value of $K = 0.8$ was used in all the cases. Our initial estimates of $a_0 = 1 \times 10^{-3}(m^{-1})$, $a_1 = 1 \times 10^{-9}(S/m)$ and $K = 1$ were not too far from the final values, though further tuning of these parameters was required to obtain a better fit to the measured data as seen in Table 3.1. The frequency-dependent attenuation $\alpha(f)$ given by (3.4) is thus fairly linear within the frequency band considered here, as reflected by the value of K in all cases. It is also noticed that it took a considerably smaller number of paths to model channel 3 as compared

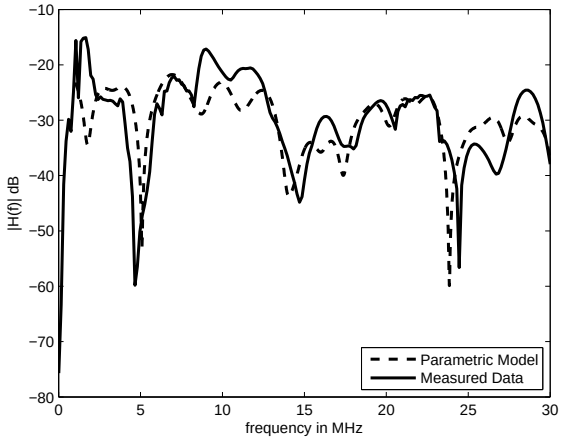

(a) Magnitude of CFR: simulated and measured results for channel 1

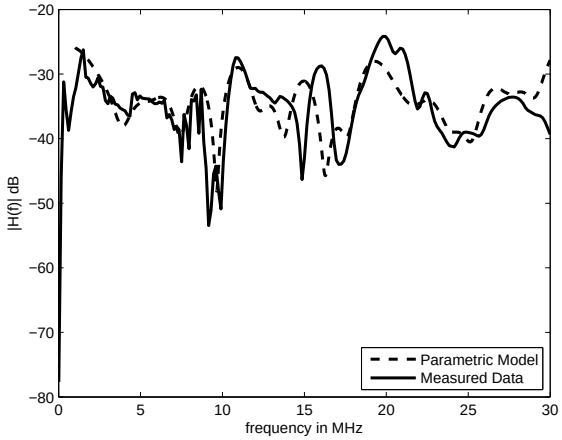

(b) Magnitude of CFR: simulated and measured results for channel 2

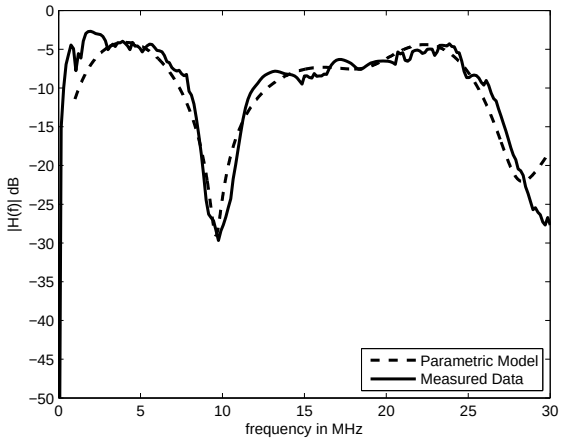

(c) Magnitude of CFR: simulated and measured results for channel 3

Figure 3-4: Modeling of three indoor PLC channels

Table 3.1: Model parameters for three simulated channels of Figure 3.3.

Channel #	$a_0(m^{-1})$	$a_1(s/m)$	N_i	K
1	5.0×10^{-3}	4.5×10^{-9}	50	0.8
2	2.5×10^{-3}	5.5×10^{-9}	40	0.8
3	4.0×10^{-3}	2.0×10^{-11}	15	0.8

to both Channel 1 and 2. This is foreseeable from the magnitude of the CFRs of Figure 3-4 given the spread of notches within the band considered. Thus, channel 1 and 2 have many significant signal paths leading to the receiver. The parameter N_i thus acts as the accuracy controller for the model, with certain channels requiring consideration of more number of paths than others for the same accuracy. Once the optimal number of paths are considered, it is not rewarding to include the less significant paths in the calculation as they will hardly effect any further change towards the channel frequency response.

3.2.4 Channel Impulse Response

The channel impulsive response $h(t)$, can be determined by means of the inverse Fourier transform (IFT) derived from the absolute value and phase of a measured channel frequency response [74] in the continuous time domain. Thus the time domain channel impulse response, including cable loss, can be determined as follows:

$$h(t) = \sum_{i=1}^{N_i} I_i[A_t(t, vT_i) \otimes \delta(t - T_i)] \tag{3.5}$$

where I_i and T_i are magnitude and delay of the i^{th} path respectively; v is the transverse electromagnetic (TEM) wave propagation speed in the cable which can be calculated according to the permittivity of the insulating material of the cable ($v = c/\sqrt{\varepsilon_r}$); $A_t(t, vT_i)$ is the cable loss effect in the time domain evaluated as the inverse Fourier transform of (3.2) [65]; the operator $\otimes$ indicates tensor product. The results presented in Table 3.2 show the channel impulse response peak times of the three sample channels of Figure 3-4. The time delay parameters of the three channels of Figure 3-4 are also shown in Table 3.2 which demonstrates the multipath characteristics of PLC channels for indoor communication applications. The main peak is represented by the first arrival time followed by several subsequent peaks with descending magnitudes. The characteristic summary of the channel impulse responses is populated in Table 3.2. The occurrence of the dominant peaks in each channel are recorded

Table 3.2: Channel impulse response summary of the three channels of Figure 3.3

CH #	Peak #	$\tau_A(s)$	$(P_i - P_{i-1})$	$d(m)$	$\tau_m(\mu s)$	$m_\tau(\mu s)$	$\sigma_\tau(\mu s)$
1	1	5.00×10^{-8}	5.00×10^{-8}	10	1.95	0.196	1.08
	2	1.33×10^{-7}	8.33×10^{-8}	17			
2	1	5.00×10^{-8}	5.00×10^{-8}	10	1.71	0.144	0.84
	2	1.00×10^{-7}	5.00×10^{-8}	10			
	3	1.33×10^{-7}	3.33×10^{-8}	7			
	4	1.66×10^{-7}	3.33×10^{-8}	7			
	5	2.33×10^{-7}	6.67×10^{-8}	13			
3	1	5.00×10^{-8}	5.00×10^{-8}	10	1.22	0.136	0.89
	2	8.33×10^{-8}	3.33×10^{-8}	7			

and their time of occurrence is presented as peak time (s). The time interval between the peaks is calculated as $P_i - P_{i-1}$ which can be translated into the difference in path lengths using $d = c\Delta t$, where Δt is the time difference between successive peaks. Considering a fairly linear phase characteristic, the group delay can be determined as follows [75]:

$$\tau_g = -\frac{1}{2\pi}\frac{d\vartheta(f,t,l)}{df}, \tag{3.6}$$

$\vartheta(f,t,l)$ is the phase of the signal as it propagates through the channel. Parameters f, t, and l represent frequency, time and path length respectively. The impulse response of PLC channels can be described by various time-domain parameters. There have been some thorough studies on PLC channels undertaken in the frequency range 1 - 30 MHz by [76,77]. In their campaign, they observed that for 90% of the channels studied, a root mean square (RMS) delay spread was below 0.5 μs. In [78], considering the transmission frequency band 0.5 - 15 MHz, the maximum excess delay was found to be below 3 μs.

In the frequency range up to 30 MHz, the authors found that, for 95% of the channels studied, the mean delay spread is between 0.16 μs and 3.2 μs and the same percentage of channels exhibit a delay spread between 0.24 μs and 2.5 μs [79]. This kind of study has not been explored in great deal as opposed to frequency domain based modeling, yet it provides an enhanced opportunity towards a determination of a unified statistical generalized representation. Since the channel impulse response (CIR) and the CFR of a PL channel have a relationship based on the Fourier transform, intuitively one would deduce that if the transfer magnitude is characterized by more fades per bandwidth, a longer CIR is expected. This can be quantified in terms of maximum excess delay of the channel. The results in Table 3.2 show that channel 1 and 2 have longer maximum excess delays (1.95 μs and 1.71 μs,

respectively) compared to channel 3 with 1.22 μs. This correlates with the results of Figure 3-4 where channel 1 and 2 are dominated by deep fades throughout the bandwidth. Channel 3, however, comprises of a single deep fade at 10 MHz. Furthermore, an investigation into the dispersive nature of the PLC channel derived from an ensemble of measurements performed as described in Section 3.2.1 and present the delay parameters statistically.

3.2.5 Power Delay Profile

The multipath nature of the PLC channel results in severe dispersion of the propagating signal [80]. The intensity of the received signal after the dispersion is a function of the time delay and its representation is called the power delay profile (PDP). This quantity provides information pertaining to the signal intensity as it traverses the multipath channel. The channel power delay profile gives the strength of a signal received through a multipath channel as a function of time delay as shown below.

$$p(\tau) = \frac{|h(\tau)|^2}{\int_{-\infty}^{\infty}|h(\tau)|^2 d\tau}. \tag{3.7}$$

An ensemble of PDPs is obtained, each representing a power dispersion due to the multipath propagation of the measured PLC channel. A typical plot of the power delay profile is shown in Figure 3-5. Time delay multi-path channel parameters are derived from the power delay profile. Time dispersion varies widely in PLC channels due to the random distribution of multiple reflectors (branches) in the electrical power network and random load profiles, resulting in random time-dependent channel impulse responses [80].

3.2.6 Time-Delay Spread Parameters

Since time dispersion is dependent on factors such as the electrical power network topology, load characteristics, transmitter-receiver distance, just to name a few, some parameters that can be used to grossly quantify multipath characteristics of PLC channel are described [81].

3.2.6.1 First-Arrival Delay (τ_A)

The numerous signal paths between the transmitter and the receiver translates to different times of transmission. Since multiple copies of the propagating signal are received at different moments, the signal that traverses the shortest path arrives first at the receiver. This is

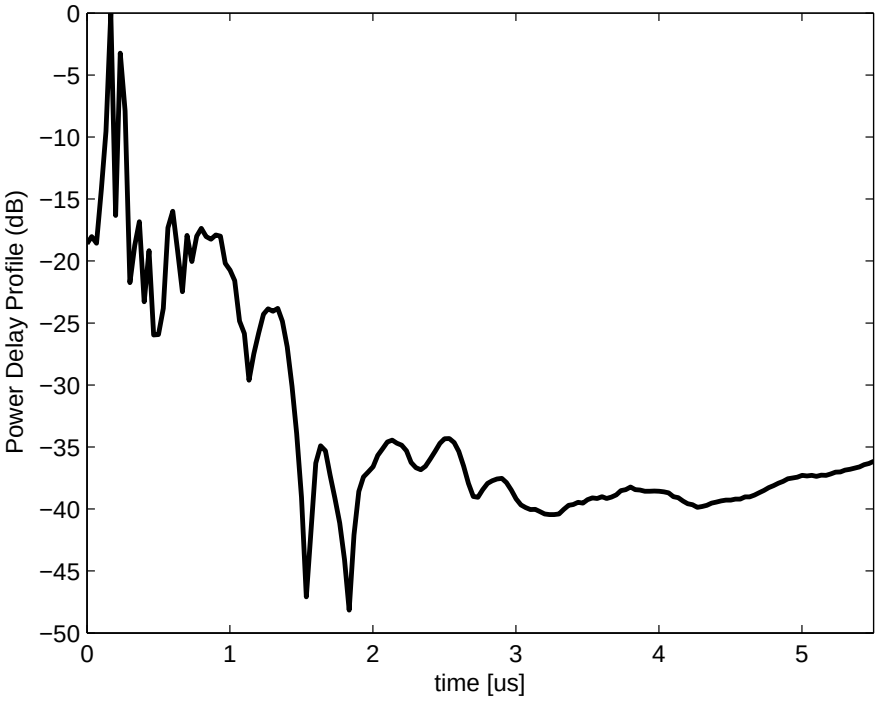

Figure 3-5: A sample PDP plot

called the first arrival delay and it is the minimum possible propagation delay between the Tx and Rx. As the first detectable received signal, it serves as a reference, thus, other propagation delay parameters are defined in relation to it. Therefore, any delay parameter defined beyond the first arrival delay is considered excess delay.

3.2.6.2 Mean Excess Delay (τ_e)

The mean excess delay characterizes the first moment of the power-delay spread with reference to the first arrival path. It is a dispersive property of wideband multipath channels commonly used to quantify these channels. PLC channels are characterized by multipath propagation, and then the following expression is used to determine the mean excess delay

$$\tau_e = \int (\tau - \tau_A) p(\tau) d(\tau). \tag{3.8}$$

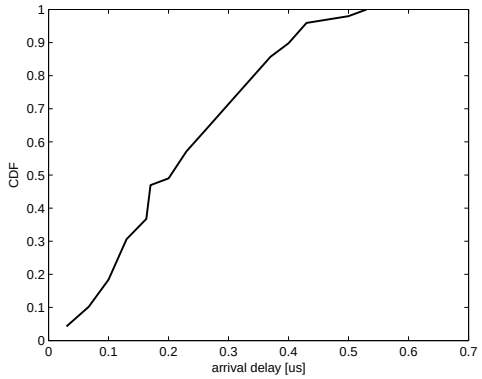

(a) Cumulative distribution for arrival delay

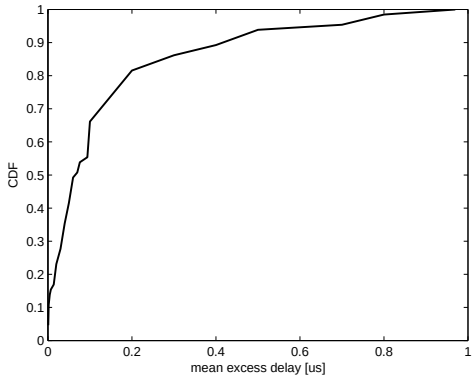

(b) Cumulative distribution for mean excess delay

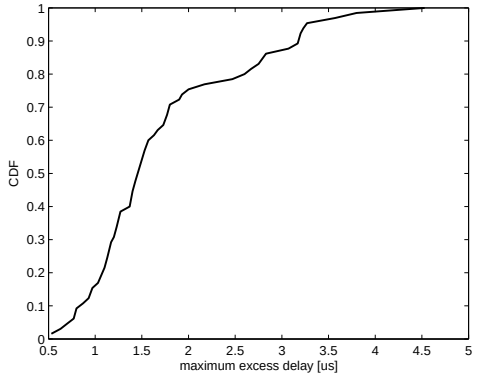

(c) Cumulative distribution for maximum excess delay

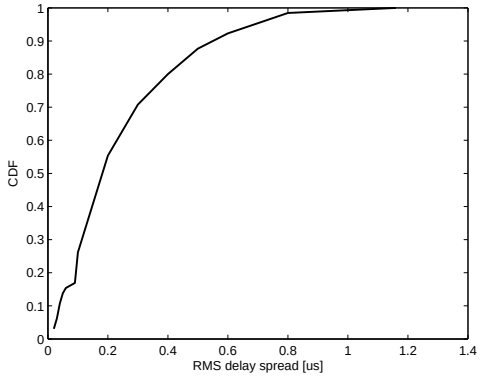

(d) Cumulative distribution for RMS delay spread

Figure 3-6: Cumulative distributions (CDFs) for the time delay parameters

3.2.6.3 RMS Delay Spread (τ_{rms})

Defined as the square root of the second central moment of the power-delay spread, this parameter determines the frequency selectivity of a PLC fading channel. This frequency selectivity has a strong relationship with the channel time dispersion. It is the standard deviation about the mean excess delay and can thus be determined as by:

$$\tau_{rms} = \left[\int (\tau - \tau_e - \tau_A)^2 p(\tau) d(\tau) \right]^{\frac{1}{2}}. \tag{3.9}$$

The RMS delay spread serves as a good indicator of the severity of the multipath phenomenon. The presence of inter-symbol interference (ISI) in data communication channels is determined from this parameter. Signal delays of high magnitude (relative to the shortest path) with long delay time contribute immensely to the τ_{rms} [81]. Regardless of the shape

of the PDP, the dispersion effects on digital receiver performance are related only to the RMS delay spread. ISI will be avoided as long as the RMS delay spread is small compared to the symbol period (T) of the digital modulation. Data rates for transmission can also be estimated using this parameter.

3.2.6.4 Maximum Excess Delay (τ_m)

The maximum excess delay is specified as the excess delay for which $p(\tau)$ falls below a specified threshold of the signal. Researchers have considered different threshold levels, but mostly consider -30 dB with respect to the peak value [74], and the same threshold is utilized in this work. The lower signal levels, below the threshold, are then processed as noise. Consequently, the mean excess delay (τ_e) and the RMS delay spread (τ_{rms}) are calculated based on impulses that exists during a time lower than τ_m.

3.2.7 Relationship between RMS Delay Spread and Mean Delay

The dependence of the RMS delay spread on the mean excess delay has been analyzed in the measured CFR. In the previous section, the RMS delay spread and the mean excess delay have been determined and presented statistically. The paper proceeds to determine the relationship between these two parameters. In this work, it is established that these parameters are related by a power law relationship. The high correlation value of $R^2 = 0.993$ suggests that a power law relation in the form given by

$$\tau_{rms}(\mu s) = 1.23\tau_e(\mu s)^{1.923} \tag{3.10}$$

can model the dependence between the RMS delay spread and the mean excess delay. The result of this fit is presented in Figure 3-7. Since the CIRs used to determine the two parameters are derived from CFR measurements of practical electrical power network of unknown topology or structure, this results is expected to be consistent, regardless of the environment. Thus, this relationship may not have other underlying dependence on parameters such as transmitter-receiver distance, cable type or geometry. In that case, the relationship is expected to maintain its scale invariance property. However, a larger measurement campaign is still required in an effort aimed towards a firm establishment of this relationship.

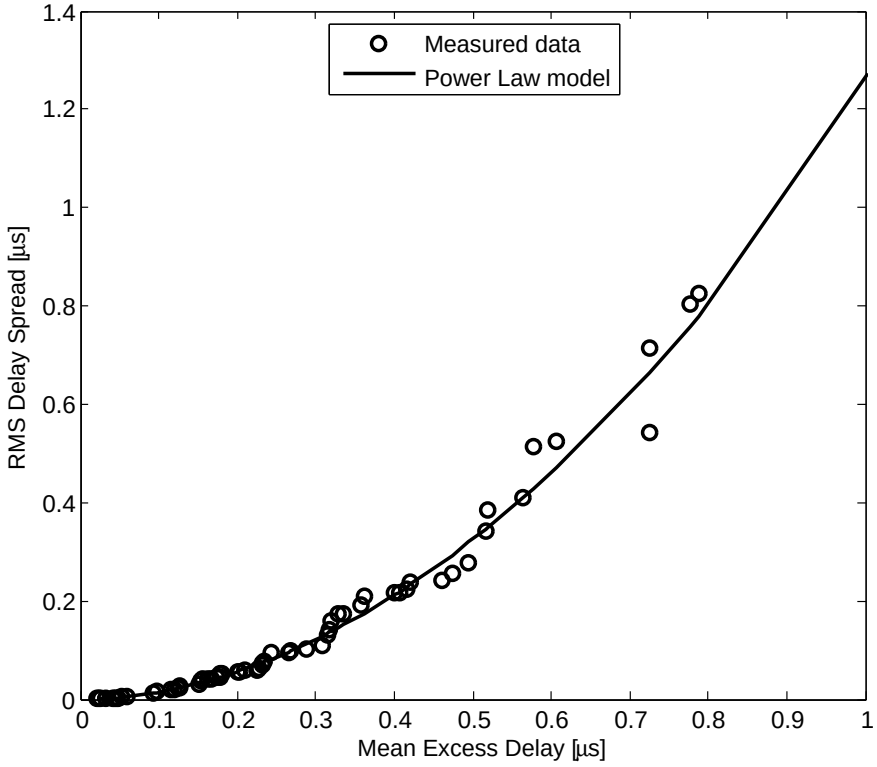

Figure 3-7: RMS delay vs mean excess delay

3.2.8 Results Analysis of Dispersion

The time dispersion characteristics of PLC channels are presented statistically in Table 3.3. For completeness, the results are presented graphically in Figure 3-6. The analysis entails the evaluated minimum, maximum, mean, standard deviation and the 90th percentiles of each time-delay parameter. Alongside our results is that of an extensive measurement campaign carried out in France [74] for comparison (here shown with a subscript (1)). It should be noted that their measurements extends to frequencies up to 100 MHz, though for the same threshold signal level, similar delay characteristics are expected and it is macroscopically the case here. In this study, the first arrival delay (τ_A) was observed to have a minimum value of 0.033 μs, standard deviation of 0.143 μs, and a mean value of 0.179 μs. For 90% of the time, the value of was found to be less than 0.37 μs and above 0.06 μs. On the other hand, the mean excess delay (τ_e) has a mean value of 0.163 μs, and a standard deviation of 0.216 μs. Though τ_e is confined between 0.00082 μs and 0.97 μs, it is found that for 90%

Table 3.3: Statistics of the time delay parameters

$\tau(\mu s)$	$Min(\mu s)$	$Max(\mu s)$	$Mean(\mu s)$	$STDev(\mu s)$	90% above	90% below
τ_A	0.033	0.534	0.179	0.143	0.067	0.37
τ_{A1}	0.010	0.410	0.152	0.097	0.05	0.30
τ_e	0.00082	0.97	0.163	0.216	0.02	0.40
τ_{e1}	0.0003	0.88	0.182	0.157	0.025	0.36
τ_{rms}	0.0215	1.16	0.287	0.222	0.04	0.55
τ_{rms1}	0.026	1.039	0.309	0.212	0.06	0.60
τ_m	0.534	4.535	1.749	0.867	0.83	3.27
τ_{m1}	0.18	6.26	2.228	1.327	0.55	3.81

of the time, its values are between 0.02 μs and 0.4 μs.

For 90% of the measured channels, the maximum excess delay (τ_m) was observed to lie between 0.83 μs and 3.27 μs. Its mean and standard deviation were found to be 1.749 μs and 0.867 μs, respectively. Of the measured channels, 90% of them exhibit an RMS delay spread between 0.04 μs and 0.55 μs. The percentiles for the time delay parameters are displayed in Figure 3-6 in the form of cumulative distributions (CDFs). Other percentiles not discussed in this paper can easily be deduced from the presented CDFs.

3.2.9 Coherence Bandwidth

It is common practice to characterize a radio communication channel with what is known as coherence bandwidth. This parameter measures the statistical extent to which a channel is flat observed over a specified window. In this work, an analysis of coherence bandwidth in PLC networks is presented. In the quest to design robust and reliable PLC systems, a remarkable amount of effort is placed on the choice of channel equalization, modulation, coding and receiver architecture schemes. The primary objective of this initiative is to mitigate the harsh effects of the PLC channel [82]. The multipath nature of the PLC channel results in deep fades (nulls) in the channel frequency response. This behaviour of channel frequency response is quantified by the coherence bandwidth B_c. Over some minimum spectral windows in the frequency domain, the magnitude of the channel transfer function preserves a quasi-constant state. This band has an inverse relationship with the maximum delay spread, over which the phase response is also quasi-linear. Such a band of frequencies are statistically defined by the coherence bandwidth and thus has a dependence on the RMS delay spread. In general, it is a statistical measure of a range of frequencies over which a channel can be considered flat, thereby defining a range of frequencies over which

a designer may consider the frequency correlation function (FCF) flat [74]. Practically, the coherence bandwidth indicates the amount of bandwidth the signal can use without implementing advanced techniques such as channel equalization. The frequency correlation function of the frequency selective PLC channel can be defined by considering this channel to be a wide sense stationary uncorrelated scattering (WSSUS) channel. By evaluating its autocorrelation function, the frequency correlation function can be determined by:

$$R(\Delta f) = \int_{-\infty}^{\infty} H(f)H^*(f + \Delta f)df, \tag{3.11}$$

where $H(f)$ represents the channel frequency response, Δf is the frequency shift and $[*]$ denotes the complex conjugate. For illustration, typical frequency correlation functions are sampled for four transmitter-receiver scenarios and depicted in Figure 3-8. It is observed that there is a rapid degradation of the FCF with respect to frequency separation. There is no definitive value of correlation that has been put forward for specification, but generally accepted coefficients are 0.5, 0.7, and 0.9. In this work we have considered the latter, which is more stringent and will further be referred to as $B_{0.9}$. Due to the frequency selective characteristics of PLC channels, the decrease of FCF with increasing frequency is non-monotonic. In Figure 3-8, the upper graph (up to just above 5 MHz) represents a good channel due to its high coherence bandwidth for a given RMS delay spread. The worst channel would be the lower-most graph as it exhibits the lowest coherence bandwidth for a given RMS delay spread throughout the frequency separation. A good channel can be assumed to have the least multipath contributions, hence it can be associated with a topology having fewer branches. The correlation coefficient was computed using the smallest frequency separation, 150 kHz in this work. The estimate of the coherence bandwidth is derived from the FCF graph. Figure 3-9 shows the scatter plot of the RMS delay spread against the coherence bandwidth $B_{0.9}$ for the measured PLC channels. An approximation of their relationship is also shown, and is determined to be:

$$B_{0.9}(kHz) = \frac{60}{\tau_{rms}(\mu s)} \tag{3.12}$$

The results show that RMS delay spread values less than 0.09 μs achieve a coherence bandwidth of at least 600 kHz. On the other hand, in the range 0.09 μs - 1.16 μs, the coherence bandwidth is between 80 kHz and 600 kHz. Thus, PLC channels with high RMS

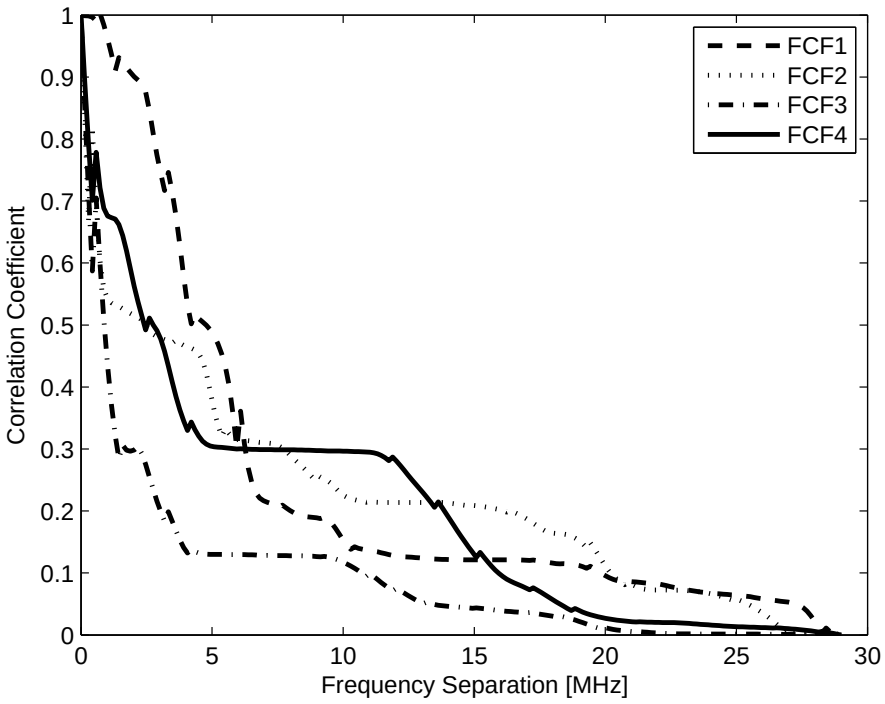

Figure 3-8: Frequency correlation function of four sample channels

delay spread are not desirable for data communication purposes. In terms of system design, desired values of τ_{rms} are those that result in high coherence bandwidth as this translates into faster symbol transmission rates [83]. The coherence bandwidth of the channel is particularly relevant to frequency-hopping spread spectrum (FHSS) scheme and multi-carrier schemes such as OFDM [84].

3.3 Deterministic Channel Modeling

The growing appeal for electrical power networks usage as data communication media necessitates a thorough study of this expansive infrastructure found in nearly each building. The ever growing demand for in-house broadband services in conjunction with dramatic increase in the number of digital radio communication systems within indoor environments has seen power line communication become a viable option for indoor broadband provision [85]. However, this interesting prospect of utilizing the electrical power network for data transmission poses regulatory and technical issues. The characteristics of electrical power networks, originally designed for energy distribution, are not favourable to data transmission due varying

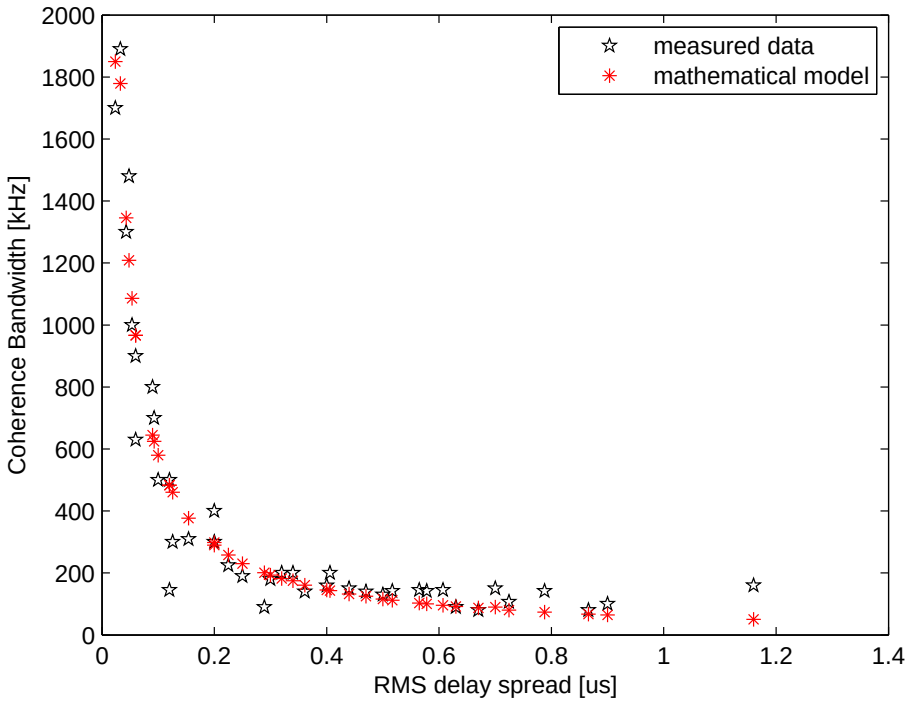

Figure 3-9: Coherence bandwidth relation to RMS delay spread

impedance, significant noise and high discrimination of high frequency signals [86]. Appropriate physical and link layers' techniques (e.g. modulation, channel access, and error correction) are required for building communication systems and it is through simulations that such techniques are determined. The PLC channel characteristics models are the primary inputs to these simulations and it is desirable to describe the channel with as few parameters as possible whilst conjointly realistic. It is common practice to describe a transmission line by its transfer characteristics with the parameters determined either by measurements or theoretical derivations [27,66,67,87–89]. These models are necessary for PLC system design and implementation. The objective of this section is to develop a simple deterministic model of a PLC channel with few parameters. The model is based on transmission line theory and basic resonance concepts of electrical circuits.

3.3.1 Powerline Cable Parameters

The cable parameters are evaluated for a three core symmetrical indoor wiring for high frequency signalling, befitting the assumption of a two-wire transmission [90]. With the

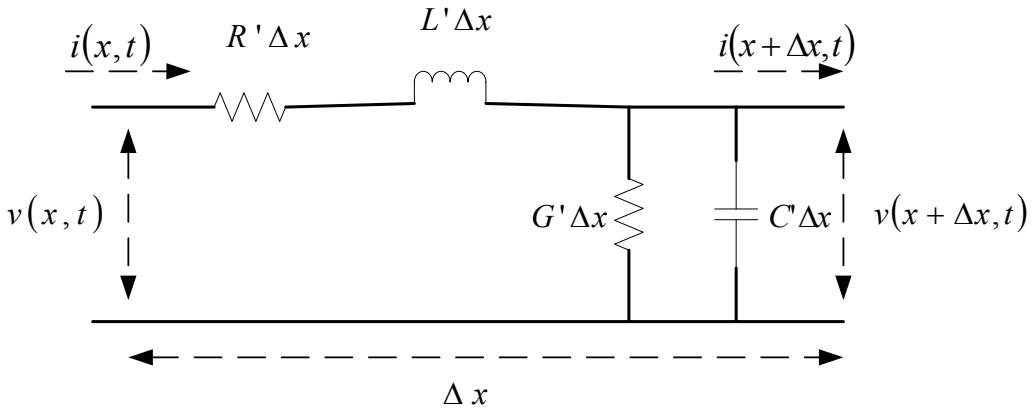

Figure 3-10: Transmission line equivalent circuit

transverse electromagnetic (TEM) wave consideration, the propagation mechanism is such that the magnetic and electric fields maintain orthogonality between them as well as to the direction of propagation [91]. A section of a transmission line represented by a differential length Δx can be described by distributed line parameters which can be derived through the analysis of electromagnetic propagation along a transmission line. These parameters, as shown in Figure 3-10, are influenced by the electrical characteristics and physical dimensions of the transmission line concerned. The per unit parameters are defined such that the series inductance L' describes the combined self-inductance of the two conductors, while the shunt capacitance C' arises as a result of the two conductors' propinquity. The finite conductivity of the conductors give rise to the resistance R' and G' represents the shunt conductance due to the dielectric loss of the material separating the two conductors [92].

The power line as a distributed parameter network can be viewed as cascade of such sections as shown in Figure 3-10 for a finite length of the line. The voltages and currents vary in magnitude and phase over the length of the line. By applying common propagation techniques, the propagation constant γ can be determined as [92]:

$$\gamma = \alpha + j\beta = \sqrt{(R' + j\omega L')(G' + j\omega C')}. \tag{3.13}$$

The characteristic impedance Z_0 can be defined as:

$$\begin{aligned} Z_0 &= \frac{R' + j\omega L'}{\gamma} \\ &= \sqrt{\frac{R' + j\omega L'}{G' + j\omega C'}}, \end{aligned} \tag{3.14}$$

where $\omega = 2\pi f$ is the angular frequency, α is the attenuation constant in Np/m and β is the phase constant in rad/m.

3.3.2 Determination of Propagation Parameters

The power line propagation parameters are determined through measurements for this work. A typical indoor power cable, Cu 3×2.5 mm^2 Cabtyre flexible PVC, of length 100 m is used as a test cable for this purpose. We measure the input impedance of the cable at one end under short and open circuit conditions at the other end. A well calibrated (one-port calibration) ZVL Rhode & Schwartz Vector network analyzer is used to take the measurements in the 1 - 30 MHz frequency range. The input impedance, Z_{in} of a terminated lossy transmission line of length l can be determined using transmission line theory. At the measurement port

$$Z_{\text{in}}(l=0) = \frac{V(-l)}{I(-l)} = Z_0 \left[\frac{Z_L + Z_0 \tanh(\gamma l)}{Z_0 + Z_L \tanh(\gamma l)}\right]. \tag{3.15}$$

For an open ended cable, the impedance is given by

$$Z_{oc} = Z_0 \coth(\gamma l) \tag{3.16}$$

and for a short circuit the impedance is expressed by

$$Z_{sc} = Z_0 \tanh(\gamma l). \tag{3.17}$$

The characteristic impedance and propagation constant can thus be calculated as follows:

$$Z_0 = \sqrt{Z_{oc} Z_{sc}} \tag{3.18}$$

and

$$\gamma = \frac{1}{l} \tanh^{-1}\left(\sqrt{\frac{Z_{sc}}{Z_{oc}}}\right). \tag{3.19}$$

The measured characteristic impedance and attenuation constant for the cable mentioned above are used as input parameters to the model. The mean value of the characteristic impedance, Z_0 is 80 Ω while the attenuation constant's variability with frequency is examined within 1- 30 MHz. The lossy power line cable causes an attenuation, $A(f, l)$ which increases with frequency and length and is given by [26]

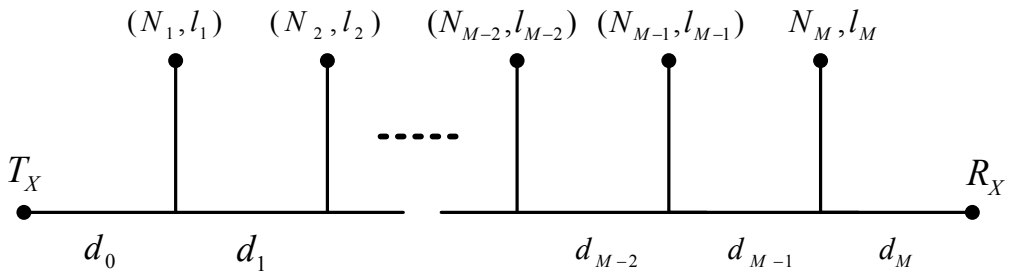

Figure 3-11: Multi-tapped transmission line topology

$$A(f, l) = e^{-\alpha(f)l} = e^{-(a_0 + a_1 f^K)l}. \tag{3.20}$$

The structure of (3.20) is derived from cable physical effects; however, the model parameters a_0 , a_1 and K cannot be easily determined from previously known cable parameters. The attenuation constant from (3.20) is given by

$$\alpha(f) = a_0 + a_1 f^K. \tag{3.21}$$

And in some cases, the value of K has been reported to be around unity, which makes the determination of the other parameters simple in the form of y-intercept and the slope of the linear relationship. This is certainly not the case here so other approaches are required. From the measured attenuation constant, a fit is generated using the Least Absolute Residual (LAR) robust method. The obtained attenuation parameters are $a_0 = -1.25 \times 10^{-3}\ m^{-1}$, $a_1 = 1.44 \times 10^{-6}$ s/m and $K = 0.589$.

3.3.3 Channel Model Description

A typical indoor electrical power network is heavily branched due the multiple power operated appliances found in homes and offices. As a multiple access network, an electrical power network has a bus topology because a common transmission line is accessed at numerous points along its length. Such a scenario is depicted in Figure 3-11. The branching elements are shown as $N_1, N_2, \ldots, N_m, N_{m+1}, \ldots, N_M$ with the inter-tap distances denoted by $d_1, d_2, \ldots, d_m, d_{m+1}, \ldots, d_{M-1}$.

In this approach, we consider the branching elements of a loaded transmission line as generalized parallel RLC circuits [93]. This approach reduces the computation complexity

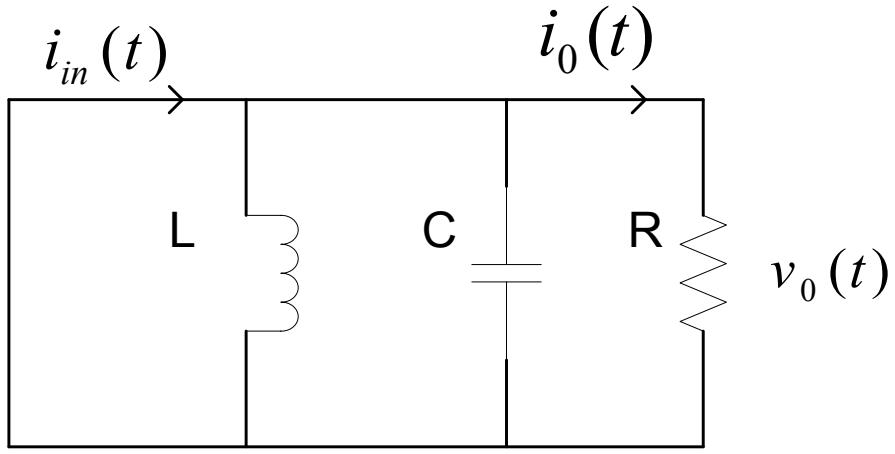

Figure 3-12: Current entering a branch

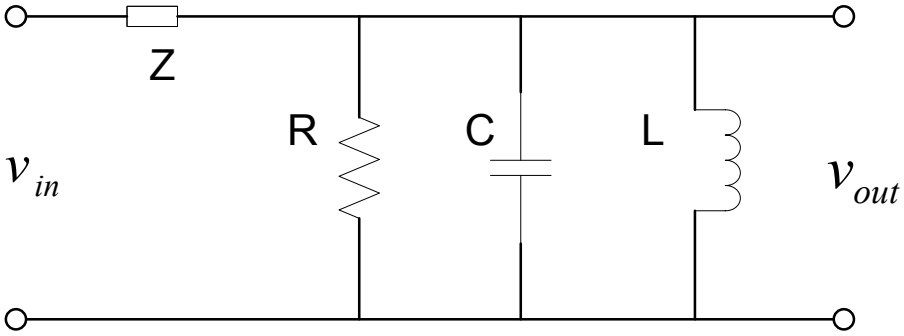

Figure 3-13: Equivalent voltage model at a branch

at the branching points, peculiar with numerical techniques. We consider a circuit of Figure 3-12 which consists of the R, L, and C components connected in parallel to represent a branch element. A current source, $i_{in}(t)$ supplies the circuit with current and $i_0(t)$ is the current through the resistor R. The voltage across the circuit is shown as $v_0(t)$ across the resistor R. The equivalent transmission section into a branch is depicted in Figure 3-13.

By applying Kirchhoff's current law to Figure 3-12, the input current can be represented as follows [94]:

$$i_{in}(t) = \frac{1}{L_p}\int_{-\infty}^{t} R_p i_o(t)dt + C_p\frac{d(R_p i_o(t))}{dt} + i_o(t). \tag{3.22}$$

If we assume that the circuit contains no prior energy stored in it, the Laplace transform of (3.22) result in

$$I_{in}(s) = \left(\frac{R_p}{sL_p} + sR_pC_p + 1\right) I_o s \tag{3.23}$$

and hence;

$$\frac{I_o(s)}{I_{in}(s)} = \frac{s\frac{L_p}{R_p}}{s^2L_pC_p + s\left(\frac{L_p}{R_p}\right) + 1}. \tag{3.24}$$

The impedance, Z_p, of the parallel resonant circuit of Figure 3-12 can be determined as follows:

$$Z_p = \frac{V_o(j\omega)}{I_{in}(j\omega)} = \frac{I_o(j\omega)R_p}{I_{in}(j\omega)} = \frac{j\omega L_p}{-\omega^2 L_pC_p + j\omega\left(\frac{L_p}{R_p}\right) + 1}. \tag{3.25}$$

3.3.3.1 Derivation of Model Parameters

A parallel type of resonance (anti-resonance) can be achieved using a short-circuited transmission line of length $\lambda/4$. The input impedance of the shorted line of length l is:

$$Z_{in} = Z_0\tanh(\alpha + j\beta)l = Z_0\frac{1 - j\tanh(\alpha l)\cot(\beta l)}{\tanh(\alpha l) - j\cot(\beta l)} \tag{3.26}$$

The input impedance of (3.26) can be simplified near resonance by letting $\omega = \omega_0 + \Delta\omega$ where $\Delta\omega$ is small and as a consequence,

$$\beta l = \frac{\omega_0 l}{v_p} + \frac{\Delta\omega l}{v_p} = \frac{\pi}{2} + \frac{\pi\Delta\omega}{2\omega_0}. \tag{3.27}$$

and

$$\cot(\beta l) = \cot\left(\frac{\pi}{2} + \frac{\pi\Delta\omega}{2\omega_0}\right) = -\tan\left(\frac{\pi\Delta\omega}{2\omega_0}\right) \approx -\frac{\pi\Delta\omega}{2\omega_0}. \tag{3.28}$$

It is also considered that for a low loss transmission line $\tanh(\alpha l) = \alpha l$, hence the input impedance can be represented as follows:

$$Z_{in} = Z_0\frac{1 + j\alpha l\pi\Delta\omega/2\omega_0}{\alpha l + j\pi\Delta\omega/2\omega_0} \approx \frac{Z_0}{\alpha l + \frac{j\pi\Delta\omega}{2\omega_0}}. \tag{3.29}$$

Since $\alpha l\pi\Delta\omega/2\omega_0 \ll 1$, this result is of the same form as the impedance of a parallel RLC circuit as derived in [92], see below:

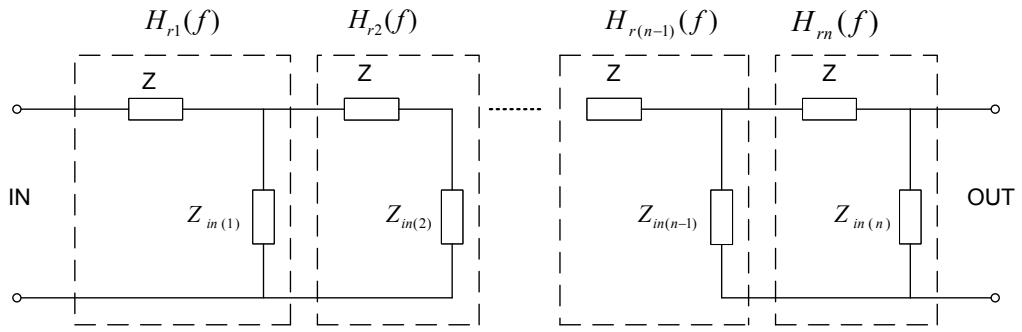

Figure 3-14: Powerline descriptive model

$$Z_{in} = \frac{1}{\left(\frac{1}{R}\right) + 2j\Delta\omega C}. \tag{3.30}$$

Then we can identify the resistance of the equivalent circuit as

$$R = \frac{Z_0}{\alpha l} \tag{3.31}$$

and the capacitance of the equivalent circuit as

$$C = \frac{\pi}{4\omega_0 Z_0}. \tag{3.32}$$

The inductance of the equivalent circuit can be expressed by

$$L = \frac{1}{\omega_0^2 C}. \tag{3.33}$$

3.3.3.2 Model Description

The multi-tapped power line is described by cascaded discrete line components as shown in Figure 3-14. Each block is defined by its own transfer function $H_{r1}(f), H_{r2}(f), \ldots, H_{r(n-1)}(f)$, $H_{rn}(f), H_{r(n+1)}(f), \ldots, H_{(r(N-1)}(f), H_{rN}(f)$. The components of these transfer functions are a parallel combination of $Z_{in(n)}$ and Z which are the frequency dependent branch impedance and main section impedance respectively.

The resultant Z_{in} at every branching point is given by (3.25). For a given branch length l, the circuit experiences multiple resonances in the frequency domain, bounded at 30 MHz in our consideration. Due to the different lengths of the branches, individual parallel resonant sections will have different resonant frequencies, f_0 in the frequency domain. The electrical

length of a cable can be expressed in terms of the wavelength, λ, which has a relationship with the propagation velocity v_p and the operating frequency f given by $\lambda = v_p/f$ [95]. It has been found in numerous literature [96, 97] that the notches in the frequency response can be viewed as resonant points in the frequency domain. We simply then view the overall transfer function as resultant from a cascade of several resonant circuits. For a branch terminated with an open circuit, the first resonance (notch) occurs at $f_0 = v_p/4l$ [96], with the subsequent notches occurring at frequencies defined by:

$$f_{ok} = \frac{v_p}{4l}(2k+1), \qquad k = 1, 2, \ldots \tag{3.34}$$

However, for a branch terminated with a short circuit, the first resonance point is at $f = 0$ with subsequent resonance points given by:

$$f_{sk} = \frac{v_p}{4l}(2k), \qquad k = 1, 2, \ldots \tag{3.35}$$

The transfer function H_{rn} of the individual resonant blocks can be determined by:

$$H_{rn}(f) = \frac{Z}{Z_{pn}(f) + Z}. \tag{3.36}$$

The resulting transfer function is then given by

$$H_r(f) = \prod_{r=1}^{N} H_{rn}(f), \tag{3.37}$$

where N is the total number of resonant points within a given frequency range for a given branch length. For network topologies having more than one branches, the resultant transfer function is calculated as a cascade of de-coupled resonant circuits, thus we calculate the $H(f)$ as

$$H(f) = \prod_{r=1}^{M} H_r(f), \tag{3.38}$$

where M is the total number of branches in the network.

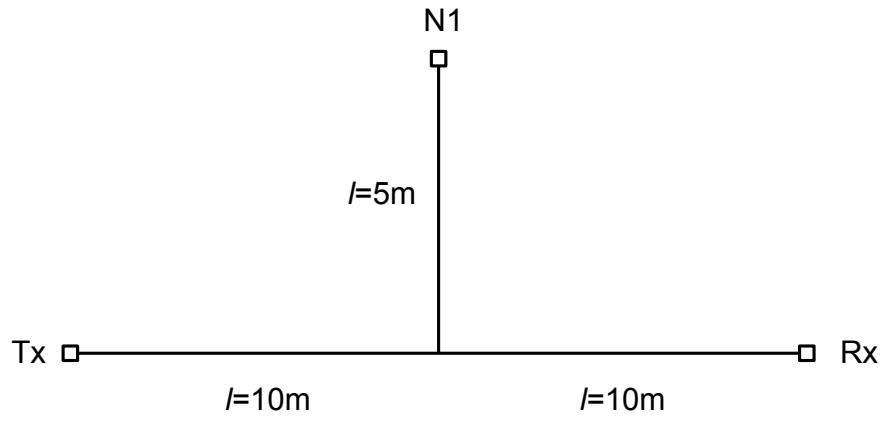

Figure 3-15: Single branch electrical power network

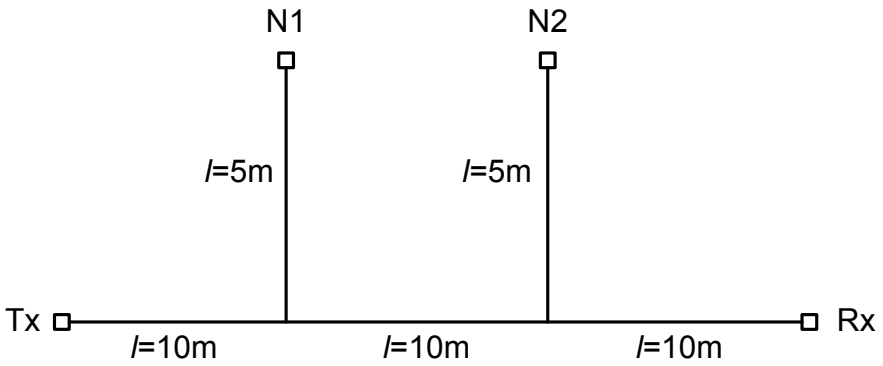

Figure 3-16: Two-branch electrical power network

3.3.4 Simulation Results

The validity of the model was evaluated by taking measurements from a power line cable of known dimensions using the ZVL Rhode & Schwartz network analyzer with full two-port calibration. The test networks, as shown in Figure 3-15, 3-16 and 3-17, were open circuited at the unused branch terminals and with the knowledge of the branch lengths, characteristic impedance and attenuation constant the transfer function estimate was determined. The measured and estimated transfer responses of the topologies of Figure 3-15, 3-16 and 3-17 are shown in Figure 3-18, 3-19 and 3-20 respectively. In the three cases, we observe a deep notch at $f \approx 7$ MHz which is due to the first two branches having the same length. Branches of the same length will cause resonance at the same frequencies, but will aggravate the notch depth at those frequencies. The same behaviour is observed at $f \approx 23$ MHz.

For simple electrical power networks (i.e. single and two-branch networks in this work),

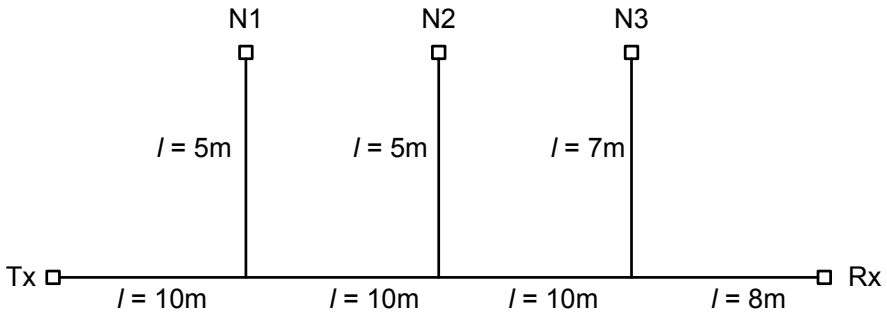

Figure 3-17: Three-branch electrical power network

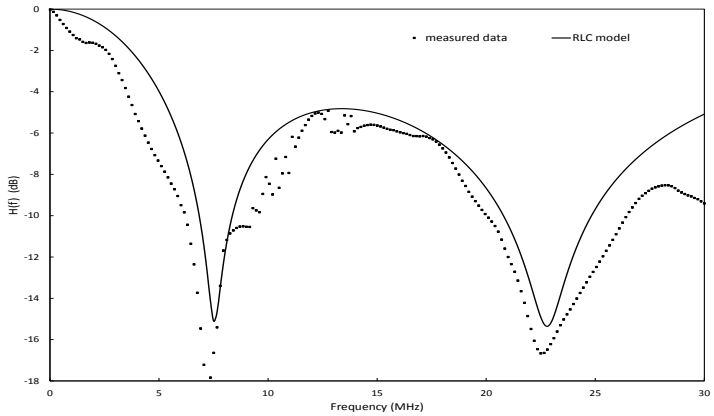

Figure 3-18: Measured and estimated magnitude of CFR of a single-branch electrical power network

the model performs better than with the more complex three-branch network. This is evident in Figure 3-20 in the frequency range from 10 MHz to 20 MHz. This is more likely a result of the increased distance traversed by the signal between the branches, which is not taken into account in the model development and implementation. The accuracy is likely to deteriorate as the number of branches increase and its spread may differ within the band of interest.

Data communication systems' performance through the electrical power grid as a transmission media, as it is with any other media, relies heavily on the availability of reasonably accurate channel models [24]. The deterministic model presented here is simple and requires very few parameters to estimate the channel transfer function. Due to the unpredictable nature of the load profile, this model is developed by considering the open/short circuited branches which presents the worst case loading scenario. From Figure 3-18 through 3-20, the ability of the model to track the deep fades across the frequency band is evident. These

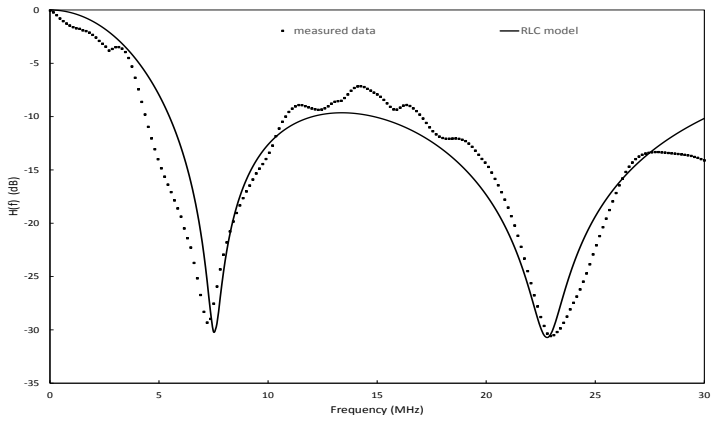

Figure 3-19: Measured and estimated magnitude of CFR of a two-branch electrical power network

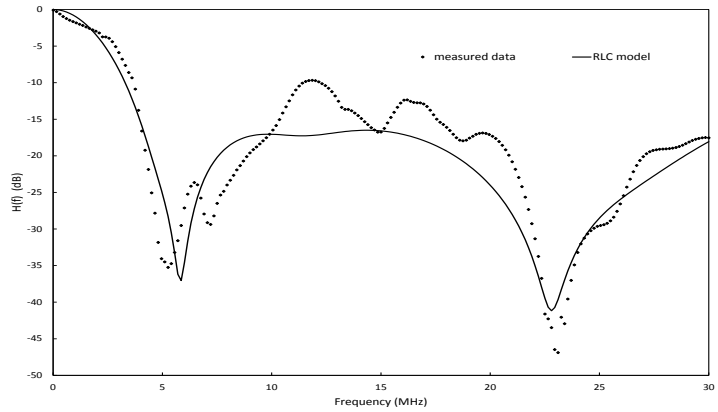

Figure 3-20: Measured and estimated magnitude of CFR of a three-branch electrical power network

deep fades are responsible for signal degradation in a communication channel, hence they cannot be under-estimated or simply ignored.

3.4 Summary and Conclusions

In this chapter, we have taken two approaches towards modeling PLC channels. Firstly, a multipath model is developed for real electrical power networks of unknown characteristics or architecture. Secondly, a deterministic approach is adopted to model known electrical power grid topologies through a built testbed. we have modelled the complex frequency response of real-world PLC channels using multipath signal propagation technique in the frequency

range 1-30 MHz. The applicability of the model to large networks with unknown parameters is demonstrated with good agreement between simulation and measurement results as shown in Figure 3-4. The motivation for this approach derives from the desire to utilize existing indoor electrical power networks to establish high speed communication links. In most cases the topology of the network is not readily available; hence we sought for solutions that require little knowledge about the network. To compare different multipath channels in the quest to develop some general guidelines for PLC systems, parameters which grossly quantify the multipath channel have been used. These are in the form of maximum excess delay τ_m, mean excess delay τ_e, and RMS delay spread τ_{rms}. It has been found that typical values of RMS delay spread are in the order of μs in practical PLC channels, comparable to outdoor mobile radio channels. The RMS delay spread provides a good indication of the multipath spread. In digital communications, the RMS delay spread in comparison with the symbol duration gives an indication as to whether the channel requires equalization to avoid inter-symbol interference (ISI) or not. This is popular in OFDM and CDMA communication systems. The most significant contribution to larger RMS delay spread is due to strong signal reflections with long delays. This work includes the statistics of time delay parameters as well as coherence bandwidth and its relation to RMS delay spread in the frequency range up to 30 MHz. It is observed that the inverse relationship between coherence bandwidth and RMS delay spread as given by (3.12). Utilizing the results presented in Figure 3-9 and Figure 3-6(d), it is possible to determine statistically, the probability of encountering a flat channel for a specified coherence bandwidth. For example, for a coherence bandwidth of 200 kHz or more, suitable channels are those with an RMS delay spread less or equal to approximately 0.2 μs. For this specification, according to Fig. 10, about 50% of the measured channels may not require equalization. 80% of the measured channels exhibit estimated values of coherence bandwidth between 600 kHz and 90 kHz. The 90th percentile of the RMS delay spread is found to be between 0.04 μs and 0.55 μs with a mean of 0.287 μs and standard deviation of 0.222 μs. Comparatively, the relationship between coherence bandwidth and RMS delay spread as shown by (3.12) is very close to that obtained by [74]. Though this result is expected to differ from site to site, with more measurement campaigns, this relationship could be established without loss of generality and possibly arrive at a unified representation. The comparisons in Table 3.3 also show closeness in terms of bounds for other time delay parameters for indoor PLC channels.

In the deterministic approach, basic transmission line parameters are determined to derive the transfer characteristic to model the PLC channel. The propagation parameters required to build the model are obtained from measurements of typical indoor electrical power network. Though deterministic approaches remain topology dependent, for a given topology, only the cable propagation parameters and load impedances are required. The low voltage (LV) power line network is regarded as a cascade of several parallel resonant circuits. The notch position clearly depend on the length of the branching elements and their depth increases with increasing branch number. The proposed model is used to analyze three scenarios of network topology. Though there are some noticeable differences in the frequency range, the model captures the notch positions and depths satisfactorily. Compared to the approach by Phillips [27], which requires knowledge of the transfer characteristics, this model only relies on the knowledge of the topology. The model can be improved by taking into consideration the inter-branch lengths.

CHAPTER 4

Channel Modeling for High Speed Indoor PowerLine Communication Systems: The Lattice Approach

4.1 Introduction

The transmission of data signals through electrical power networks plays an important role in contributing towards global goals for broadband services inside the home and office. In this chapter the aim is to contribute to this ideal by presenting a PLC channel modeling approach which describes a electrical power network as a lattice structure. In a lattice structure, a signal propagates from one end into a network of boundaries (branches) through numerous paths characterized by different reflection/transmission properties. Due to theoretically infinite number of reflections likely to be experienced by a propagating wave, the optimum number of paths required for meaningful contribution towards the overall signal level at the receiver is determined. The propagation parameters are obtained through measurements and other model parameters are derived from deterministic electrical power networks. It is observed that the notch positions in the frequency response are associated with the branch lengths in the electrical power network. Short branches will result in fewer notches in a fixed bandwidth as compared to longer branches. Generally, the channel attenuation increases with the electrical power network size in terms of number of branches. The proposed model compares well with experimental data.

Recently, due to the advances in computing and data communication, it is apparent that technological advances and demand of information technology will continue to rise [98]. Furthermore, this rapid increase is accompanied by the declining cost of data communications as a result of both technological improvements and increased competition. With the advent of technology and continued demand for multimedia services, human dependency on power and data communications has reached new heights. Numerous efforts are in place to progressively enhance and expand the efficiency in both sectors. Accompanied by the deregulation of the telecommunication and electricity markets, provision of innovative solutions by new operators is born [99]. In data communications, applications such as broadband

internet, smart grid etc, require easy installation procedures at minimum cost to attract new customers. Due to the universal existence of the electrical power network, PLC is a viable option for the provision of numerous indoor broadband services [100].

PLC is a technology where high frequency signals are transmitted over power lines originally designed to carry the normal 50/60 Hz power signal. PLC thus has the obvious advantage due to its expansive network (reduced infrastructural costs) over conventional communication media such as coaxial and fibre optic cables. However, there are major inherent peculiarities in this channel which influences broadband transmission over the PLC network. The powerline network is designed optimally to deliver power as opposed to data. The significant difference in terms of structure and physical characteristics generally presents a harsh environment for the low-power high frequency signals. Since the quality of the transmission is largely dependent on the characteristics of the channel, developing accurate PLC channel models is of fundamental importance. The topology of a PLC channel is such that there exist other terminal connections between the transmitting and receiving ends of a communication link. These terminals are in the form of loaded branches. In principle, the attenuation increases with increasing distance, but there is no simple correlation [75]. The principal factors that influence channel attenuation are the network topology, cable characteristics as well as the loading profile at the terminals. The channel frequency response shows that even short distance links exhibit deep narrowband fades having attenuation which can be higher than that experienced by longer distance links.

These deep fades are a result of reflection and multipath propagation. Several techniques have been proposed to model a PLC channel. It is common practice to consider a power line channel as a "black box" and describe its transfer function [87], [27]. The most significant disadvantage of this approach is that a large number of measurements are required to estimate the model parameters. The process of parameter estimation requires application of complex fitting algorithms in order to determine the model that fits the measurements adequately. Global extensive channel measurements may be required to develop a generalized model. Different approaches are then employed to determine the system parameters, either through experimental data and measurements or deriving them theoretically [88], [67]. Other approaches consider the PLC channel as a multipath environment due to signal reflections at branching points and connected loads [27], [26, 28, 30, 65, 66, 97, 101–104]. The accuracy of the model generally relies on the proper selection of the parameters of the signal

propagation properties [65]. The multipath model is a subset of top-down strategies, which tends to have a high computational cost in determining the dominant paths and the corresponding parameters. The complexity grows with increasing number of dominant paths. This process is inherently computational intensive due to the large number of dominant paths in indoor environments, owing to the low attenuation resultant from generally short path lengths. Moreover, top-down approaches lack the physical connection with reality, thus they do not describe signal propagation in the electrical power network. Transmission line theory based models are also common [25, 31, 70, 71, 77, 96, 105–111], which describe the PLC channel as a series of cascaded two-port networks and can thus be adapted to different network topologies using popular transmission matrices [65]. Though this approach has a direct relationship with signal propagation in the network, determination of such matrices is usually not straightforward and the difficulty grows with the size of the given electrical power network. The other drawback is that this approach cannot simply be extended for application in networks with interconnected cables having different number of conductors.

In this chapter, a deterministic PLC channel model based on the lattice structure is presented [112]. This approach is a bottom-up strategy which describes wave propagation in an electrical power network by utilizing transmission and reflection coefficients. Thus, it has a direct relationship with signal propagation in an electrical power network. Therefore, it can flexibly be extended to different electrical power networks of different structures. Additionally, this approach addresses the physics of electrical power networks since its derivation is based on the physical interpretation of electromagnetic wave propagation in transmission line networks. We consider the branches in the electrical power network as consolidated point loads and use transmission line theory to describe their input impedance. We derive an analytical expression of the channel frequency response that captures the reflection/transmission profile of a signal propagating through an electrical power network. As a graphical tool, all signals are seamlessly traced and the total signal level at any point in the electrical power network is the superposition of all the waves arriving at that point. The history of any signal is easily traceable and its composition identifiable. Due to possible infinite paths presented to a propagating signal as it travels towards the receiver, we derive an expression that represents only the dominant paths. This is usually a complex exercise in other methods, leading to some researchers simply assuming what they perceive as a reasonable number. The lattice approach simplifies its determination and the developed expression is

well suited to all networks with no further complexity introduced regardless of the network size or complexity. A comparison is then made between this model, experimental data and other deterministic models.

4.2 Channel Description

Typically, an indoor electrical power network consists of several branches required to supply power to the household appliances and office equipment. The structure of aa electrical power network is analogous to that of a bus topology with multiple access ports between the transmitter and the receiver. Such a topology is as shown in Figure 4-1 with branching elements $b_{r1}, b_{r2}, b_{r3}, \ldots, b_{r(N-2)}, b_{r(N-1)}, b_{rN}$ and the inter-branch distance denoted by $d_1, d_2, d_3, \ldots, d_{N-2}, d_{N-1}$. The receiver could be placed at any of the available open terminals in the network for access to the information transmitted. The branching elements present impedance discontinuities as the signal propagates from the transmitter (T_X) to the receiver (R_X). The signal encounters further discontinuities due to the numerous loads connected at the branching ends in the network. Such unpredictable change in the electrical power network impedance makes it difficult to trace the channel state, primarily because appliances are continuously plugged in and out of the network at random by the users. Some appliances also bears varying impedance states depending on their mode of operation even over a sustained connection. Other powerline topologies exist varying from country to country as well as different indoor wiring practices. The topology shown in Figure 4-1, commonly known as the T-topology, is the most popular and thus provide the basis of this work.

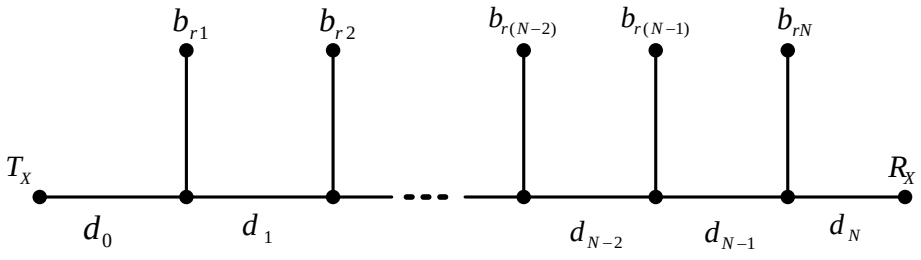

Figure 4-1: Typical multi-access powerline topology

4.3 The Lattice Approach

The electrical power network, as discussed above, presents numerous reflection boundaries. At a branching point, the superposition of all the forward and backward travelling signals forms a lattice. As the injected voltage from the source travels back and forth in the network, its behaviour is captured by a bouncing diagram as shown in Figure 4-2. A bouncing diagram is a convenient representation of signal propagation within a branched PLC network. The powerline network is decomposed into N dissimilar segments (branches), each having an impedance of $Z_{in}(n)$, $(n = 1, 2, 3, \ldots, N)$. Thus there exist $(N - 1)$ discontinuities in the path of a voltage waveform travelling from the source to a receiver placed at the nth branch. The initial voltage signal reaches a branching element which sets up a reflected wave. The reflected wave propagates back to the source, which in turn gives rise to another reflection and so on, with this process continuing indefinitely. It should be noted here that, in terms of reflections, a source may not always refer to the transmitting terminal. Branching nodes prior to the subsequent ones may also be regarded as their source as they become the feeder nodes.

As the signal propagates from the source to the destination, it experiences reflections and transmissions at the branching nodes. The signal is analyzed as it reaches the branching nodes and properly apply the boundary conditions at each junction. By defining basic lattices at the branching nodes, as shown in Figure 4-2, it is possible to track all the signal replicas and numerically determine the voltage level at each branching node. Similar ap-

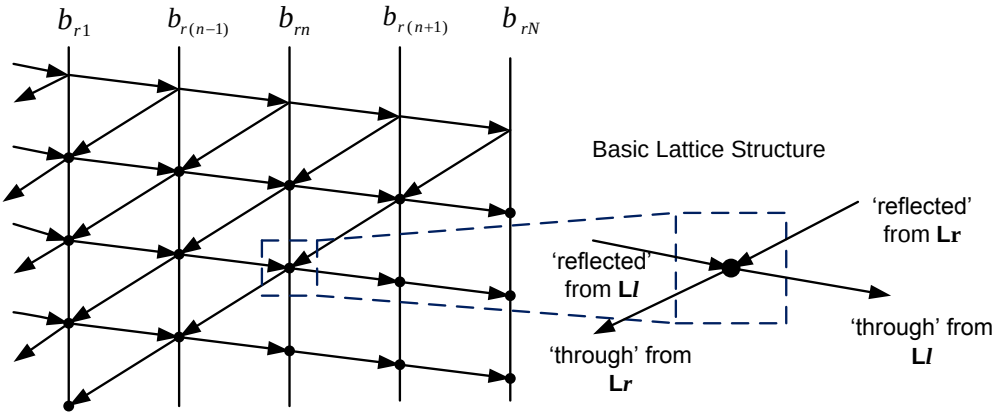

Figure 4-2: A Basic Lattice Structure

proaches in similar areas have been used in [113] and [114]. At each branching node, there are $(N+1)$ lattices, where N is the total number of branches in a network. Figure 4-2 shows how a typical lattice is derived from a bouncing diagram of an electrical power network of size N. In the same figure we also show how signal replicas combine at a lattice. At a branching node there are signal replicas that reach a node after being reflected from the left lattice (L_l), reflected from the right lattice (L_r), pass through from the right lattice (L_r), and through from the left lattice (L_l). Thus the total voltage level at a branching node is given by $\sum_{i=1}^{N+1} V_{L_i}$. This is simply the overall voltage sum of individual lattice voltages at a node.

4.4 Model Formulation

The electrical power network is modeled as a lattice structure with numerous reflection points (at the lattices) in the path of a propagating signal. Over a period of time, there are infinitely many reflection/transmission combinations that take place before a signal reaches the receiving end. The lattice representation, through a bouncing diagram, allows us to trace all possible paths traversed by the signal en route to the receiving terminal. While part of the signal reaches the receiver through a direct path, other replicas of the original signal branch off the main path, effectively arriving at the receiver at a later stage. PLC channels can thus be regarded as a multipath environment. Such numerous paths can be seen on the bouncing diagram shown in Figure A-1 in the appendix. The lattice diagram illustrates a voltage travelling back and forth between a pair of branches as well as being transmitted through to the next branch progressively towards the receiving end. Effectively, the portion of the signal that reaches the receiver has encountered several reflection/transmission combinations and travelled a certain distance, l_p, where p is the pth path concerned. It is also notable that signal replicas that travel a considerably long distance before reaching the receiver will have insignificant contribution to the signal level at the receiver. These replicas are not considered in the solution. The attenuation of a signal propagating along a transmission line is dependent on the length of the path as follows [26]:

$$A(f,l) = e^{-\alpha(f)l} = e^{-(a_0+a_1 f^k)l}, \tag{4.1}$$

where $\alpha(f) = (a_0 + a_1 f^K)$ is the frequency dependent attenuation constant and l is the

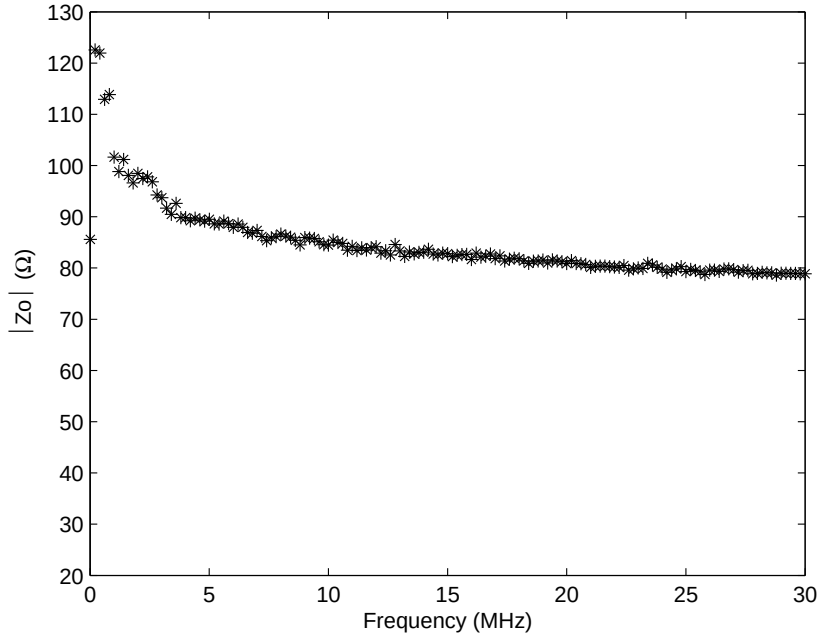

(a) Characteristic Impedance

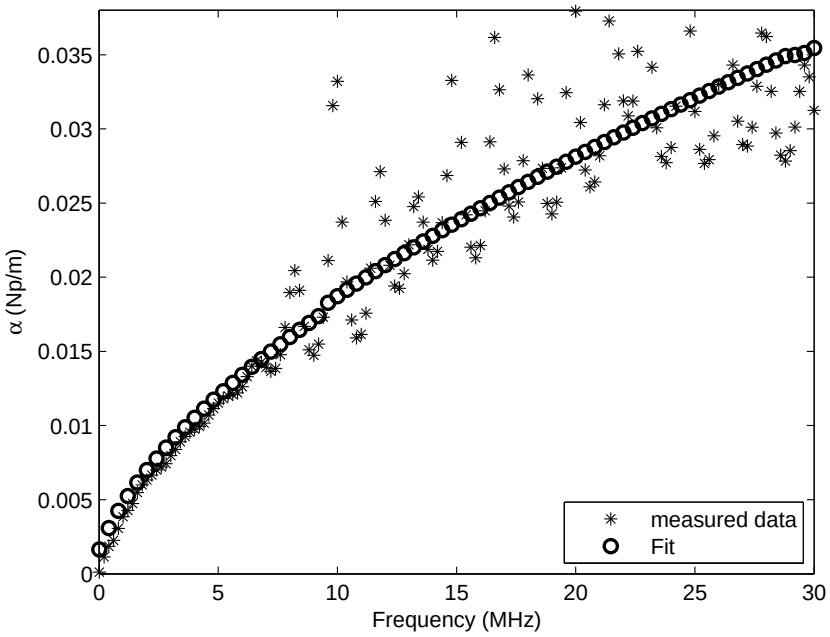

(b) Attenuation Constant

Figure 4-3: Cabtyre Flexible PVC Copper (Cu) Cable Parameters: (a) Characteristic Impedance Magnitude and (b) Attenuation Constant

path length. Variables a_0, a_1 and K are determined from measurements through a Least-Absolute Residual (LAR) robust analysis of the attenuation constant. The mismatches encountered by the wave front as it travels on the line at every junction results in reflection and transmission factors. In this context, a junction is defined as an impedance discontinuity along a transmission line. The impedance discontinuity may arise due to a section of a transmission line having a different characteristic impedance, a terminating load or the input impedance to other circuit elements. In this work, branches are represented with their input impedances and considered as consolidated loads to the main line. It should be noticed that the branches are parallel to the main line hence the definition of the junction reflection and transmission factors as follows [115]:

$$r = \frac{(Z_L \parallel Z_0) - Z_0}{(Z_L \parallel Z_0) + Z_0} = \frac{-Z_0}{2Z_L + Z_0}, \tag{4.2}$$

and

$$T = 1 + r, \tag{4.3}$$

where Z_0 is the characteristic impedance of the main line, r and T are the reflection and transmission factors at the junctions respectively. The operator ($\parallel$) indicates a parallel operation while Z_L is the input impedance of the branching element. A loaded branch is considered as a consolidated point load and apply transmission line theory to determine its impedance. In other words, we sought to find the input impedance at the junction due to the branch and the load that might be connected at its end. The junction impedance can thus be calculated as follows [116]:

$$Z_L(l) = Z_{in}(l) = Z_0 \left(\frac{Z_t + Z_0 \tanh(\gamma \cdot l)}{Z_0 + Z_t \tanh(\gamma \cdot l)} \right), \tag{4.4}$$

where Z_t is the load impedance that terminates the branch line and $\gamma = \alpha + j\beta$ is the propagation constant. The propagation parameters of the powerline are obtained from measurements. Typical indoor cables used by the local utility are of three-wire copper (Cu) 2.5 mm^2 Cabtyre flexible PVC type. Other cable diameters are also available in 1.5 mm^2 and 4 mm^2. The characteristic impedance Z_0 and the attenuation constant $\alpha(f)$ are determined as described in [109]. These parameters are examined in the frequency range 1 - 30 MHz as shown in Figure 4-3.

For the purpose of illustration, Figure A-1 in appendix shows an electrical power network representation with four branches and a sending end of voltage V_s. The lattice diagram obviously does not show all the possible reflection/transmission scenarios but rather depicts how these factors are formulated to determine voltage levels at every branching point. In our method, a homogeneous electrical power network is considered as this is consistent with many indoor wiring practices, thus the characteristic impedance of the main line is the same as that of the branches and does not vary between branches. The distance between the branches may vary depending on the network design. Secondly, since it is of minimum benefit to consider all the infinite (theoretical) paths, we only consider first order reflections [115] as the associated signals are likely to reach the receiver with meaningful energy according to (4.1). Therefore, another restriction is placed on the number of branches between which the signal ought to bounce for consideration. Signals which bounce off too many branches take a long time to reach the receiver, so we have limited this number to two. This is peculiar with large networks with many branches. As a matter of fact, a signal that bounces off too many branches might even take a longer time to reach the receiver as compared to a particular second order reflection signal. With these conditions set forth, the process of tracing a voltage signal propagating from the source to the rest of the network is carried out. There are propagation paths with similar characteristics in terms of their reflection profile, so these are grouped together and a general model developed thereof. Four groups of such paths as shown in Figure 4-4 have been identified and defined as follows:

- **TYPE (1)**: Direct paths: these paths exhibit no reflection as the signal travels towards the receiver.
- **TYPE (2)**: Single-reflection paths: these paths lead to the receiver after just one reflection. They are generally backward traveling replicas reflected by branches succeeding the receiving node.
- **TYPE (3)**: Double-reflection paths: these signal replicas will reach the receiver after bouncing off two branches. The said branches could be the receiving node itself, leading or lagging branches.
- **TYPE (4)**: Source-branch reflection paths: these paths will reach the receiver after bouncing off any one branch and off the sending end.

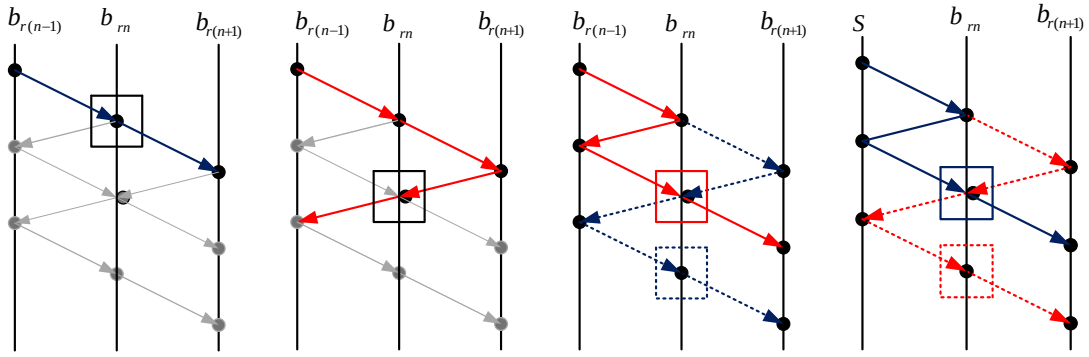

(a) TYPE (1) (b) TYPE (2) (c) TYPE (3) (d) TYPE (4)

Figure 4-4: Path Types Observed at a Lattice: (a) Type (1), (b) Type (2), (c) Type (3), and (d) Type (4)

The expected voltage level at a receiver placed at any of the branching elements is then determined. For clarity of solution formulation, we will follow the four types mentioned above in the derivation process. Each of the characteristic path will consistently be denoted with superscripts (1) to (4) to describe its reflection path profile. A single vector $\mathbf{S_n}$ containing transmission factors is defined such that [112]:

$$S_n = T_1T_2T_3...T_{n-1}T_n = \prod_{i=0}^{n} T_i \mid T_0 = 1, \tag{4.5}$$

where n is the branch number. The operator (|) denotes "whereby", providing a condition for the variable. The size of $\mathbf{S_n}$ depends on the size of the electrical power network. The voltage at a branching point due to reflection/transmissions is also defined in the following manner:

$$V_{br,n}^{(k)}(\gamma) = V_s(\gamma) \times \Psi_{br,n}^{(k)}, \tag{4.6}$$

where n, V_s, and $k \in [1, 2, 3, 4]$ are branch number, source voltage, and path type, respectively. $\Psi_{br,n}^{(k)}$ represents all the reflection/transmissions at a branch as shown in the appendix. The direct path voltage expected at the four ($n = 1, 2, 3, 4$) branches depicted in Figure A-1 can be determined as follows [112]:

$$V_{br,1}^{(1)}(\gamma) = V_s(\gamma)T_1, \tag{4.7a}$$

$$V_{br,2}^{(1)}(\gamma) = V_s(\gamma)T_1T_2, \tag{4.7b}$$

$$V_{br,3}^{(1)}(\gamma) = V_s(\gamma)T_1T_2T_3, \tag{4.7c}$$

$$V_{br,4}^{(1)}(\gamma) = V_s(\gamma)T_1T_2T_3T_4, \tag{4.7d}$$

and hence a general expression describing these voltages at any branch number n in a network containing N branches is as follows:

$$V_{br,n}^{(1)}(\gamma) = V_s(\gamma)\prod_{i=1}^{n} T_i. \tag{4.8}$$

The second group of voltage replicas reaching the first four branches within a powerline network of size $N = 5$ can be determined through the following set of equations [112]:

$$V_{br,1}^{(2)}(\gamma) = V_s(\gamma)\left\{T_1^2\left[r_2 + r_3T_2^2 + r_4T_2^2T_3^2T_4^2\right]\right\} \tag{4.9a}$$

$$V_{br,2}^{(2)}(\gamma) = V_s(\gamma)\left\{T_1T_2^2\left[r_3 + r_4T_3^2 + r_5T_3^2T_4^2\right]\right\} \tag{4.9b}$$

$$V_{br,3}^{(2)}(\gamma) = V_s(\gamma)\left\{T_1T_2T_3^2\left[r_4 + r_5T_4^2\right]\right\} \tag{4.9c}$$

$$V_{br,4}^{(2)}(\gamma) = V_s(\gamma)\left\{T_1T_2T_3T_4^2[r_5]\right\}. \tag{4.9d}$$

The general expression for these group of replica voltages at any branch number n in a given powerline network of N total branches is given by [112]:

$$V_{br,n}^{(2)}(\gamma) = V_s(\gamma)T_n\prod_{i=1}^{n} T_i\left[\sum_{j=n+1}^{N} r_j\left(\frac{S_{j-1}}{S_n}\right)^2\right]. \tag{4.10}$$

Considering the third group of voltage replicas, it is noticeable that these does not exist at the first branch. A receiver at this node will not record any TYPE (3) voltage replicas. Signals resultant from reflections between any two branches will not cross the first branch even if one such reflection takes place at the first branch itself. These kinds of reflections will only have a contribution at the branches subsequent to the first. The first four branches have such replicas determined by the following expressions [112]:

$$V_{br,1}^{(3)}(\gamma) = 0 \tag{4.11a}$$

$$\begin{aligned} V_{br,2}^{(3)}(\gamma) = V_s(\gamma) \{ & T_1 T_2 \left[r_1 r_2 + r_1 r_3 T_2^2 \right. \\ & \left. + r_1 r_4 T_2^2 T_3^2 + r_1 r_5 T_2^2 T_3^2 T_4^2 \right] \} \end{aligned} \tag{4.11b}$$

$$\begin{aligned} V_{br,3}^{(3)}(\gamma) = V_s(\gamma) \{ & T_1 T_2 T_3 \left[r_1 r_2 + r_2 r_3 \right. \\ & + r_1 r_3 T_2^2 + r_2 r_4 T_3^2 + r_1 r_4 T_2^2 T_3^2 \\ & \left. + r_2 r_5 T_3^2 T_4^2 + r_1 r_5 T_2^2 T_3^2 T_4^2 \right] \} \end{aligned} \tag{4.11c}$$

$$\begin{aligned} V_{br,4}^{(3)}(\gamma) = V_s(\gamma) \{ & T_1 T_2 T_3 T_4 \left[r_1 r_2 + r_2 r_3 \right. \\ & + r_3 r_4 + r_1 r_3 T_2^2 + r_2 r_4 T_3^2 + r_1 r_4 T_2^2 T_3^2 \\ & \left. + r_3 r_5 T_4^2 + r_2 r_5 T_3^2 T_4^2 + r_1 r_5 T_2^2 T_3^2 T_4^2 \right] \} . \end{aligned} \tag{4.11d}$$

Extending the above derivation to a general case, the contribution of such replicas at an arbitrary branch number n within a network of size N, it is determined that [112]:

$$V_{br,n}^{(3)}(\gamma) = V_s(\gamma) \prod_{i=1}^{n} T_i \left[\sum_{k=1}^{N-1} \sum_{i=1}^{n-1} \prod_{j=0}^{1} r_{i+jk} \left(\frac{S_{i+k+1}}{S_i} \right) \right] . \tag{4.12}$$

The final group of replicas with meaningful contribution at an arbitrarily placed receiver are of TYPE (4), those which are reflected off a branch element and the source. Such signals can be determined as shown in 4.13(a) through 4.13(d) [112] by using

$$\begin{aligned} V_{br,1}^{(4)}(\gamma) = V_s(\gamma) \{ & r_s T_1 \left[r_1 + r_2 T_1^2 \right. \\ & \left. + r_3 T_1^2 T_2^2 + r_4 T_1^2 T_2^2 T_3^2 + r_5 T_1^2 T_2^2 T_3^2 T_4^2 \right] \} \end{aligned} \tag{4.13a}$$

$$\begin{aligned} V_{br,2}^{(4)}(\gamma) = V_s(\gamma) \{ & r_s T_1 T_2 \left[r_1 + r_2 T_1^2 \right. \\ & \left. + r_3 T_1^2 T_2^2 + r_4 T_1^2 T_2^2 T_3^2 + r_5 T_1^2 T_2^2 T_3^2 T_4^2 \right] \} \end{aligned} \tag{4.13b}$$

$$\begin{aligned} V_{br,3}^{(4)}(\gamma) = V_s(\gamma) \{ & r_s T_1 T_2 T_3 \left[r_1 + r_2 T_1^2 \right. \\ & \left. + r_3 T_1^2 T_2^2 + r_4 T_1^2 T_2^2 T_3^2 + r_5 T_1^2 T_2^2 T_3^2 T_4^2 \right] \} \end{aligned} \tag{4.13c}$$

$$\begin{aligned} V_{br,4}^{(4)}(\gamma) = V_s(\gamma) \{ & r_s T_1 T_2 T_3 T_4 \left[r_1 + r_2 T_1^2 \right. \\ & \left. + r_3 T_1^2 T_2^2 + r_4 T_1^2 T_2^2 T_3^2 + r_5 T_1^2 T_2^2 T_3^2 T_4^2 \right] \} , \end{aligned} \tag{4.13d}$$

and in general [112];

$$V_{br,n}^{(4)}(\gamma) = V_s(\gamma) r_s \prod_{i=1}^{n} T_i \sum_{j=1}^{N} r_j \left(S_{j-1}\right)^2 . \tag{4.14}$$

The resultant received signal level at a receiver placed at branch number n in a network is thus the sum of all the individual contributions as described above. This can be represented as shown in (4.15) and detailed in (4.16).

$$V_{br,n}^{(tot)}(\gamma) = V_{brn}^{(1)}(\gamma) + V_{brn}^{(2)}(\gamma) + V_{brn}^{(3)}(\gamma) + V_{brn}^{(4)}(\gamma). \tag{4.15}$$

$$\begin{aligned} V_{br,n}(\gamma) = V_s(\gamma) \prod_{i=1}^{n} T_i + \left\{ V_s(\gamma) T_n \prod_{i=1}^{n} T_i \left[\sum_{j=n+1}^{N} r_j \right.\right. \\ \left.\left. \left(\frac{S_{j-1}}{S_n} \right)^2 \right] \right\} + \left\{ V_s(\gamma) \prod_{i=1}^{n} T_i \left[\sum_{k=1}^{N-1} \sum_{i=1}^{n-1} \prod_{j=0}^{1} r_{i+jk} \left(\frac{S_{i+k+1}}{S_i} \right) \right] \right\} \\ + V_s(\gamma) r_s \prod_{i=1}^{n} T_i \sum_{j=1}^{N} r_j \left(S_{j-1}\right)^2 , \end{aligned} \tag{4.16}$$

which can be simplified by factoring out the common terms and reduced to [112]:

$$\begin{aligned} V_{br,n}(\gamma) = V_s(\gamma) \prod_{i=1}^{n} T_i \left\{ 1 + T_n \left[\sum_{j=n+1}^{N} r_j \right.\right. \\ \left. \left(\frac{S_{j-1}}{S_n} \right)^2 \right] + \left[\sum_{k=1}^{N-1} \sum_{i=1}^{n-1} \prod_{j=0}^{1} r_{i+jk} \right. \\ \left.\left. \left(\frac{S_{i+k+1}}{S_i} \right) \right] + r_s \sum_{j=1}^{N} r_j \left(S_{j-1}\right)^2 \right\} . \end{aligned} \tag{4.17}$$

The effects of cable attenuation which is both frequency and line length dependent are then taken into account as shown in (4.1). Again, the attenuation profiles are separated by using the same classification of replicas as it has been done previously, hence the same notation is maintained for consistency. The variables used herein carry the same meaning as previously defined except where specific mention is made. It is not common in practice to have equally spaced branches in the electrical power network, but the variation of the inter-branch spacing d, in indoor environments is minimal. Therefore, an average spacing is considered since it will have minimal impact on the overall propagation distance. The

attenuation profiles for each group is determined as shown by 4.18(a) through 4.18(d).

$$A_n^{(1)} = e^{-\gamma(nd)} \tag{4.18a}$$

$$A_n^{(2)} = e^{-\gamma(2j-n)d} \qquad j = n+1, \cdots, N \tag{4.18b}$$

$$A_n^{(3)} = e^{-\gamma d\left\{2\times\text{floor}\left[\left(\frac{m-1}{n-1}\right)+2\right]+(n-2)\right\}}; \quad m \in \left[1, -0.5n^2 + 5.5n - 5\right] \tag{4.18c}$$

$$A_n^{(4)} = e^{-\gamma(n+2j)d} \qquad j = 1, \cdots, N. \tag{4.18d}$$

where the operator (floor) rounds off its elements to the nearest integer less or equal to the elements. The resultant voltage level, taking into account the effects of attenuation can thus be defined by [112]:

$$V_{br,n}(\gamma) = V_{br,n}^{(1)}(\gamma)A_n^{(1)} + V_{br,n}^{(2)}(\gamma)A_n^{(2)} + V_{br,n}^{(3)}(\gamma)A_n^{(3)} + V_{br,n}^{(4)}(\gamma)A_n^{(4)}. \tag{4.19}$$

The frequency response of an electrical power network at a node can be determined given (4.19) in the frequency domain. The relationship between the input and output of a system can be described by the equation below:

$$V_{br,n}(\gamma) = H(f)V_s(\gamma), \tag{4.20}$$

where $H(f)$ is the transfer function of the electrical power network. Therefore we can use (4.17) such that we obtain the frequency response of an electrical power network as shown below [112]:

$$\begin{aligned} H(f) = \prod_{i=1}^{n} T_i \Bigg\{ A^{(1)} + T_n \Bigg[\sum_{j=n+1}^{N} r_j \left(\frac{S_{j-1}}{S_n} \right)^2 A^{(2)} \Bigg] \\ + \Bigg[\sum_{k=1}^{N-1} \sum_{i=1}^{n-1} \prod_{j=0}^{1} r_{i+jk} \left(\frac{S_{i+k+1}}{S_i} \right) A^{(3)} \Bigg] \\ + r_s \sum_{j=1}^{N} r_j \left(S_{j-1} \right)^2 A^{(4)} \Bigg\}. \end{aligned} \tag{4.21}$$

4.5 Multipath Model

The model of (4.21) is a summation due to superposition of the signal components traversing the paths from source to receiver. With its numerous reflections resulting from impedance discontinuities, the various paths traversed by several components of the signal indicates that a PLC channel can be described as a multipath environment. The discontinuities are characterized by the reflection coefficient $r(f)$ and a transmission coefficient $T(f)$ [117]. This approach was initially formalized by [26]. Considering a channel with K_p dominant paths, the multipath model is described as follows [26]:

$$H(f) = A\sum_{p=1}^{K_p} \underbrace{\left(\prod_{k=1}^{K} r_k(f) \prod_{m=1}^{M} T_m(f)\right)}_{g_p(f)} \underbrace{e^{-j\left(\frac{2\pi l_p}{v_p}\right)f}}_{\text{phase}} \underbrace{e^{-(\alpha)l_p}}_{\text{attenuation}}, \tag{4.22}$$

where $g_p(f), l_p, \alpha, f$, and v_p represent the weighting factor, path length, attenuation constant, frequency and the speed of electromagnetic waves in the cable material, respectively. The weighting factor represents the product of the reflection/transmission factors along a path p. The overall path gain for the path after j interactions is expressed as:

$$g_p(f) = \prod_j g_{pj}(f), \tag{4.23}$$

with $g_{pj}(f)$ as either the reflection or transmission factor ($g_{pj}(f) = r(f)$ for a reflection and $g_{pj}(f) = T(f)$ for a transmission). Typically, all reflection and transmission factors in power lines are less than or equal to one. This is primarily because the electrical power network is constituted by passive components. Transmission only occurs at the nodes where the loading parallel connection of two or more cables results in impedance lower than the characteristic impedance of the feeder cable. Accordingly, the magnitude of the weighting factor will be less than or equal to one.

$$\mid g_p(f) \mid \leq 1. \tag{4.24}$$

The paths with increased interactions will have a reduced resultant weighting factor. Moreover, the longer the path the higher the attenuation and hence minimized impact at the receiver. Therefore, only K_p dominant paths are considered. The selection of these

Table 4.1: Optimum number of paths K_p at branch n in an N size network

n	$N=1$	$N=2$	$N=3$	$N=4$	$N=5$	$N=6$
1	2	4	6	8	10	12
2	-	4	7	10	13	16
3	-	-	7	11	15	19
4	-	-	-	11	16	21
5	-	-	-	-	16	22
6	-	-	-	-	-	22

paths follows the same definition as in the previous section. The number of paths depends on the size of the network and the position in the network where the receiver is placed. With the simplicity of the lattice diagram, it is possible to quantify the number of paths at any node in the network. The results of such an analysis are presented in Table 4.1 for a network of maximum size $N = 6$.

As the network grows in complexity, the challenge of tracing these paths becomes increasingly difficult. Therefore, the results of Table 4.1 are modeled as a mathematical function, through pattern recognition techniques that can seamlessly adapt to any size of the network for a receiver placed anywhere in it. The number of paths can be expressed as [112]:

$$K_p(N,n) = 2Nn - \left[\frac{1}{2}n^2 + \left(N+\frac{1}{2}\right)n - (N+1)\right] \quad N \geq n. \tag{4.25}$$

The path length l_p, which defines the individual distance travelled by a signal along a path p can be defined using the same derivations presented in 4.18(a) through 4.18(d) considering the four defined path groups. The fact that there exist several paths having the same length though traversing different paths is taken into account. However, their reflection/transmission profile will always differ depending on the characteristics of their respective paths. The analysis of path lengths, given our path definitions, can be summarized by the following equations within each path type.

$$l_p = \begin{cases} (1) & nd, & n \leq N \\ (2) & (2i-n)d, & i \in [n+1, N] \\ (3) & \left\{2 \times \text{floor}\left[\left(\frac{m-1}{n-1}\right)+2\right] + (n-2)\right\} d, & m \in [1, -\frac{1}{2}n^2 + \frac{11}{2}n - 5] \\ (4) & (n+2j)d, & j \in [1, N] \end{cases} \tag{4.26}$$

4.6 Model Validation

The model presented in (4.21), also represented as a multipath propagation model in (4.22), is used to determine the frequency response of known powerline networks. Three test networks are built in a laboratory using typical utility cables and their transfer characteristics measured using a Rhode & Schwartz ZVL13 vector network analyzer. The channel frequency response (CFR) is evaluated in the frequency 9 kHz - 30 MHz. During the measurements, the branch ends were left open. The node input impedances can then be calculated using (4.4) with $Z_t = \infty$, following which both the reflection and transmission coefficients can be calculated using (4.2) and (4.3) respectively. The results from three test beds are shown in Figure 4-5 through 4-7.

Due to the size of the network, reaching the end terminals of the network can be difficult, hence a port extension is required to reach measurement ports of the network analyzer. To avoid port extensions interfering with the measured network characteristics, a full two-port calibration is performed prior to measurements to nullify its effects.

4.7 Discussion of Results

The effects of reflections due to branching elements are observable in the transfer characteristics in the form of notches spaced evenly in the frequency span. The first notch will appear when the phase shift between the direct and reflected waves is exactly one half wavelength, leading to a subtraction. This is especially clear when observing a single branch topology as shown in Figure 4-5(a). For a branch terminated with an open circuit, the first notch will appear at $f_0 = v_p/4l$ [109], [96] and subsequent notches will occur at odd multiples of f_0 within the fixed bandwidth such that:

$$f_k = \frac{v_p}{4l}(2k+1) \quad k = 1, 2, 3, \cdots, \tag{4.27}$$

where v_p is the propagation speed and l is the branch length. The first notch frequency in Figure 4-5(b) is $f_0 = 7.5$ MHz as expected, and corresponds to a time period of 133 ns. The subsequent notch satisfying the frequency span is expected at $f_1 = 22.5$ MHz according to (4.27) which is the case as shown in Figure 4-5(b). Beyond f_1 the notch frequencies lie outside the frequency span considered. Given the upper frequency of the bandwidth,

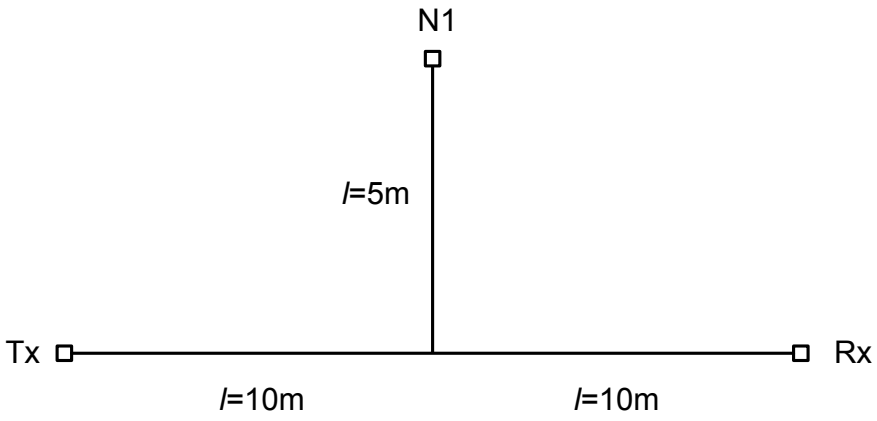

(a) Single-branch

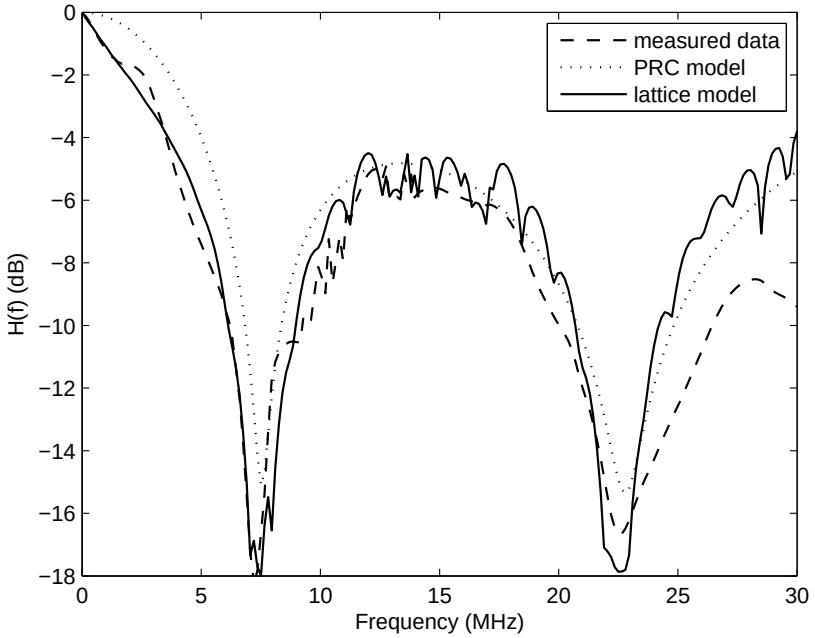

(b) Single-branch results

Figure 4-5: Measured frequency response magnitude Experiment 1: (a) Single-branch Topology and (b) results

30 MHz, notches generated by branches of length less than 1.25 m will exist outside the bandwidth considered. The resultant propagation speed in the cable, due to insulation was found through measurements to be $v_p = 1.5 \times 10^8$ m/s. The first wave that traverses a direct path from T_x to R_x of 20 m, will thus appear after $t = 20/(1.5 \times 10^8) = 133$ ns. Considering the test topology of Figure 4-5(a), the second wave will appear after $t = 30/(1.5 \times 10^8) = 200$ ns. The time period of the first notch ($t_0 = 133$ ns) should correspond to twice the difference

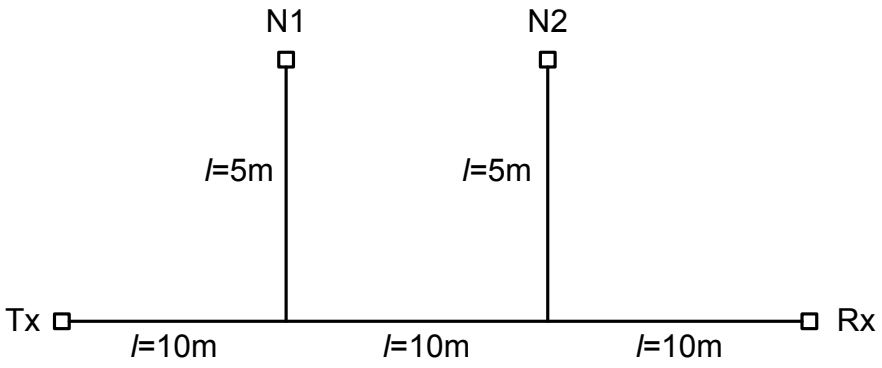

(a) Two branches

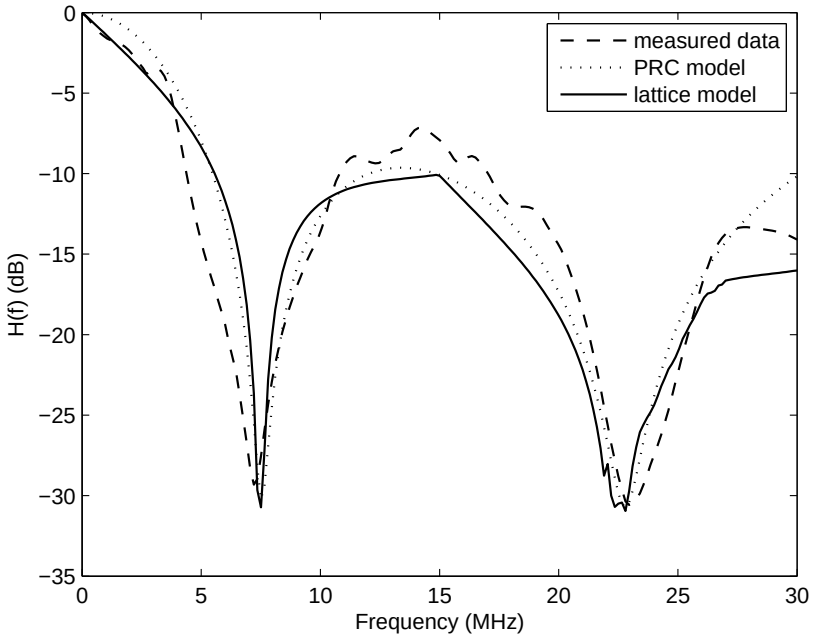

(b) Two-branch results

Figure 4-6: Experiment 2: (a) Two-branch Topology and (b) Results

(full wavelength) between these two times $2\times(200-133) = 134$ ns. Subsequent time periods corresponding to subsequent notch frequencies can be obtained as follows:

$$t_k = \frac{t_0}{(2k+1)} \quad k = 1, 2, 3, \cdots. \tag{4.28}$$

In Figure 4-5 through 4-7, the lattice model of three test topologies and comparison with measured data and the parallel resonant circuit (PRC) model of [109] are shown. Evidently, there is a good agreement between the model and measurements. These results validates the

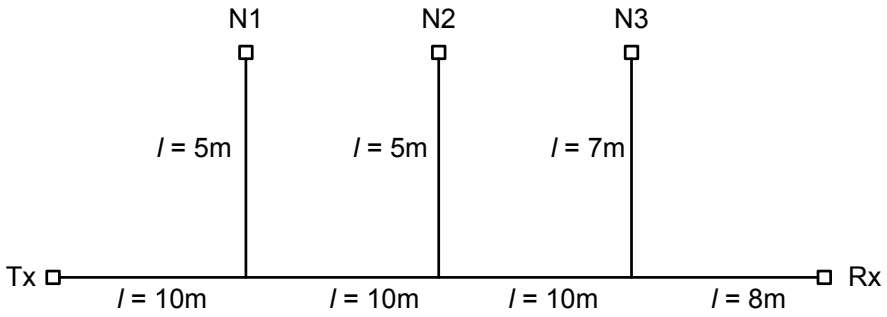

(a) Three branches

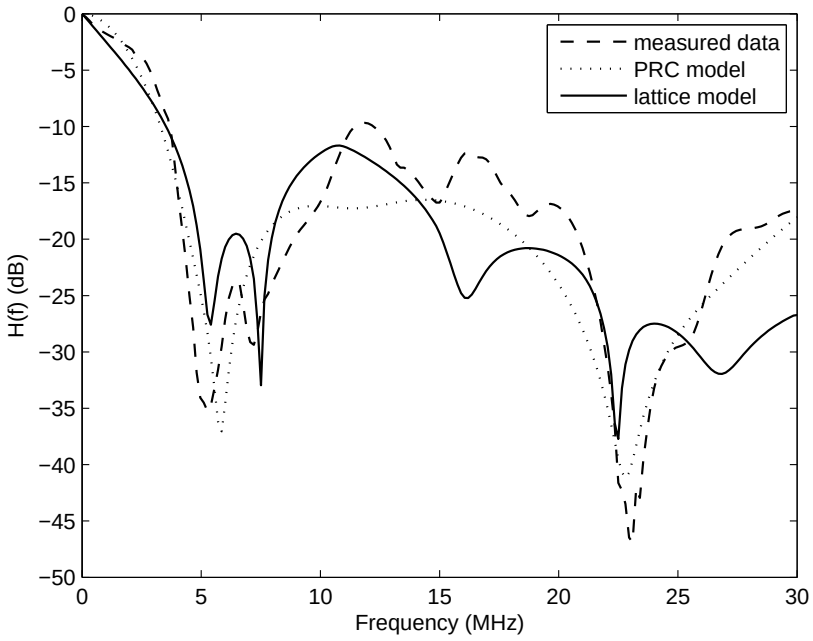

(b) Three-branch results

Figure 4-7: Experiment 3: (a) Three-branch Topology and (b) Results

applicability of the lattice approach in powerline modeling. The structure of the topology of Figure 4-6 is such that the second branch has the same length as the first. This strategic choice of branch lengths has a profound result. According to (4.27), the two branches, having equal lengths, will result in notch occurrences at the same frequencies. However, it is noticed that the depth of the notches has increased. It is therefore valid to deduce that multiple branches of the same length will always result in constant notch distribution in the frequency bandwidth, with the notch depth dependent on the number of such branches. In Figure 4-7, a third branch is added having a different branch length of 7 m. Again, using (4.27) it is expected that the notches will appear at $f_0 = 5.36$ MHz, $f_1 = 16$ MHz, and $f_2 = 26.8$ MHz.

Table 4.2: Determination of First Notch Frequency and Inter-Notch Separation

Branch	Path (p)	τ_p (ns)	$\tau_2 - \tau_1$ (ns)	F (MHz)	f_0 (MHz)
$5m$	direct path second path	$l_{1;5}/c = 253$ $l_{2;5}/c = 320$	$= \Delta t = 67$	$= \frac{1}{\Delta t} = 15$	$= \frac{F_5}{2} = 7.5$
$7m$	direct path second path	$l_{1;7}/c = 253$ $l_{2;7}/c = 347$	$= \Delta t = 93$	$= \frac{1}{\Delta t} = 10.75$	$= \frac{F_7}{2} = 5.38$

From the measurements/simulations, $f_0 \approx 5.26$ MHz, $f_1 \approx 15.2$ MHz, and $f_2 \approx 25.6$ MHz. The time taken by the direct wave to traverse 38 m will be given by $t = 38/1.5 \times 10^8 = 253.3$ ns. The second wave will appear after $t = 48/1.5 \times 10^8 = 320$ ns after travelling along one of the 5m branches. Owing to the two branches having equal lengths and also being the shortest in the network, two signals will appear at the receiver at the same time ($t = 320$ ns) provided the network is homogeneous. This explains why branches of the same length results in increased notch depth. If it is desired to determine the time period of the first notch due to the 7 m branch, we can follow the same procedure as before. In fact, the impact of each branch can be studied independently. The notch positions of a given PLC network can be determined in the time domain by evaluating the channel impulse response. By taking the inverse Fourier transform (IFT) of (4.22) it is possible to analyze the channel in time domain, defined as:

$$h(t,\tau) = \sum_{p=1}^{K_p} \beta_p \delta\left(t - \tau_p\right) e^{j\phi_p}, \tag{4.29}$$

where β_p is the amplitude gain, τ_p is the time of arrival (TOA) and ϕ_p is the phase of the pth arriving path. The characteristics of the direct path are such that it takes variables β_1, τ_1 and ϕ_1. In that case, the receiver distance from the transmitter is $l_1 = \tau_1 \nu_p$. With purely time domain characteristics the position of the first notch f_0 as well as the inter-notch spacing F can be predicted in the frequency domain. For the network of Figure 4-7 having two distinct types of branches, the results are shown in Table 4.2.

The notch locations play an important role in many deterministic approaches such as using resonant circuits or filter combinations. In the transfer function, all the notches due to the three branches are observable. Hence we can view the powerline channel transfer

characteristics as a superposition of several cascaded responses.

4.8 Conclussion

In this work we describe the powerline network as a lattice structure with traceable reflection/transmission combinations. Assuming a uniform inter-branch spacing we are able to trace all the significant paths and develop a model based on voltage levels at any port in the network. The lattice approach, typical of bottom-up approaches, has an inherent drawback in that the topology of the network in typical indoor powerline environments is not always readily available, hence this kind of solution serves as a guideline towards estimation of channel performance and other relevant channel metrics. The unpredictability of the network topology due to the ever changing branch loading presents a complex problem that may require adaptive modeling techniques. Furthermore, the model derivation, though relatively less complex, remains a manual exercise that requires a meticulous approach. In this approach, we considered open branches as a worst case scenario which serves as a boundary solution. Similarly, branches may be short circuited or terminated with characteristic impedance to evaluate other boundary conditions.

The results obtained using the three test networks show that signal attenuation is directly proportional to the number of branches in a network. This is evident in Figure 4-5 through 4-7. As an example, at 15 MHz the signal attenuation is approximately -6 dB, -10 dB, and -16 dB for single-, two-, and three-branch networks respectively. The network resultant transfer function is the superposition of the individual branch transfer functions. The shape of the transfer characteristics is heavily influenced by the branch lengths as seen throughout the results. When the length of the branch increases, so does the number of periodical notches within the frequency span. In Section 4.7, we have shown that the 5 m branches for the lattice and the PRC models, as well as for the measurements, will only result in two notches (at 7.5 MHz and 22.5 MHz) while the 7 m branch will result in three notches (at 5.36 MHz, 16 MHz, and 26.8 MHz) in the frequency range 1 - 30 MHz.

The results of the lattice model are compared with measured data as well as the parallel resonant circuit (PRC) model developed by [109]. Both approaches are deterministic in nature and represents the transfer function adequately. Deterministic models are computation intensive. Determination of model parameters and matrix formulations tends to be a daunt-

ing task. However, the lattice model is less complex and requires fewer input parameters. Its flexibility and close relationship with the physics of the power network makes it suitable for network related system modeling such as in multi-user systems and relay systems. For homogeneous networks, typical of indoor environments, the characteristic impedance and the propagation constant are the same throughout the cabling. Thus, the only input variable is the length of the branches. This model is basically a transmission line theory based multipath approach, and can thus be applied as usual.

CHAPTER 5

Analysis and Prediction of Asynchronous Impulsive Noise Volatility for Indoor PLC Systems using GARCH Models

5.1 Introduction

Originally, electrical power networks attracted utility companies considerably to further employ them as communication media [51]. The majority of developed countries have somewhat instituted reliable digital subscriber lines (DSL) as well as other wired services, hence, in their view there is little incentive in the deployment of outdoor PLC systems. However, owing to the accessibility of triple-play solutions, the objective to utilize indoor wiring for computer and multimedia connectivity presents an appealing prospect. Moreover, developments in digital communications have made internet access feasible off the premises wall electrical points of connection [85]. All these desirable possibilities of electrical grid usage as a communication medium has been deterred by lack of an international standard regulated by a globally recognized standardization body. Since the inception of the IEEE 1901 standard for broadband over power line, a new era has been unlocked in the powerline communication sector. Notwithstanding this development, the intrinsic properties of the electrical power network poses other technical challenges for effective and reliable broadband transmission. Besides the topology and cable characteristics, PLC systems experience impulsive noise generated by the numerous equipments connected to the network including other narrowband interferences coupled onto the electrical power network [85]. The overall level of noise is the sum of all the noises in the network.

The undesirable effects of PLC noise has prompted a lot of research in the area [21, 46, 76, 77, 118–120] in various regions across the world. As mentioned earlier, the noise generated by appliances is typically synchronous with the mains harmonics (50 or 100 Hz). This cyclic noise is generally referred to as cyclostationary impulsive noise. It is commonly generated by silicon controlled rectifiers in power supplies [51]. Cyclostationary impulsive

noise can also attain frequencies much higher than the mains frequency as found in the measurements in this work. Occasionally, due to switching on and off of appliances in the network, sporadic impulses occur without any regularity and this noise is particularly arbitrary. In the frequency band 1-30 MHz, there is a presence of various radio services such as amateur radio, sharing the spectrum with broadband PLC systems. At high frequencies, the unshielded nature of the electrical wiring results in them behaving like antennas, picking up other radio signals in the process. Besides the acknowledged noise sources above, there still exist several additional sources of noise in the grid, some of which their origin is not known. Due to the ever presence of this noise in the network, it is usually referred to as background noise.

Typically, when determining the background noise [23, 77], it is common to include both the impulsive and narrowband interference aspects when calculating its probability distribution and power spectral density. Considering the impulsive noise, its analysis has been accomplished in the time domain by employing digital storage oscilloscopes (DSO) triggered by a peak detector output. The acquired sequence is processed to determine the statistics of interval arrival time, pulse width and pulse magnitude [76, 119]. This process makes it difficult to identify different aspects of the noise and their periodicity. Noise registers having low magnitude are entirely concealed under high power ones resulting to a biased amplitude statistics.

In this work, all the numerous noise signals appearing at a power outlet regardless of their energy level are captured. The noise registers are colour coded according to their frequency of appearance over a period of time across the working frequency band. Even when impulses from different components overlap, each one will statistically contribute to the density of the bitmap at the correct level. Due to the burstiness of the PLC noise, we have developed a model suitable for capturing the volatile nature of the impulsive noise. This arises from the fact that statistical models based on impulse amplitudes and impulse times are highly biased due to increased overlapping of noise registers during measurements.

5.1.1 Noise Measurements

The noise generated by numerous electrical appliances in the electrical power network can be obtained at an electrical outlet of an indoor environment. Various appliances in the premises generate noise sequences with distinctive properties. While some equipments inject negligible

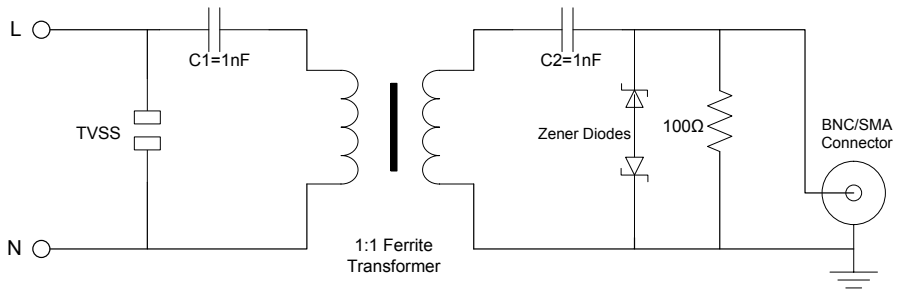

Figure 5-1: Coupling circuitry

levels of noise, some produce high level noise disturbances.

5.1.1.1 Measurement Setup

Communication equipment such as modems generally permit minimal voltage at their ports, which is entirely the contradiction in the electrical power network. The 220 V mains voltage used in indoor power lines therefore poses a genuine threat to communication systems' equipment. To effectively couple signals to and from the "live" electrical power network, a coupling circuit is necessary to filter out the high power mains voltage. Such a circuit is depicted in Figure 5-1 and exhibits high-pass characteristics with a cut-off frequency of 200 kHz with a satisfactorily uniform response in the desired working band. The coupler has an attenuation of at most 1.59 dB in the working band. For galvanic isolation, the coupler incorporates a 1:1 RF transformer with a transient voltage surge suppressor (TVSS) connected on either side.

5.1.1.2 Measurement Instrumentation

Contrary to numerous measurement campaigns on electrical power network, the discussion in this work is based on the measurement of power spectral density of noise data sequences over an extended acquisition time. Conventional swept spectrum analyzers employs line traces with a singular capability of displaying one signal magnitude for every frequency point, which basically represents the largest, smallest or the average power, depending on the settings. To circumvent this shortcoming we have used the Tektronix RSA5126A Real-Time signal analyser in the frequency span 1-30 MHz. The instrument is equipped with a 16 bit analogue to digital converter. The sampling rate that was chosen is 200 MS/s. The analyzer

is equipped with the revolutionary Digital Phosphor Technology (DPX) which provides an intuitive live colour view of signal transients as they vary over time in the frequency domain. The DPX spectrum display can detect and accurately measure transients as brief as 10.3 μs. The instrument has a 16 bit analogue to digital conversion (ADC) rate with a sampling rate of 200 MHz. Furthermore, its dedicated hardware computes up to 292 000 spectrums per second on the digitized input signal. All these spectrums are then displayed as colour-graded bitmap that reveals low-amplitude signals beneath stronger signals occupying the same frequency at different times. The bitmap image, as opposed to a line trace, gives more insight, enabling one to distinguish numerous versions of the same signal as it varies over time. The colour scheme used in this work ("temperature") is such that the hot red colour indicates a signal that appears more frequently than those shown in cooler colours.

5.1.2 Measurement Results

It often desirable to evaluate the contribution to the noise register due to background noise. This is challenging because the background noise generally exhibits lower magnitudes in comparison with the more deleterious impulsive noise. The RSA5126 real-time signal analyser makes this possible with its DPX spectrum capability. Figures 5-2, 5-3, 5-4 and 5-5 show noise measurement results acquired in an indoor electrical power network and four distinct types of measurements are presented. The DPX spectrum bitmap (amplitude vs. frequency) is shown in Figure 5-2. It can be observed that various noise sequences have been captured over time and the bitmap is continuously updated with every measurement cycle. The bitmap indicates that some signal amplitudes appear more frequently compared to others at the same frequency point. The most frequent signals are shown in red/yellow colour in the spectrum while the less frequent ones are shown in blue. It can easily deduce that the "hottest" region represent the background noise. Regardless of this noise being buried under high amplitude impulsive noise components, it can still be detected as evident from Figure 5-2.

The spectrogram (time vs. frequency) in Figure 5-3 shows the time-frequency characteristics of PLC noise. There has been numerous reports that powerline impulsive noise is dominated by synchronous impulsive components generated by appliances connected to the network; as is observed here, however, we can simultaneously identify noise components at higher frequencies. This is not easily observable, for example, using the time-domain graph

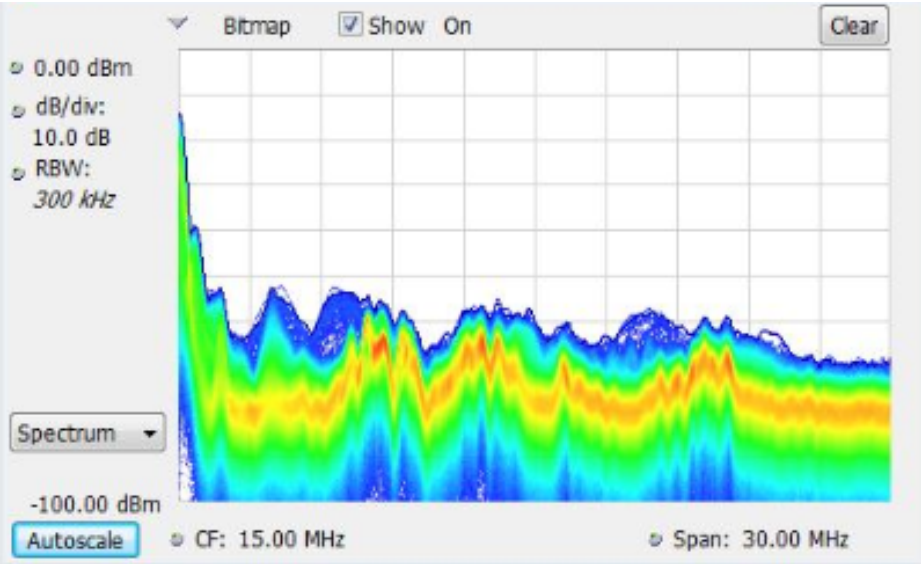

Figure 5-2: Colour spectrum of PLC noise density captured in an office

displayed in Figure 5-4. Clearly we can identify the synchronous impulsive component (at the second harmonic, 100 Hz), whereas other aspects are not easy to identify. The frequency domain noise representation is shown in Figure 5-5 and we can only capture one trace at a time, either the maximum, minimum, or average of the noise level. In the same figure it is also seen that the instantaneous plot of noise, which is essentially continuously varying around the peak average value.

Considering Figure 5-2, though there is the benefit of identifying all the noise over time, obviously such a randomly varying process should be classified statistically over time. This variability of noise level occurrences is characterized statistically over time.

5.1.3 Noise Distribution

The instantaneous noise power envelope such as that shown in Figure 5-2 is captured by the measuring instrument and can be defined by:

$$\text{power} = I^2 + Q^2 \tag{5.1}$$

where I and Q are the in-phase and quadrature components of the waveform. Unfortunately, the power line noise signal is difficult to characterize due to its intrinsic random behaviour. In order to extract meaningful information from such a random process, a statistical description of the PLC noise power level is required. A statistical analysis of the PLC signal is provided

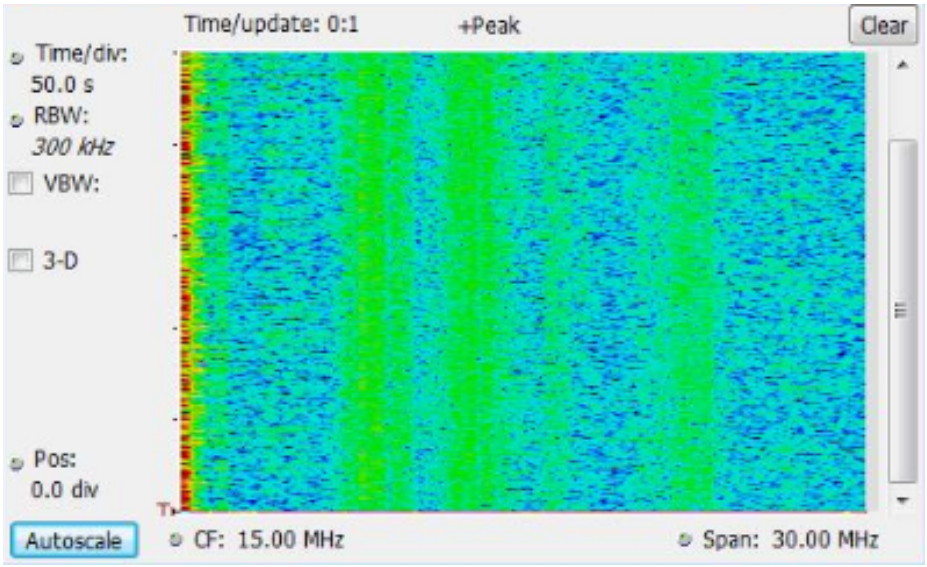

Figure 5-3: Time-Frequency spectrum of PLC noise captured in an office

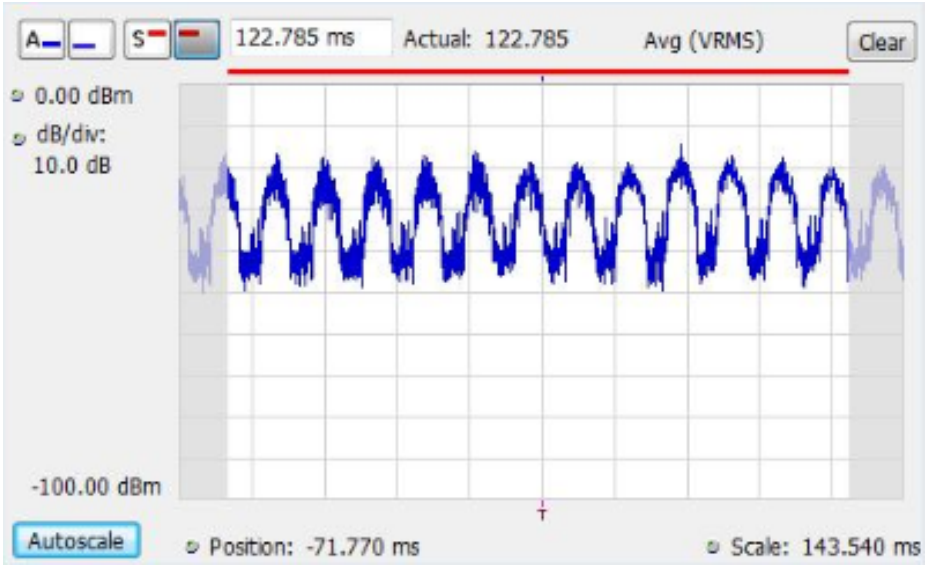

Figure 5-4: Time-Domain spectrum of PLC noise captured in an office

through the complimentary cumulative distribution function (CCDF). A CCDF curve shows how much time the signal spends at or above a given power level. In this work, we observe the signal level relative to its average power. Thus, the peak-to-average ratio is actually being measured as opposed to the absolute power level. This deviation will be expressed in dB. The percentage of time the signal spends at or above a certain power level defines the probability for that particular power level. A CCDF curve is thus a plot of relative power levels vs. probability. Figure 5-6(a) shows a CCDF of PLC noise registered in an office. In

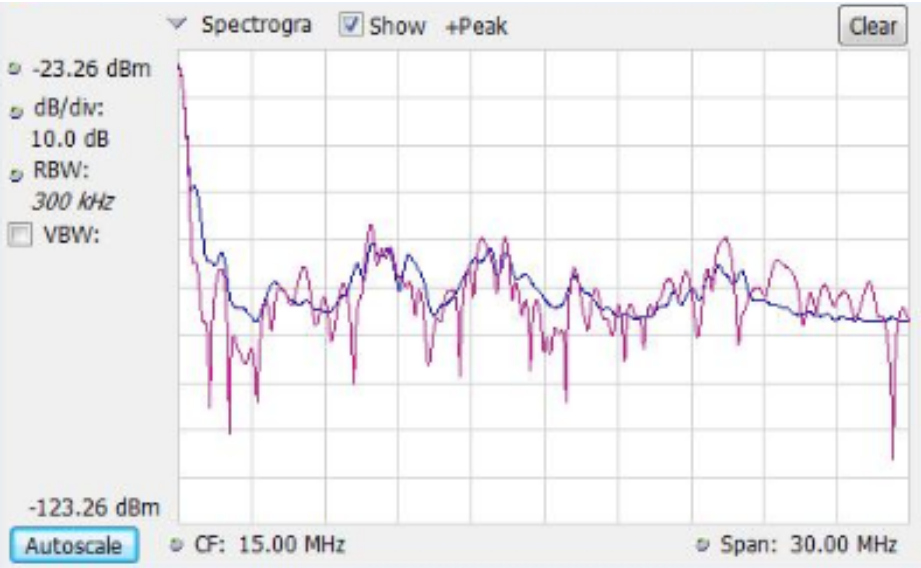

Figure 5-5: Spectrogram of PLC noise captured in an office

the same plot, a Gaussian noise CCDF is plotted for reference. The cumulative distribution (CDF) and the probability distribution functions are also shown in Figure 5-6(b) and 5-6(c) respectively. We derive the CDF from the CCDF in the following manner:

$$F(x) = 1 - \bar{F}(x), \tag{5.2}$$

where $F(x)$ is the CDF and $\bar{F}(x)$ is the CCDF. The cumulative distribution function is ideally the opposite of its compliment and is defined as follows:

$$F(x) = P(X \leq x) = \sum_{y:y \leq x} p(y) \tag{5.3}$$

The cumulative distribution describes the probability that a random variable X with a given probability distribution will exhibit values less than or equal to x. Once the CDF is obtained, the probability density function can also be determined. The relationship between the CDF and the PDF is such that the PDF is the derivative of the CDF. It can thus be determined as follows, provided f_x is continuous at x:

$$f_X(x) = \frac{d}{dx} F_X(x) \tag{5.4}$$

where $f_X(x)$ is the PDF and $F_X(x)$ is the CDF. The probability distribution can be represented as follows:

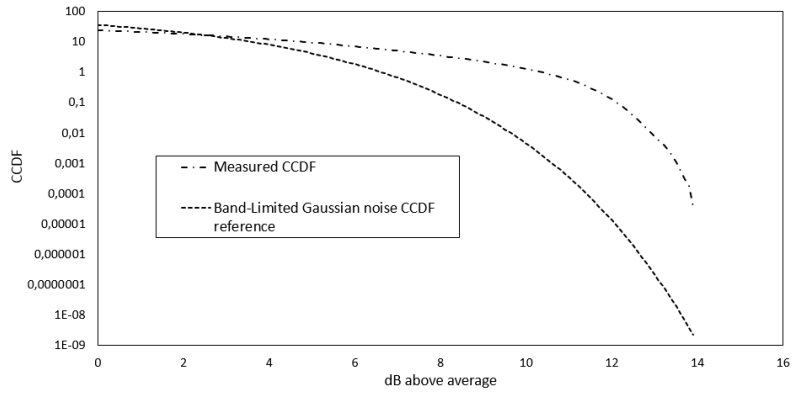

(a) CCDF of PLC noise registered in an office

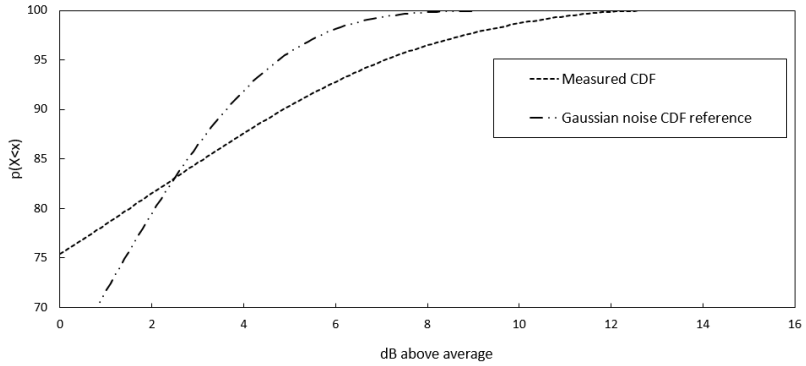

(b) CDF of PLC noise registered in an office

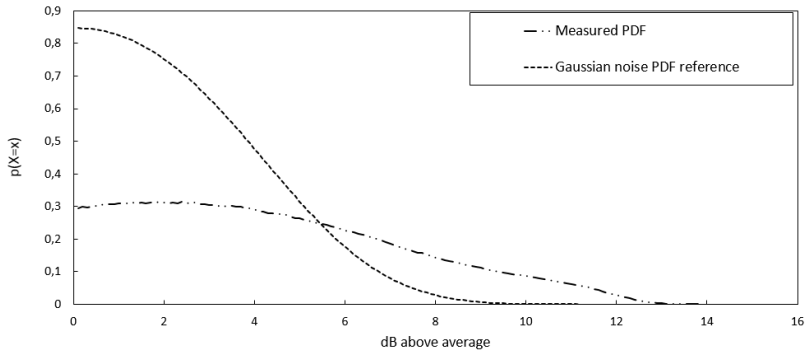

(c) PDF of PLC noise registered in an office

Figure 5-6: Statistical distribution of impulsive noise measured at a wall plug

$$f_X(x) = P(X = x) \tag{5.5}$$

Which is the probability that a certain power level above the average power occurs.

This work has presented a detailed measurement procedure for noise measurement for broadband power line communication systems. The measurements are acquired using a high

resolution signal analyser from Tektronix that is capable of providing high resolution noise spectrums both in time and frequency domain. Some characteristics which are normally difficult to observe with conventional digital oscilloscopes or vector spectrum analyzers are shown with adequate clarity. The time-frequency characteristics of PLC noise shows that there is a strong presence of high frequency cyclostationary noise well beyond that which is synchronous with the mains frequency. Through measurements, we are able to determine the complementary cumulative distribution function (CCDF) of the noise powers that equals or exceed the average power of the noise. Though, this is not a measure of absolute noise power, it provides valuable information as to how often certain exceedance power levels are attained. We can see from Figure 5-6(a) that the most stressful noise (further right of the graph) occurs less often compared to that which is closer to the average power in magnitude. The same conclusion can be drawn from the DPX spectrum shown in Figure 5-2. The blue coloured signals occurring above the yellow/red signals are of higher magnitude and appears less frequent.

The distribution of the power levels above the average power level represents the distribution of impulsive noise occurrences. It is evident in Figure 5-6(a) through 5-6(c) that this noise definitely does not follow the classical additive white Gaussian noise (AWGN). Clearly, there is a large presence of high power impulsive noise components in the PLC environment than suggested by the AWGN assumption. As an example: the Gaussian distribution suggests that the probability of a noise component being 7.5 dB above the average power is 0.5, whereas according to measurements for the same power exceedance of 7.5 dB, the probability is 0.15. On the other hand, the AWGN assumption exaggerates the presence of noise components with a power level within the vicinity of the average power level. As an example: The Gaussian distribution predicts that the probability of a noise component being 2.5 dB above the average power is 0.7. According to the measurements, the probability of a noise component being 2.5 dB more that the average noise power is approximately 0.3.

This power statistics gives us a perspective of how often there is presence of impulsive noise. In that case, impulsive noise is not classified as whether cyclostationary, synchronous or asynchronous. It is rather presented as seen at the receiver. Since the distribution of these impulsive components does not follow any standard probability distribution, it is most likely that it could be modelled by a combination of known probability distributions or a completely new model. It is also of note that this distribution will vary from location to

location as well as time to time. However, with intensive measurements a unified model or class of models could possibly be developed and defined for typical indoor scenarios.

5.2 Prediction of Asynchronous Impulsive Noise Volatility

The recent dramatic increase in the number of digital radio communication systems within indoor environments has brought about an increased appeal in developing high-speed data transmission systems. The idea of utilizing the ubiquitous electrical power network for data communication purposes within residential areas has seen a great deal of research activity aimed at characterizing both the channel and noise associated with indoor power lines. PLC channels experience numerous impairments, of which noise has a significant contribution in quantifying possible data rates that can be achieved. Unfortunately, power line communications noise cannot be characterized by standard statistical specifications. This is simply because PLC noise originates from numerous sources connected to the power grid. It is common practice in literature to classify noise based on its power spectral density and behaviour, leading to the following five classes of noise: *colored background noise, narrowband noise, periodic impulsive noise asynchronous to the mains frequency, periodic impulsive noise synchronous to the mains frequency, and asynchronous impulsive noise* [21]. Recently, a lot of work has been focused on modeling the periodic impulsive components of noise. This noise is generally produced by the user equipments and the SCR-based power supplies plugged in the electrical power networks. Its power spectral density (PSD) as well as its periodic short-term variations have been examined especially in [23] and [46], respectively; with the results of [46] been utilized comprehensively in the development of a powerline communication channel simulator [47]. Moreover, with regards to the principal characteristics of the periodic impulsive noise, empirical results for parameters such as PSD and the noise pulse characteristics (i.e repetition rate, shape, duration and amplitude) have been presented in [48–51]. Accordingly, the derivation of the models that adequately fits these results has been provided. It is observed, nonetheless, that a completely statistical model of the periodic impulsive noise has only been developed in [50]. The noise is represented by specific statistical laws governing the duration, magnitude and inter-arrival times of a sequence of pulses. Other statistical models, [37] and [52], have been presented based on Poison processes, but unfortunately they do not depend on measurement data.

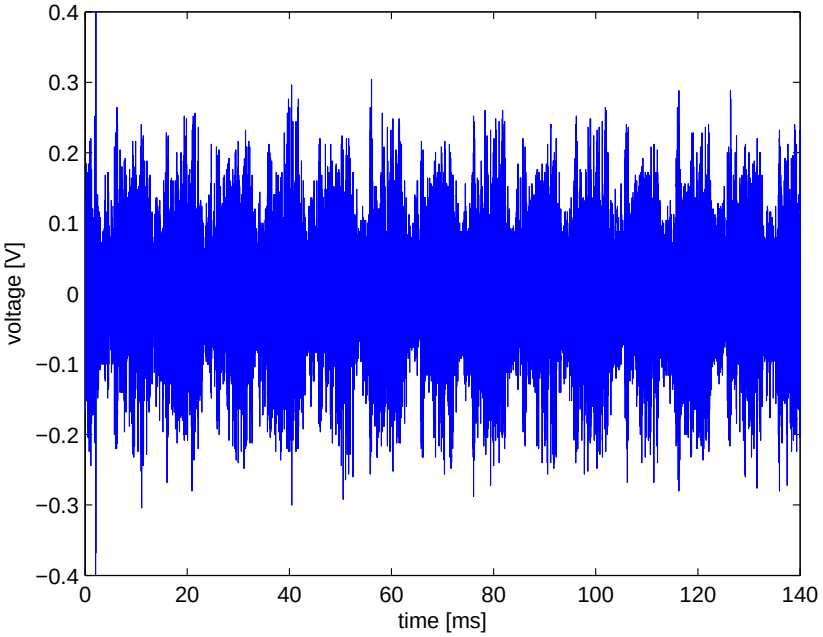

Figure 5-7: Measured asynchronous noise time sequence

In this work, PLC asynchronous impulsive noise is described as a GARCH process. This process is based on the idea that PLC noise exhibits volatility clustering i.e. periods of high volatility are followed by periods of high volatility and periods of low volatility are followed br periods of low volatility. This observation is derived from the residuals of the time series after performing an OLS regression of the noise data sequence. The noise data sequence is then referred to as suffering from heteroskedasticity. This approach differs from common approaches such as that of [50] which studies the properties of individual pulses. Understanding noise volatility is important as it provides long-term predictions of expected impairment experienced at the receiver under bursty noise. GARCH models addresses the deficiencies of common regression models such as Autoregressive Moving Average (ARMA) which models the conditional expectation of a process given the past, but regards the past conditional variances to be constant. In our approach, the time-varying volatility is predicted by using past time-varying variances in the error terms of the noise data series. Subsequent variances are predicted as a weighted average of past squared residuals with declining weights that never completely diminish.

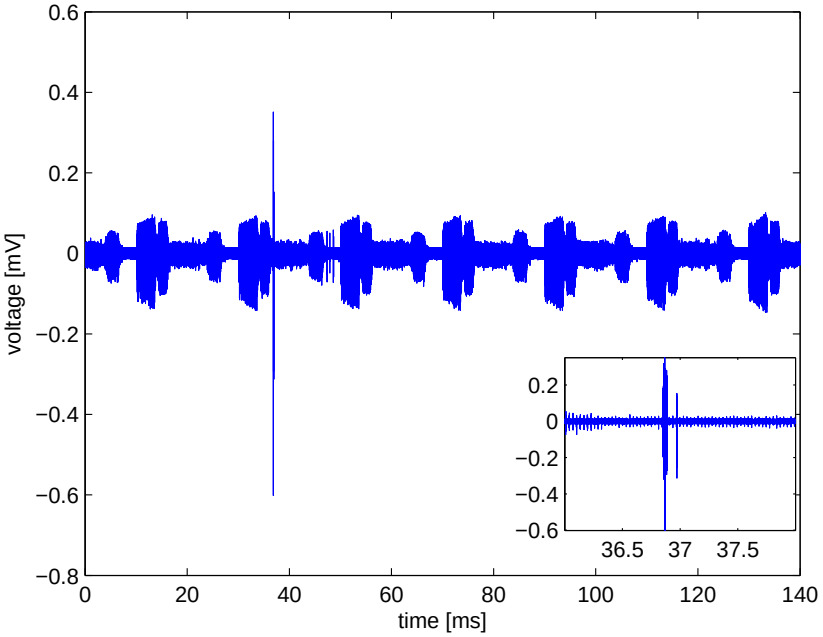

Figure 5-8: Heteroskedastic Residuals

5.2.1 Time Series Data Acquisition & Treatment

Noise data sequences have been acquired using a RIGOL DS2202A digital oscilloscope (DSO) at a sampling rate $f_s = 100$ MHz. With this sampling rate, the maximum storage capability of the oscilloscope is exploited, allowing the system to capture 14 million data points. The time limitation imposed by the data length in memory is not desirable, but it is still possible to capture noise sequences of more than 10 mains cycles with this setting. Thus, modeling such lengths of data can be considered *long-term modeling*. The oscilloscope is connected to the electrical power network via a coupling circuit to ensure its safety from the mains and control the operating frequency to within (1 - 30 MHz) band.

In this work, our focus is on asynchronous impulsive noise. This noise is composed of random impulses of varying durations generally caused by switching supplies and various other indoor appliances. Narrowband noise may also be present due to other radio services operating in the same frequency band. Asynchronous impulsive noise is the most unpredictable PLC noise and thus causes a lot of concern in terms of achievable bit error rates during data communication. Such a noise was measured in the kitchen of a detached house

and the results are shown in Figure 5-7. In its randomness, one can still notice that there is a heavy presence of synchronous impulsive noise (synchronous with the mains voltage signal). This is simply because noise generated by appliances tends to aggregate every mains cycle. Nonetheless, this can be regarded as *cyclic* heteroskedasticity. In order to test for heteroskedasticity, an OLS regression of the measured noise time series is performed. The results, as shown in Figure 5-8, indicate that the noise data exhibits volatility clustering i.e. periods of high volatility and periods of low volatility. It is noticed from the residuals, through the zoomed portion, that the observed spike is an impulsive event. This is most likely caused by a turn ON/OFF event of an appliance.

5.2.2 Generalized ARCH (GARCH)

As is common with many natural time series processes, PLC noise data sequences often exhibit volatility clustering, where time series show periods of high volatility and periods of low volatility; see, for example Figure 5-8. In fact, with powerline impulsive noise scenario, time-varying volatility is more common than constant volatility, and accurate modeling of this time-varying volatility is of great significance in assessing the performance of the channel for digital communications. Prediction of transmission metrics such as signal to noise ratio (SNR) and bit error rate (BER) depend a great deal on accurate prediction of noise processes.

Consider noise as a dependent variable y_t which is supposedly generated by

$$y_t = x_t^{'}\gamma + \varepsilon_t \qquad t = 1, \cdots, T, \tag{5.6}$$

where x_t is a $k \times 1$ vector of lagged endogenous variables and possibly exogenous variables, and γ is an $k \times 1$ vector of parameters. The ARCH model characterizes the distribution of the stochastic error term ε_t conditionally on a set of lagged variables $\Omega_{t-1} = \{y_{t-1}, x_{t-1}, y_{t-2}, x_{t-2}, ...\}$. In the original model developed by [121], it was assumed that the error term conditionally follows a normal distribution;

$$\varepsilon_t | \Omega_{t-1} \sim N(0, h_t), \tag{5.7}$$

where

$$h_t = \alpha_0 + \alpha_1 \varepsilon_{t-1}^2 + \alpha_2 \varepsilon_{t-2}^2 + \cdots + \alpha_q \varepsilon_{t-q}^2, \tag{5.8}$$

with $\alpha_0 > 0$ and $\alpha_j \geq 0$ for $j = 1, \cdots, q$, in order to ensure a positive conditional variance. Here, q is the order of the ARCH process. The model presented in (5.6) - (5.8) is attractive in that the conditional variance h_t depends on the past Ω_{t-1} and is a positive function of the size of the past errors in absolute value. Thus a large positive or negative error tends to be followed by a large (in absolute value) error, and similarly a small error tends to be followed by a small error. The order q determines the length of the period within which a certain disturbance persists in conditioning the variance of the subsequent disturbances. The larger is q, the longer the periods of volatility clustering. Additionally, a significant property of ARCH processes is that the combinations resulting from the conditional variance instigates additional kurtosis in the unconditional distribution. In fact, the parametrization does not impose $textita - priori$ the existence of unconditional moments, which may well lead to infinite variance.

It does not take long in applied work to realize that the specification of the conditional variance as an ARCH(q) requires a large number of lags and therefore the approximation of several parameters subject to inequality constraints. In consequence, [122] made a proposal towards a generalization of the ARCH model, (which was then designated as GARCH) which makes provision for a parsimonious representation of a high order ARCH model. The conditional variance function of a GARCH(p, q) model has the following form

$$h_t = \alpha_0 + \alpha_1 \varepsilon_{t-1}^2 + \cdots + \alpha_q \varepsilon_{t-q}^2 + \beta_1 h_{t-1} + \cdots + \beta_p h_{t-p} \tag{5.9}$$

with

$$\alpha_0 \qquad > 0 \tag{5.10}$$

$$\alpha_j \quad \geq 0 \quad \text{for} \quad j = 1, \cdots, q \tag{5.11}$$

$$\beta_k \quad \geq 0 \quad \text{for} \quad k = 1, \cdots, p \tag{5.12}$$

where the constraints (5.10) through (5.12) ensure a positive conditional variance.

5.2.3 Determination of Conditional Means and Variances

In light of utilizing GARCH models, some general principles pertaining to modeling non-constant conditional variance are presented. In our consideration we begin with regression

modeling with a *constant* conditional variance, $Var(Y_t \mid X_{1,t}, ..., X_{p,t}) = \sigma^2$. The general form for the regression of Y_t on $X_{1,t}, ..., X_{p,t}$ then becomes

$$Y_t = f_e(X_{1,t}, ..., X_{p,t}) + \epsilon_t \tag{5.13}$$

where ϵ_t is independent of $X_{1,t}, ..., X_{p,t}$ and has expectation equal to 0 and a constant conditional variance σ_ϵ^2. The function f_e is the conditional expectation of Y_t given $X_{1,t}, ..., X_{p,t}$. furthermore, the conditional variance of Y_t is σ_ϵ^2. With modification to Equation (5.6), it allows for conditional heteroskedasticity. Let $\sigma^2(X_{1,t}, ..., X_{p,t})$ be the conditional variance of Y_t given $X_{1,t}, ..., X_{p,t}$. Then the model

$$Y_t = f(X_{1,t}, ..., X_{p,t}) + \sigma(X_{1,t}, ..., X_{p,t})\epsilon_t, \tag{5.14}$$

where ϵ_t has conditional (given $X_{1,t}, ..., X_{p,t}$) mean equal to 0 and conditional variance equal to 1, gives the correct conditional mean and variance of Y_t. The function $\sigma(X_{1,t}, ..., X_{p,t})$, which is a standard deviation should not take negative numbers. If the function $\sigma(\cdot)$ is linear, then its coefficients must be constrained to ensure non-negativity. The implementation of such constraints can be cumbersome, therefore it is usually preferable to rather use non-linear and non-negative functions. GARCH models are a subset of a class of models of conditional variance often referred to as *variance function models*.

5.2.4 Simulation and Experimental results

The GARCH model described in prior sections is used to develop a statistical model for asynchronous impulsive noise generated at a home plug in a detached house. The model can be considered a long-term model since the data length encompasses several cycles of the mains period. Evidently, the model captures the measurement data adequately as seen in Figure 5-9 when compared with the simulated data. The statistical accuracy of our model is specified in terms of the sum of squared residuals as follows:

$$SSR = \sum_{i=1}^{n} e_i^2, \tag{5.15}$$

where

$$e_i = y_i - \hat{y}_i \tag{5.16}$$

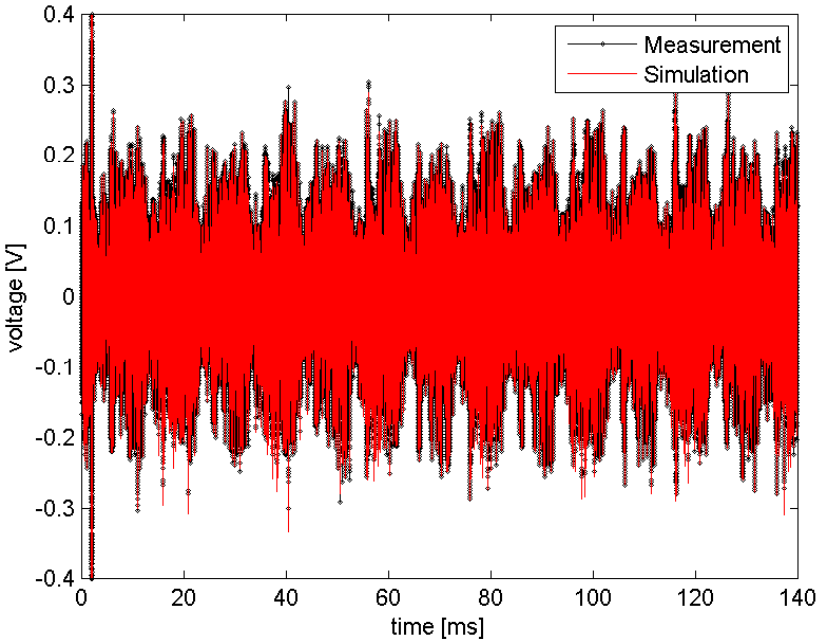

Figure 5-9: Measured and simulated noise data sequences captured in a detached house

The residuals between the simulated and measured data leads to a squared residual error, SSR=222.6 (for 14 million data points) and an $R^2 = 0.996$. R^2 is a statistical measure of how close the data are to the fitted regression line. The accuracy of the model is demonstrated through a comparison of the measured and simulated autocorrelation functions as shown in Figure 5-10(a) and 5-10(b).

5.3 Conclusion

Analysis of powerline communication impulsive noise has been carried out with the help of a high resolution signal analyzer from Tektronix. With its Digital Phosphor Technology (DPX) capable of capturing transients as brief as 10 μs and dedicated hardware that computes roughly 300 000 spectrums per second, the highly variable noise sequences are adequately captured and characterized. For reference, in this case, impulsive noise is described as the noise registers which have power greater than the average power. Furthermore, the peak-to-average ratio is used instead of absolute power. The statistical distribution of the noise deviate a great deal from the additive white Gaussian (AWGN) assumption. Often times, classical probability distributions are often employed to model impulsive noise in PLC

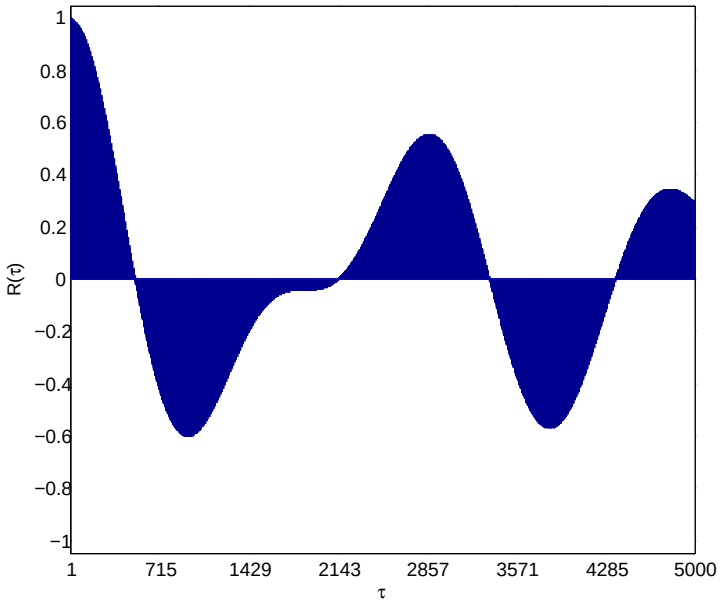

(a) Autocorrelation function of the acquired noise sequence

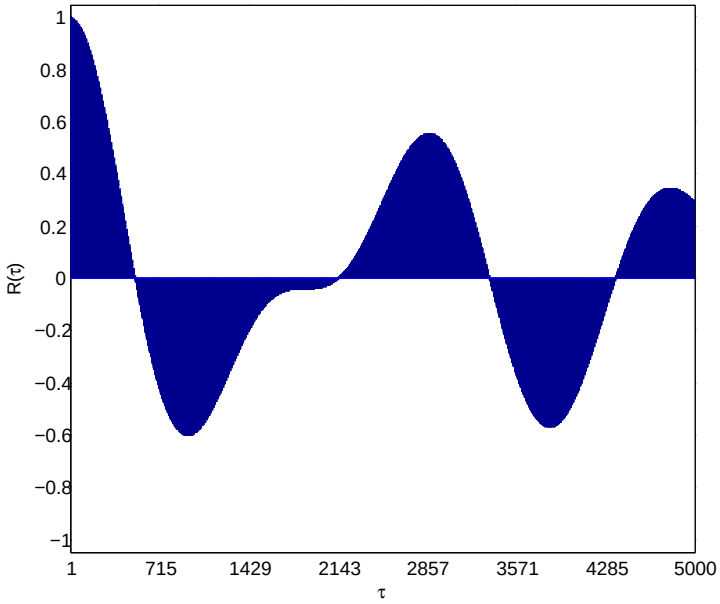

(b) Autocorrelation function of the developed statistical model

Figure 5-10: Comparison between the autocorrelation function of: (a) the measured noise data register, and (b) simulated noise scenario

channels with varying degrees of conviction as to their accuracy. In this work, it is established that the measured noise time series exhibit volatility clustering by observing the noise sequence residuals. The applicability of a GARCH process derives from this observation. We conclude that asynchronous impulsive noise is heteroskedastic both in mean and variance and we have modelled it as such. The results show that the GARCH model captures the measured data adequately as evident in Figure 5-2. This model thus provides confidence in long-term forecasting of PLC impulsive noise as it has proven its usefulness over a long period of time (in mains cycles). The volatility in this case shows a cyclic behaviour, synchronous with the mains signal. Nonetheless, its applicability to non-cyclic noise sequences remains valid.

CHAPTER 6

Cyclostationary Spectral Identification and Analysis of broadband Power-Line Communication Impulsive Noise

6.1 Introduction

Usually, the impulsive signals originates from connected loads in a power network can often be characterized as cyclostationary processes. A cyclostationary process is described as a non-stationary process whose statistics exhibit periodic time variation, and therefore can be described by virtue of its periodic order. The focus of this chapter centres on the utilization of cyclic spectral analysis technique for identification and analysis of the second-order periodicity (SOP) of time sequences like those which are generated by electrical loads connected in the vicinity of a PLC receiver. Analysis of cyclic spectrum generally incorporates determining the random features besides the periodicity of impulsive noise, through the determination of the spectral correlation density (SCD). Its effectiveness on identifying and analysing cyclostationary noise is substantiated in this work by processing data collected at indoor low voltage sites.

The idea of utilizing powerline networks for communication purposes has gained considerable momentum in recent times owing to the ever growing demand for broadband services in indoor environments. Powerline communication (PLC) presents itself as a strong candidate for broadband transmission largely enabled by the recent advances in digital transmission techniques. The major drawback of PLC channels, apart from their complex topologies and unpredictable channel impedance, is their noise characteristics. The noise characteristics experienced by PLC channels are rarely stationary [46, 48, 53, 123–127], white [49–51, 128, 129], and Gaussian [23, 37, 130, 131]. Its characteristics are such that it is a superposition of numerous unrelated components with different statistical attributes. Various efforts have been made towards the development of simple statistical parametric models. In particular, cyclostationary models have been proposed on the basis of fitting the instantaneous PSD of

the noise sequence to measured data [46, 49, 53, 123–127], [128], [129]. Other contributions determines an accurate characterization of the probability density function (PDF) of the impulsive noise [50], [37, 130, 131].

As a subset of non-stationary processes, a cyclostationary process exhibits some cyclic time-variant statistics. The structure of cyclostationarity presents a formidable framework for characterizing PLC noise data sequences from electrical appliances. These particular kinds of signals are usually distinguished through their unique order of periodicity. Power supplies and other power loads can lead to generation of impulses exhibiting characteristics of first-order periodicity processes (FOP). Furthermore, amplitude modulated impulses generated by some appliances exhibit SOP processes.

This work presents an efficient way of detecting and analysing cyclostationary impulsive noise sequences synonymous with power line networks by utilizing the SOP form of signals via the cyclic spectral analysis. It is a process where random characteristics of a signal besides its cyclic behaviour are estimated. The spectral correlation density is estimated by computing the averaged cyclic periodogram. [132–134]. The detection and analysis of cyclic impulsive noise features using cyclostationarity is substantiated in this work by analysing noise data registers from indoor scenarios.

6.1.1 PLC Noise Sequence Acquisition

The focus of the measurement exercise was to capture high frequency (short-term) cyclostationary noise sequences that are usually not readily observable in measurements. Noise from several usage scenarios was captured and its cyclostationarity analysed. In this work, two noise profiles are analysed: one captured displaying only short-term noise periodicities (relative to the mains period) and the other showing both short-term and long-term periodicities of time (multiple mains cycles). All measurements were acquired using a RIGOL DS2202A digital oscilloscope (DSO) capable of storing up to 14 million data samples. The full scale data length capability of the scope is utilized with measurements carried out at the rate of 100 MS/s. We will refer to the data with only short-term cyclostationarity as short-term noise and that with both short- and long-term cyclostationary components as long-term noise data. The classification is only made to emphasise that short-term noise scenarios are more likely to be directly observable when performing short-term measurements. Nonetheless, their underlying characteristics can still be determined with long-term

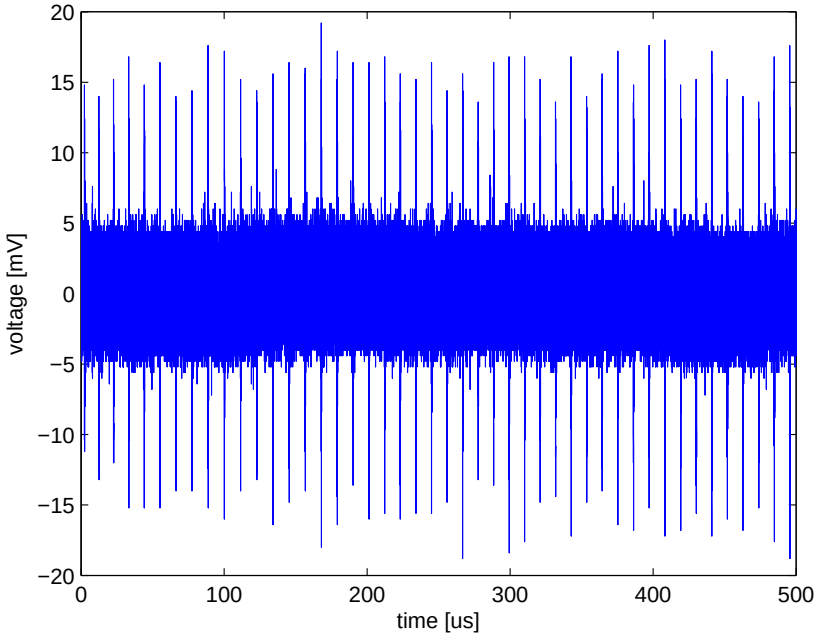

(a) Measured short-term noise sequence w_n

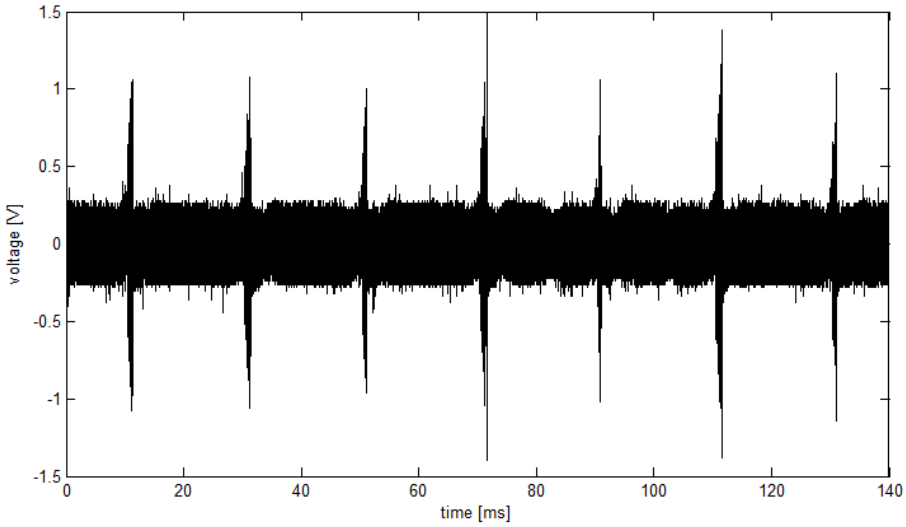

(b) Measured long-term noise sequence w_n

Figure 6-1: Noise data collected from an indoor setting (a) short-term cyclostationary noise, and (b) long-term cyclostationary noise

measurements provided high sampling rates are possible.

In order to safeguard the measuring instruments from the high mains voltage and possible surges, a broadband coupler (operating in the range 1 - 30 MHz) is used as an interface between the two contrasted environments. The coupler also serves as a relay of signals

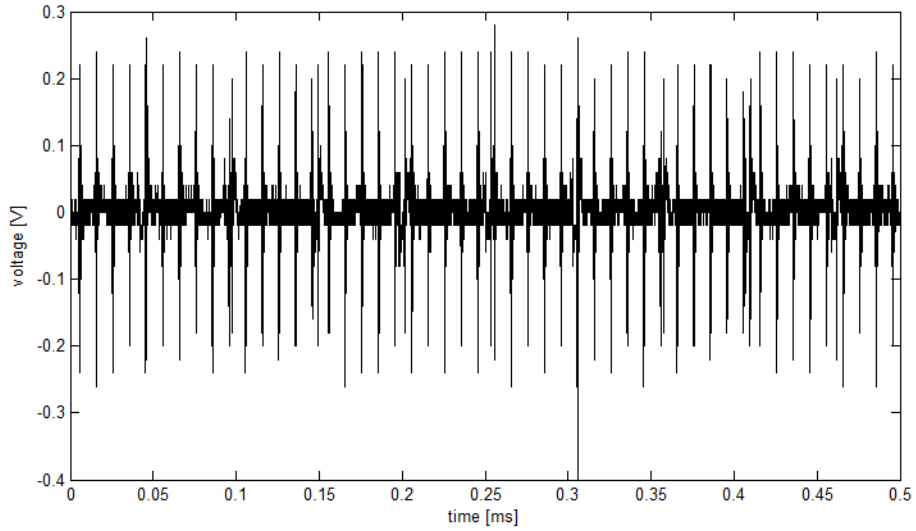

(a) zoomed-in cyclostationary noise data sequence

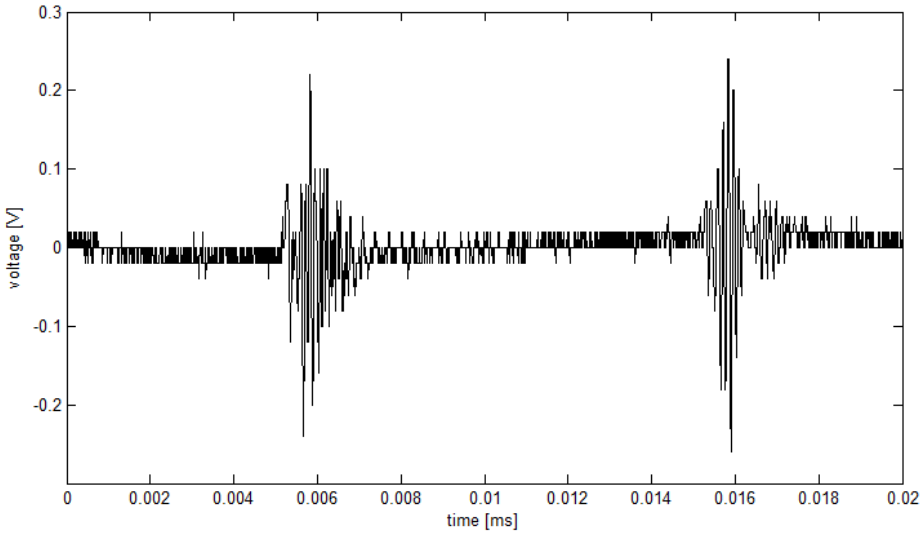

(b) Zoomed-in modulated impulsive noise

Figure 6-2: High frequency cyclostationary noise hidden within the dominant synchronous impulsive noise: (a) High frequency cyclostationary noise, and (b) Modulated noise impulses

between the mains and the measuring instruments. Samples of measured noise sequences are shown in Figure 6-1 depicting the two scenarios of short-term and long-term noise data in Figure 6-1(a) and Figure 6-1(b) respectively. However, due to the dominance (in terms of amplitude) of the noise terms synchronous with the mains frequency, the short-term noise sequences appear to be completely buried and unobservable in Figure 6-1(b). A two-stage zoom into the noise sequence of Figure 6-1(b) shows that alongside the synchronous noise components, there exists other periodicities as depicted in Figure 6-2(a) and 6-2(b). These

hidden periodicities of the signal energy flow are periodically modulated as seen in Figure 6-2(b).

6.1.2 Cyclostationarity Analysis

A cyclostationary event is generally a process of stochastic nature with evidence of unobservable periodicities often referred to as *periodically correlated* processes [133]. A non-stationary process $f_x(x,t)$ is considered cyclostationary if it exhibits periodicity in some of its statistics.

$$f_x(x,t) = f_x(x,t+T), \tag{6.1}$$

where $f_x(x,t)$ represents a suitable statistic of the signal that varies with time. Typically, cyclostationary signals can be generated through the periodic amplitude or frequency modulation of a process that is stationary in nature. A signal $x(t)$ is termed n^{th} order cyclostationary with period T provided it has moments of order n with cyclic period T. A process that exhibits first-order periodicity (FOP) has a finite magnitude additive cyclic part and thus, as a result, exhibits lines (Dirac delta functions) in its power spectral density (PSD). It is possible to resolve its components given a data sequence by synchronous averaging. Considering that its mean is time-variant, we may consider a FOP process as non-stationary. Signals which exhibit second-order periodicity (SOP) are those that can be transformed into those with FOP through quadratic time invariant transformation [135]. Although their mean may be constant, these types of signals rather exhibit time-varying autocorrelation function (ACF). Stochastic processes exhibiting either amplitude or frequency modulation are typically in the family of SOP signals. Some electrical appliances generate impulses modulated in their amplitude, resulting in SOP.

Second-order techniques derive their usefulness from the autocorrelation function. The instantaneous autocorrelation, the Wigner-Ville spectrum, as well as the spectral correlation are second order techniques obtained by linearly transforming the autocorrelation function. Consider a cyclostationary process $x(t)$, its autocorrelation function (ACF) can be calculated as

$$R_{xx}(t,\tau) = E\{x(t+\bar{\beta}\tau)x(t-\beta\tau)^*\}, \tag{6.2}$$

here $\bar{\beta} + \beta = 1$. For $x(t)$ to be cyclostationary with time T, it follows also that its

autocorrelation function is a periodic with T. Therefore,

$$R_{xx}(t,\tau) = R_{xx}(t+T,\tau), \tag{6.3}$$

which can be decomposed into their Fourier series with the Fourier terms of the autocorrelation function corresponding to the periodic ACF (CACF)

$$R_{xx}(\tau,\alpha) = \int R(t,\tau)e^{-j2\pi\alpha t}dt, \tag{6.4}$$

where α corresponds to the cyclic frequencies. The cyclic ACF indicates the amount of energy carried by the process due to cyclostationarity for every given frequency α. It should be mentioned that for $\alpha = 0$, the CACF results in the classical autocorrelation function. Its Fourier transform is called the cyclic power spectrum and it is defined as:

$$S^{\alpha}_{xx}(\alpha,f) = \int R_{xx}(\tau,\alpha)e^{-j2\pi f\tau}d\tau, \tag{6.5}$$

It is immediately noticeable that correlation in the spectrum will be continuous in frequency f while discrete in α. Considering the case $\alpha = 0$, the cyclic spectrum resembles the classical power spectrum or spectral density function (through the Wiener-Khinchin relation) [133].

6.1.3 Cyclic Spectral Analysis: Application to PLC Noise

In numerous scenarios, impulsive noise sequences generated by switch mode power supplies may be characterized as cyclostationary processes. Essentially, cyclic spectral analysis is suitable for statistically describing the stochastic aspects of a cyclostationary impulsive noise register, and also the description of its cyclic behaviour. This chapter focuses on impulsive noise sequences acquired at a plug of a typical indoor setting as opposed to acquiring noise from specific appliances. The noise sequence acquired at a wall plug generally exhibits second order cyclostationarity and even higher. Nevertheless, these components usually tend to have a negligible energy in comparison with the strong cyclic signals produced by the electrical appliances. Noise generated at a wall plug is normally *poly*-cyclostationary owing to the fact that numerous periodicities as well as cyclic modulations associated with various electrical appliances may be part of the raw data registers.

Practically, it is necessary for digital signal processing (DSP) techniques to determine the periodic statistics of a cyclostationary process. For this purpose, the Welch's *Averaged Cyclic Periodogram* (ACP) has been used, popular among other estimators employed for estimating the spectral correlation function, owing to its low computational intensity [132]. In the cycle spectrum, the cyclic frequencies α, are multiples of the reciprocal of the period of the cyclostationarity. The ACP is defined such that

$$S_{xx}^{\alpha}(f,\alpha) = \frac{1}{K\Delta t}\sum_{k=1}^{K} X_N^{(k)}(f+\beta\alpha)X_N^{(k)}(f+\beta\alpha)^*, \tag{6.6}$$

where $X_N^{(k)}$ is the discrete time Fourier transform of the k^{th} sequence. The effect of cyclic leakage is mitigated by incorporating an overlap between adjacent segments of the signal. In minimizing the prevalence of cyclic leakage, the overlap required when using a Hamming or Hanning data window should be $\geq 67\%$. [132]. For the analysis of cyclostationary signals, the cyclic coherence function is an effective tool in the determination of the strength of correlation between spectral components equally separated by a cyclic frequency. The cyclic coherence function is normalized between 0 and 1. It can be computed for a single process in the following manner:

$$\gamma_{xx}(f,\alpha) = \frac{S_{xx}(f,\alpha)}{[S_x^0(f+\bar{\beta}\alpha)S_x^0(f-\bar{\beta}\alpha)]^{\frac{1}{2}}} \tag{6.7}$$

where S_x^0 is the autocorrelation function at $\alpha = 0$. As such it is reduced to the classical spectral density function.

6.1.4 Cyclic Coherence Function for Cyclostationarity Testing

It is straightforward to realise that $|\gamma_{xx}(f,\alpha)|^2$ is normalized between 0 and 1 much as an ordinary coefficient of correlation, therefore it represents a measure of correlation having the unique property of being independent of the signal power spectrum [132]. Considering the cyclic coherence function, it is immediately evident that it is a direct generalization of the standard coherent function $\gamma_{xx}(f,0)$ of stationary processes [136]. Moreover, it can also be interpreted when $\alpha \neq 0$: a cyclic coherence near 1 for a certain cyclic frequency α shows a jointly strong cyclostationarity between the two signals at that particular cyclic frequency (regardless of the strength of their coherence at $\alpha = 0$) [132]. Additionally, the

cyclic coherence function is well suited for application on a single signal so as to determine the strength of its cyclostationarity at cyclic frequency α.

There are certain relevant results with regards to the bias and variance of the squared modulus $|\gamma_{xx}(f,\alpha)|^2$ which proves to be the principal quantity of interest in real world practices. Before the application of this quantity, the statistical analysis of $|\gamma_{xx}(f,\alpha)|^2$ compel that two cases be distinguished: (1) the case H_1 where the analysed signals are jointly cyclostationary such that $\gamma_{xx}(f,\alpha) \neq 0$, (2) the case H_0 where the analysed signals are jointly stationary such that $\gamma_{xx}(f,\alpha) \equiv 0$ [132]. It is at this point that the previous results can be used to design a straightforward and yet formidable hypothesis test for testing for the presence of cyclostationarity at a given cyclic frequency α. For any two finite length signals, the idea is to test the null hypothesis H_0 against the alternative hypothesis H_1 at the level of significance of $100p$ %. This can be accomplished by the following means: Reject H_0 if there exists some (non-singleton) frequency interval $\asymp$ where

$$|\gamma_{xx}(f,\alpha)|^2 \geqslant \frac{\Re_v}{2}\chi^2_{1-p,2}, \qquad \forall f \in \asymp \tag{6.8}$$

with $\chi^2_{1-p,2}$ the $100(1-p)$ % percentile of the χ^2_2 distribution and

$$\Re_v = \sum_{k=-K+1}^{K-1} R_w[kP]^2 . \frac{K-|k|}{K^2}, \tag{6.9}$$

where, for a data sequence of window length N_w, k represents weighted sequences, K is the number of averages and $P \in [1, \quad N_w]$ is the number of samples used for window shifting. $R_w[k] = \sum_n w[n-k]w[n]$ is the autocorrelation function of the data window $w[n]$. The proposition of (6.8) is established by observing that under the null hypothesis the quantity $2|\gamma_{xx}(f,\alpha)|^2/\Re_v$ asymptotically follows a chi-square distribution with 2 degrees of freedom with mean and variance given by $\Re_v$ and $\Re_v^2$ respectively.

6.1.5 Simulation and results

In this work, cyclic spectra as well as cyclic coherence functions are determined for two noise sequences registered in an indoor environment. As an illustration of the results obtained using the cyclic spectral analysis, Figure 6-3(a) and 6-3(b) depicts the cyclic coherence function corresponding to the measured data in Figure 6-1(a) and 6-1(b) respectively. As it is evident in the two figures, the cyclic coherence function reveals the underlying periodicities

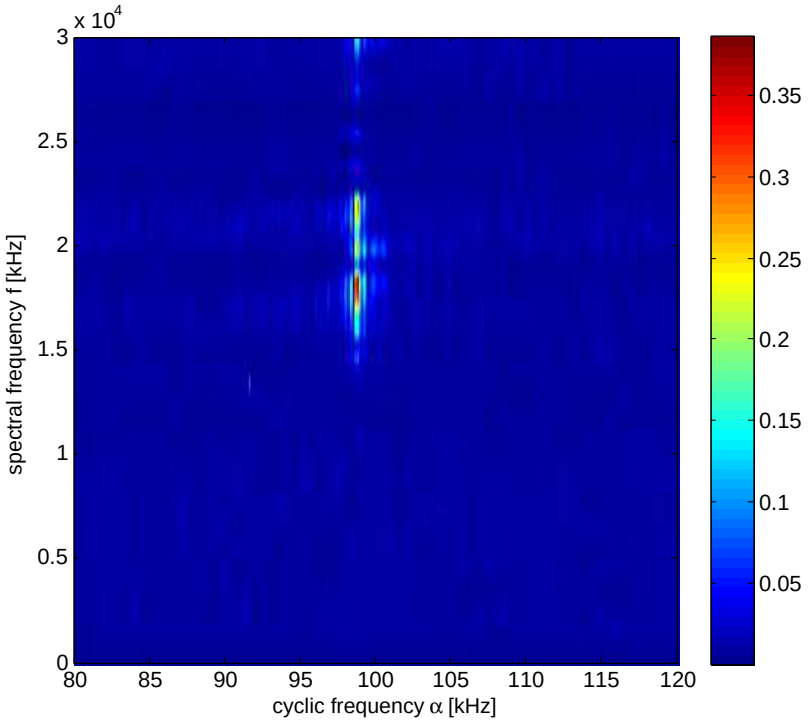

(a) Cyclic Spectral Coherence of the short-term noise

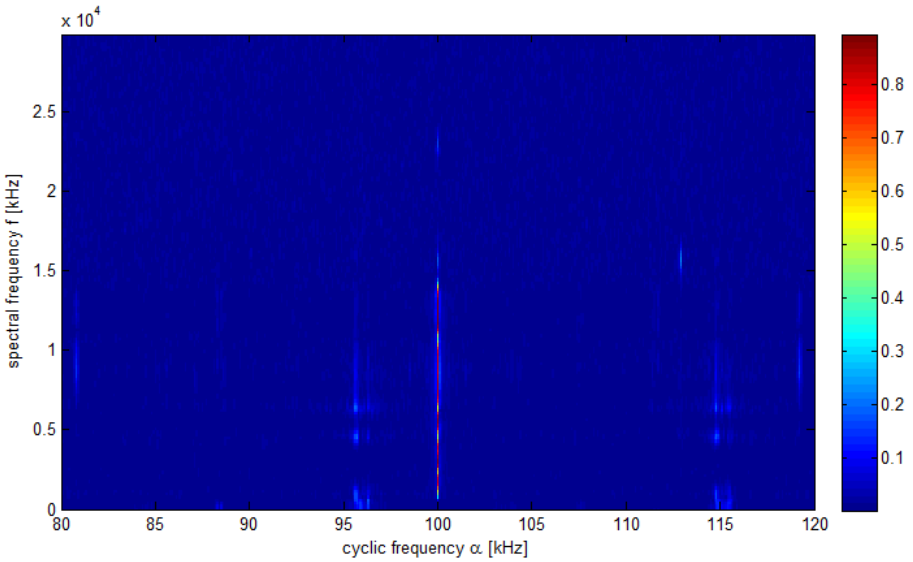

(b) Cyclic Spectral Coherence of the long-term noise

Figure 6-3: The cyclic spectral coherence of two high frequency cyclostationary signals measured at a wall plug

in each case. To clarify the presence of periodicities in the noise data, a cyclic spectral density (CSD) is calculated and presented in Figure 6-4(a) and 6-4(b). CSD, being a density function

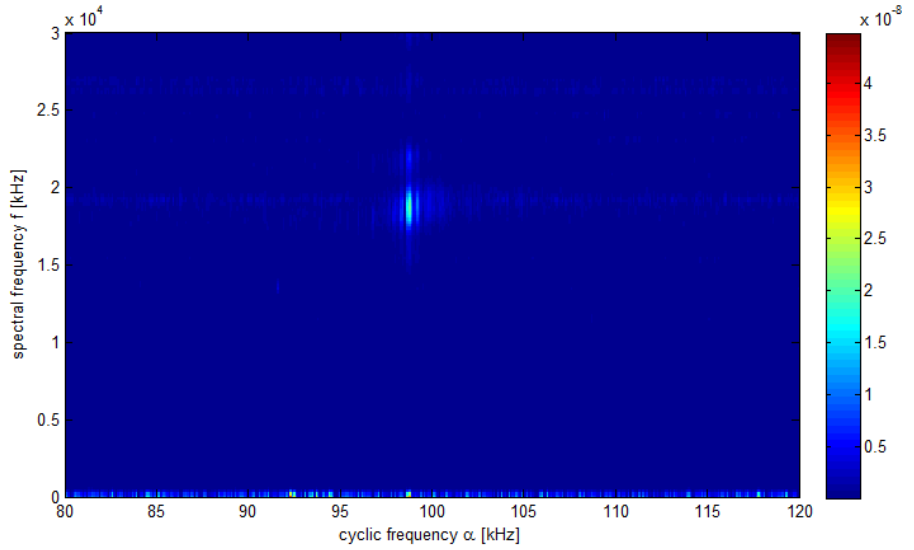

(a) Cyclic Spectral Density of the short-term noise

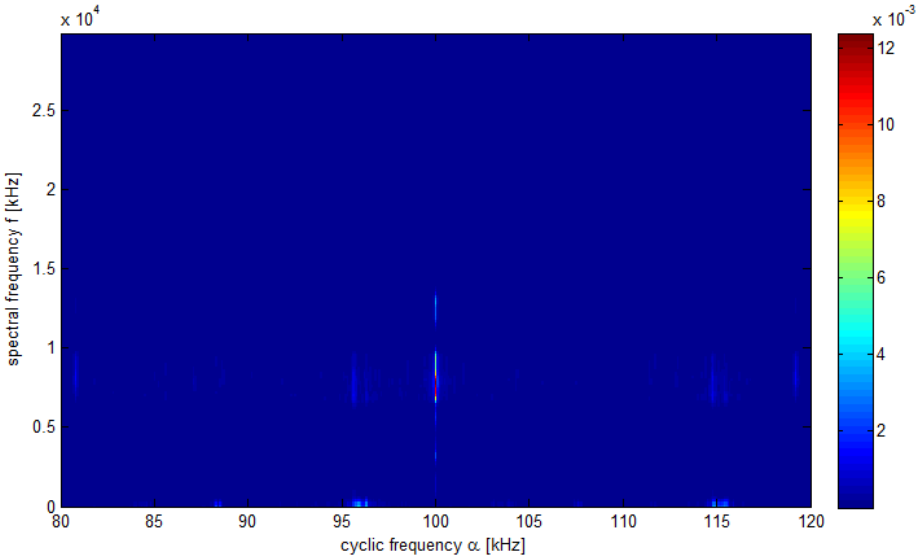

(b) Cyclic Spectral Density of the long-term noise

Figure 6-4: The cyclic spectral density of two high frequency cyclostationary signals measured at a wall plug

overcomes the problem of cyclic modulation spectrum. The energy normalization of the cyclic spectral density leads in the spectral coherence, whose magnitude squared takes only values between 0 and 1, and provides a unitless measurement of strength of correlation in the frequency domain. The results of this treatment are shown in Figure 6-5(a) and 6-5(b). The squared magnitude of the cyclic spectral coherence is shown alongside its 1% level of significance. The graphs show that the measured short-term noise has a cyclic component at

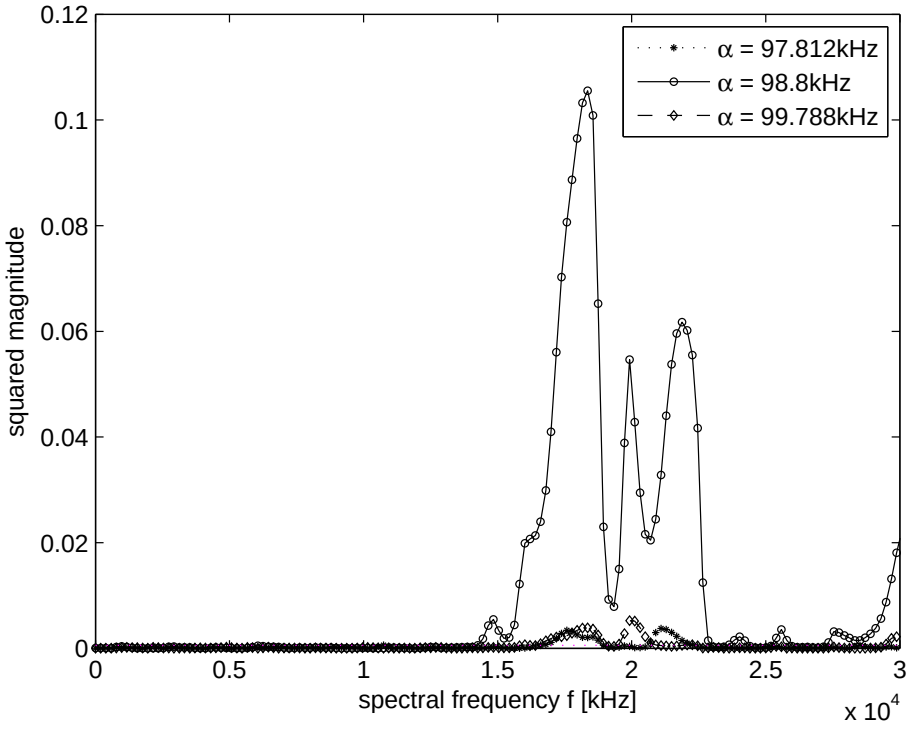

(a) Squared magnitude cyclic spectral coherence and its 1% level of significance for short-term noise

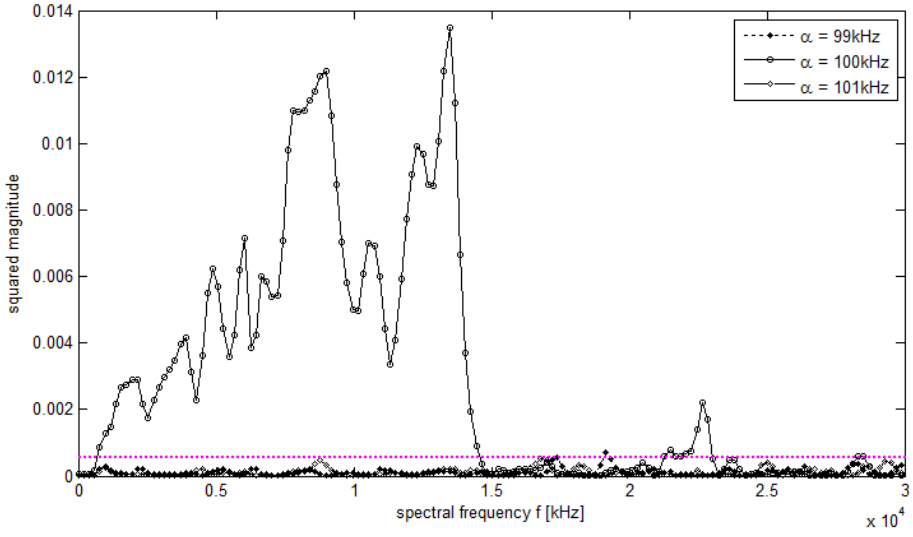

(b) Squared magnitude cyclic spectral coherence and its 1% level of significance for long-term noise

Figure 6-5: Squared magnitude cyclic spectral coherence and its 1% level of significance for two cyclostationary signals measured at a wall plug

$\alpha \simeq 98.8$ kHz while that extracted from long-term noise measurement has a cyclic frequency $\alpha \simeq 100$ kHz. Moreover, though not presented here (due to scale disparity between the

short-term and long-term periodic components), the long-term noise sequence has another periodicity at the mains first harmonic frequency $\alpha \simeq 50$ Hz. It is observed in Figure 6-5(a) and 6-5(b) that the spectral widths of these periodicities can be deduced. The spectral content of these cyclic components is measured with respect to the threshold (1% significant level) specified in (6.8). In Figure 6-5(a), the short-term noise has its spectral content in the band [0.15 0.225] normalized to the sampling frequency (100 MHz). We also observe some weak cyclostationarity at values of $\pm 1\%\alpha$. On the other hand, the spectral content of the long-term noise sequence is within [0.01 0.15] as shown in Figure 6-5(b) normalized to the sampling frequency of 100 MHz.

6.2 Parameter Estimation for Linear Regression Models

Parameter estimation of linear regression models usually employs LS and maximum likelihood estimators. While ML remains one of the best estimators within the classical statistics paradigm to date, it is highly reliant on the assumption about the joint probability distribution of the data for optimal results. In this work we use the GMM to address the deficiencies of LS/ML in order to estimate the underlying data generating process (DGP). We use GMM as a statistical technique that incorporates observed noise data with the information in population moment conditions to determine estimates of unknown parameters of the underlying model. Periodic impulsive noise (short-term) has been measured, deseasonalized and modeled using GMM. The numerical results show that the model captures the noise process accurately.

The ever increasing interest in power-line communications (PLC) has encouraged research on channel modeling for indoor power environments [137–140]. Numerous research endeavours available in the literature provide evidence that the characteristics of the noise suffered by indoor power-line channels are generally particularly different from those experienced in their wireless counterparts. Actually, PLC noise is seldom stationary [53, 123–127, 141], white [49–51, 128, 129], and Gaussian [23, 37, 130, 131], and should thus be characterized as the superposition of individual unrelated components, represented by different statistical attributes. The complexity of PLC noise modeling has not deterred researchers' efforts, with numerous endeavours been made towards developing simplified parametric statistical models. More prominently is the proposal of cyclostationary models, based on

fitting the instantaneous power spectral density (PSD) of the noise data to experimental measurements [49, 53, 123–127, 141], [128, 129]. Alternative approaches contributes by determining an accurate characterization of the PDF of the impulsive component of PLC noise [50], [37,130,131]. Most of the work done in the area of PLC noise modeling, available in the technical literature, extract the model parameters from a series of measurement data. Computer simulations are then used to asses the performance of these models as applied to powerline communication systems [37, 50, 52, 125, 127, 130].

In this work, we introduce the use of General Method of Moments (GMM) to estimate parameters of linear regression models used in the modeling of cyclostationary impulsive noise produced by electrical appliances in indoor environments. GMM estimation provides a computationally convenient way of estimating parameters of time series models. It is equally applicable to both linear and non-linear models. Irrespective of the application, GMM estimation is based on a quantity known as the population moment condition, which is a statement that some function of the data and parameters has expectation equal to 0 when evaluated at the true parameter value. The model still works even when the underlying process indicates more moment conditions than there are parameters to be estimated. Naturally it is desirable to use as much of the available information as possible. Instead of satisfying one moment condition and violate the other, we use the GMM strategy to determine an estimator that provides balance amongst population moment conditions, seeking residuals that trade off violations amongst moment restrictions. Thus, GMM is a robust semi-parametric estimation framework as it requires less information and is built on more general characteristics of the noise data. With this approach, we are able to use up to higher order moment conditions to determine model parameters and model the data generating process.

6.2.1 Data Acquistion & Treatment

In this work, the interest is to model short periodicity PLC noise caused by appliances connected in the power network. Our measurement system was set-up to capture 2.8 million noise samples at a sampling frequency f_s=2 GHz. The RIGOL DS2202A digital oscilloscope (DSO) was used for this purpose, with a coupling circuitry having a passband within 1-30 MHz. The coupler protects the measuring equipment from the mains voltage as well as provide the necessary filtering. The cyclostationary period of the measured impulsive noise corresponds to 22,222 sampling intervals and thus has a cyclic frequency of 90 kHz.

In order to develop accurate regressive models for powerline time series, it is imperative that we transform the periodic noise sequence into a stationary one. It is still practical to develop periodic (non-stationary) time series models, only that they are suitable for small sample acquisitions. It is common practice to employ differencing techniques to achieve stationarity, but unfortunately with this approach, periodicity cannot be eliminated. In this work, we adopt the approach of [53] which is specifically designed to remove periodicity. We consider a data sequence $z_{t,m}$ with a period, t (usually referred to as year) containing m seasons (periodicities) in it, that is:

$$w_{t,m} = \frac{z_{t,m} - \mu_m}{\sigma_m} \tag{6.10}$$

where μ_m and σ_m are the fitted mean and standard deviation for the m^{th} season. The fitted means and standard deviations can be obtained through standard formulae.

$$\mu_m = \frac{1}{N}\sum_{t=1}^{N} z_{t,m}, \qquad m = 1, 2, \ldots, s \tag{6.11}$$

and

$$\sigma_m = \left[\frac{1}{N}\sum_{t=1}^{N}(z_{t,m} - \mu_m)^2\right]^{1/2}, \qquad m = 1, 2, \ldots, s \tag{6.12}$$

The cyclostationarity/periodicity is then restored by reversing the process of (6.10). The measured cyclostationary time sequence is shown in Figure 6-6 with its deseasonalized sequence depicted in Figure 6-7. The deseasonalized sequence exhibits high levels of correlation between samples, indicating that it cannot be described as white noise. However, it is wide-sense stationary and Gaussian.

6.2.2 Generalized Method of Moments (GMM)

The applicability of parameter estimation based on population moment conditions has a long tradition in statistics dating back at least to the method of moments (MM) principle [142] introduced by in the late nineteenth century. The MM principle is suitable for applications where $\kappa = p$. Here p is the number of parameters to be estimated and κ is the number of moment conditions. However, there are numerous cases in time series analysis where the underlying model implies more moment conditions than there are parameters to be estimated, that is $\kappa > p$. In such cases, the MM principle does not work but *Generalised*

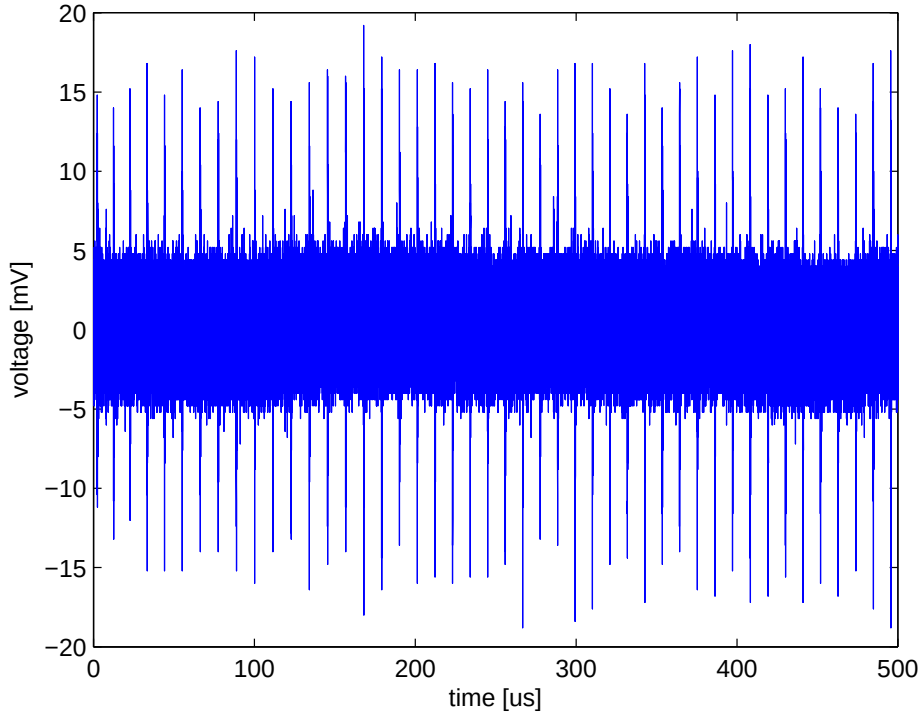

Figure 6-6: Sample time sequence of the periodic impulsive noise

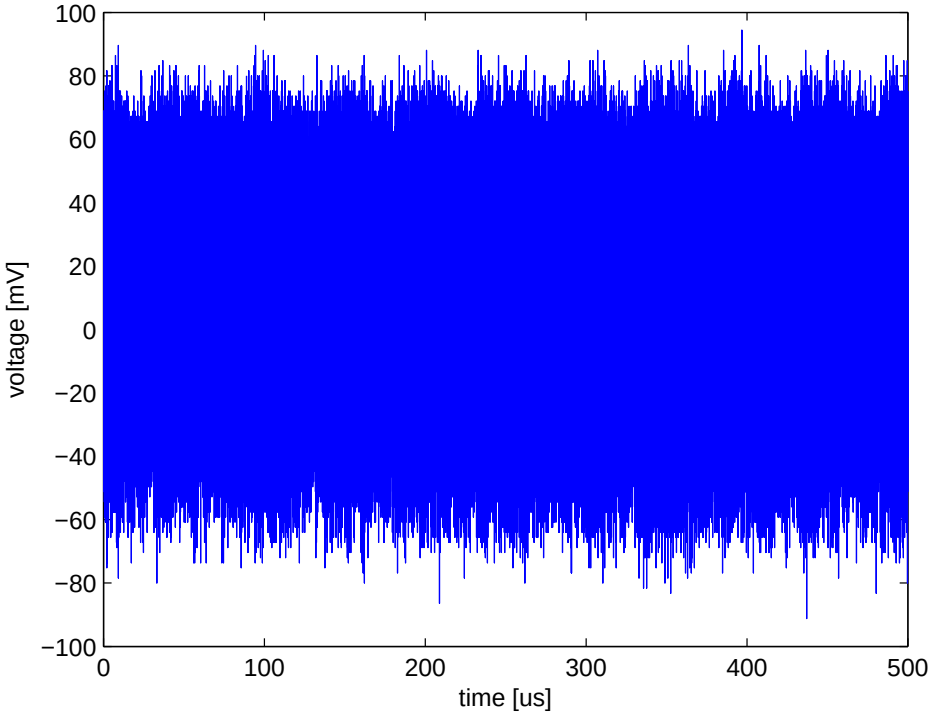

Figure 6-7: Deseasonalized noise sequence

method of moments works seamlessly. GMM sets itself apart as a technique of choice when its requirements are well comprehended in comparison with those for Maximum Likelihood (ML). Notwithstanding the fact that ML is arguably the best available estimator within the classical statistics paradigm, its optimality stems from its basis on the joint probability distribution of the data. However, in many scenarios, powerline communications in particular, this dependence on the probability distribution can become a weakness. This is because the underlying theoretical model imposes restrictions on the distribution of the data whilst not completely specifying its form. Consequently, ML is not feasible unless a decision is made to impose an arbitrary assumption regarding the distribution. The latter is not a favourable procedure primarily because in the event that the assumption about the distribution is wrong, then the optimality of ML is compromised, which may cause the estimator to be inconsistent. [142]. Fortunately, it transpires that in numerous scenarios where the time series model fails to completely specify the distribution, population moment conditions can be specified. According to these conditions, GMM would be preferable to ML since it provides a way to determine parameters based simply on the information deduced from the underlying data sequence. Generalized method of moments is an estimation strategy that enables time series models to be specified while circumventing the usual undesirable or needless assumptions, like designating a specific error distribution. It is this lack of structure that lands GMM wide applicability. It should be noted, however, that this generality may lead to questionable performance when dealing with small samples. The application can thus be a compromise between accuracy and simplicity by the researcher.

Derivation of GMM starts by determining the population moment condition.

Definition 1: (Population moment condition). Suppose w_t is a vector sequence of random variables, θ_0 be a $p \times 1$ vector of parameters, and $g(.)$ be a $\kappa \times 1$ vector valued function. The population moment condition is defined.

$$E[g(w_t, \theta_0)] = 0 \tag{6.13}$$

That is, a population moment is an assertion that some function of the data and parameters has a zero expectation under the actual parameter value evaluation. It is conceivable that $g(.)$ may vary with time and thus could be substituted with $g_t(.)$. For simplicity of

interpretation the more general illustration will not be considered.

Definition 2: (Sample moment condition). The sample moment condition is derived from the average population moment condition,

$$g_\eta(w, \theta) = \eta^{-1} \sum_{t=1}^{\eta} g(w_t, \theta). \tag{6.14}$$

The GMM estimator is defined at the value of θ that minimizes

$$Q_\eta(\theta) = \left[\frac{1}{\eta} \sum_{t=1}^{\eta} g(w_t, \theta) \right]' W_\eta \left[\frac{1}{\eta} \sum_{t=1}^{\eta} g(w_t, \theta) \right]. \tag{6.15}$$

Thus the GMM estimator is defined as

$$\hat{\theta} = \arg\min_{\theta} Q_\eta(\theta) \tag{6.16}$$

where W_η is a $\kappa \times \kappa$ positive semi-definite matrix. W_η may (and generally will) depend on the data but it is required to converge in probability to a positive definite matrix for the estimator to be well defined. In order to operationalize the GMM estimator, κ, the number of moments, will be required to be greater than or equal to p, the number of unknown parameters.

6.2.3 Simulation and Measurement Results

We have introduced GMM to drive the modeling of the time-varying PLC impulsive noise. The dynamics of the time-varying noise sequence is captured by an autoregressive process (AR) which specifies the output variable to be dependent linearly on its own previous values coupled with a stochastic error term (see full treatment in [53]). Given these moment conditions, we approximate the unknown dynamics of the time-varying parameter by an autoregressive process whose shocks are linear transformations of the scaled gradient of the conditional GMM objective function. The statistical accuracy of our model is specified in terms of the sum of squared residuals.

The simulated and measured noise sequences are depicted in Figure 6-8. The high frequency cyclostationary impulsive noise occurs rapidly over short periods of time and this model may thus be considered a short-term model. This is because over a longer period of

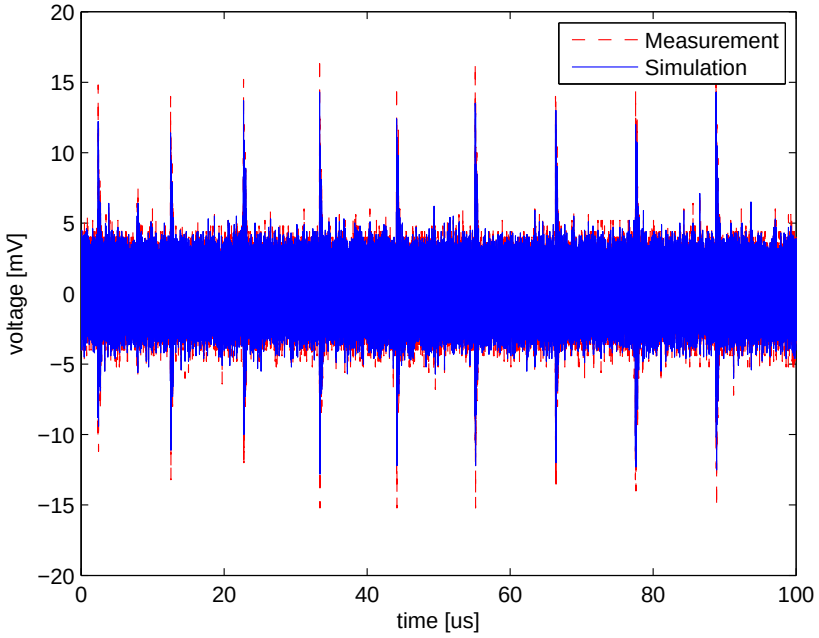

Figure 6-8: Comparison between a sample measurement of periodic impulsive noise and simulated GMM sequence

time (>mains period), there is also evidence of mains periodicity which should be modeled separately. The sum of squared residuals, SSR=0.7944 and $R^2 = 0.89$. The autocorrelation function of both the measured noise data sequence and the simulated one are shown in Figure 6-9(a) and 6-9(b), respectively, to validate the model.

6.3 Conclusion

This work has demonstrated that the impulsive cyclostationary noise in power line channels can be properly identified and analysed by applying the cyclic spectral coherence function to the noise data sequence. It is apparent, however, that this noise is dominated by synchronous impulsive components which can easily be visually inspected. It is rather the high frequency components that require detection techniques as it might not always be possible to identify these components, especially if they are buried under stationary noise. It is widely reported that noise measured in indoor environments is predominantly cyclostationary, hence this work serves to aid towards appropriate modeling of impulsive noise towards implementation in adaptive cyclic modulation schemes. The ACP estimator was employed in the determination of the spectral correlation density owing to its low computational complexity given

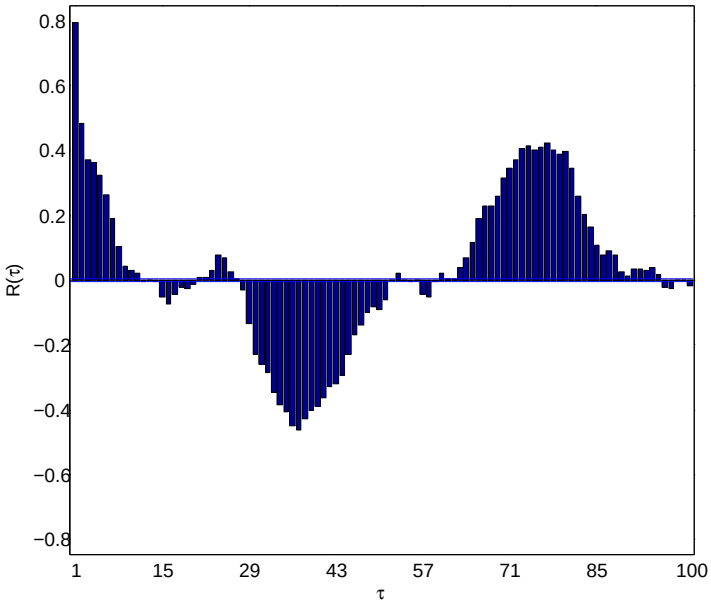

(a) Autocorrelation function of the acquired noise sequence

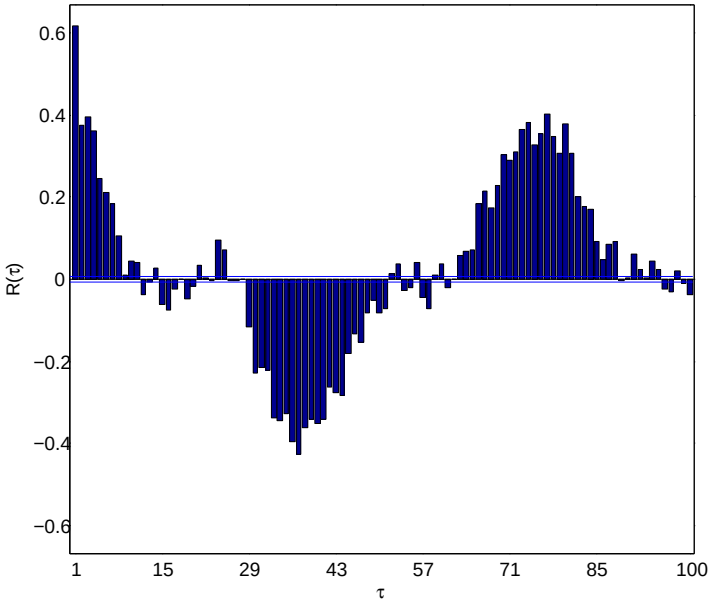

(b) Autocorrelation function of the developed statistical model

Figure 6-9: Comparison between the autocorrelation function of measured and simulated noise data sequences

the data lengths at hand (in order of millions). Nonetheless, other estimators can still be employed and compared, especially for small data lengths.

The chapter proceeds to introduce a robust approach to estimating linear regression model parameters. The generalized method of moments has been utilized to determine parameters of an autoregressive model for short-time periodic impulsive powerline communications noise in an indoor environment. The accuracy and applicability of the model relies on sample sequences measured and their subsequent deseasonalization for stationarity. The results show that the model has adequate accuracy and thus merit consideration in emulating PLC noise through computer simulations. It is however noted that in a lot of cases, traditional parameter estimators such as maximum likelihood and method of moments will suffice.

CHAPTER 7

Conclusions & Recommendations

7.1 Introduction

The future smart grid systems will autonomously monitor and control energy systems to enhance their efficiency and reliability. Intelligent control and monitoring demands low latency, highly reliable and two-way communication between customers, local utilities and regional utilities. In the present age of information technology, the current emphasis is on generation as well as dissemination of information. In order to be able to reach end users for the provision of information, alternative delivery strategies are necessary. Traditional technologies currently being employed include telephone loops, Ethernet cables, fibre optics, wireless and satellite technologies. Nonetheless, each technology is inherently limited with regards to cost and availability to reach the maximum number of consumers. Despite its potential to become a successful and widespread technology enabling high speed broadband internet and numerous network applications, PLC technology suffers from serious challenges from noise and channel attenuation which are the major channel impairments. These challenges result from the fact that the powerline network was not originally intended for data transmission, therefore PLC systems inherit the harsh intrinsic attributes of the powerline.

Smart Grids are becoming a reality all over the world. Currently, the research efforts for the introduction and deployment of these grids are predominantly focused on the development of the field of smart services. As an emerging application it requires the use of technology to access the numerous points of supply (PoS) prevalent in the grid, including the Low Voltage (LV) side with the minimum possible costs. Power Line Communications (PLC) have historically found extensive use in electrical grids for a diversity of applications and, of late, have been the focus of renewed interest. This technology is well suited for quick and inexpensive pervasive deployments. However, the fact that it is unlikely that any LV grid be the same as the other in any power utility company, and the particularities of each grid evolution, topology, conditions and materials, presents a challenge in the deployment of smart services networks with PLC technologies. Therefore, the evolution of smart ser-

vices networks and that of PLC technologies should converge to project PLC-enabled smart services networks with Smart Grid as the ultimate goal. Guidelines on strategic aspects of PLC smart services network is based on knowledge acquired on real PLC networks. The progress and evolution of PLC technology into different system specifications with subsequent application on real field to provide real services depends on the technology's low level specific details. Such details include: noise, channel characteristics, modulation schemes, MAC architectures, etc. Moreover, lack of power grid specific details in conventional scientific literature and even in the utility related associations makes it a difficult prospect in determining unified characterizations.

The core of this work relies on measurements acquired in various indoor scenarios. A detailed description of the measurements performed over these environments has been provided. The measurement setup, measurement equipment and the measurement methodologies are well stipulated in detail throughout this work. Subsequently, the analysis of the measured PLC channel transfer characteristics and noise data sequences is used to establish some preliminary grounds about the nature of the underlying generating processes.

The characterization and modeling of the indoor PLC channels has been performed during the course of this work. Considering an ensemble of measured channel transfer functions, indoor PLC channels have been characterized by statistically defining parameters such as channel correlation coefficient, RMS delay spread and coherence bandwidth. The statistics of these parameters are extracted from the data obtained in the above mentioned channel measurement campaign. To model the indoor PLC channels we have used two approaches: the top-down strategy and the bottom-up strategy. The top-down model is applied by considering the measured realistic PLC channel to be a multipath environment of unknown topology or structure. The parameters of the model are iteratively adapted to the channel transfer characteristics. In the case of the bottom-up strategy, two other channel models have been developed. In one case the model is of deterministic nature developed by considering the powerline to be a two-wire transmission line and applying the theory of transverse electromagnetic (TEM) wave propagation. The other model is developed by considering a powerline network to be a lattice structure. The lattice approach enables tracing of propagation paths hence we categorize this model as deterministic-multipath (DM). There is an added advantage to the lattice model in that the optimum number of paths can be determined for any given size of the power network, a key parameter often

reduced to vague estimates in literature. The simplicity of the models has been outlined and their validation shown in all cases.

Impulsive noise in indoor PLC networks has also been studied and characterized. We have shown that for a set of measured noise sequences, a simple automatic procedure can be adopted to extract the models from them. The highly volatile asynchronous noise has been characterized, proven to be heteroskedastic and modeled as a GARCH process. The Gaussianity of PLC noise has also been proven to be non-existent. Cyclic spectral analysis has been used to identify and analyze the second-order periodicity of the noise time series. The time-varying cyclostationary PLC noise has been modeled as an autoregressive (AR) process with the generalized method of moments (GMM) estimator employed. The models described in this work are simple and accurate, making them suitable to emulate noise effects in computer simulations of PLC systems.

7.2 Conclusions

7.2.1 Chapter 1

The work presented in this thesis is a contribution to the field of indoor powerline communications which is an emerging field in broadband communications. First and foremost the state of the art of the PLC technology is discussed. The historical evolution of PLC technology is provided and various standards developed over the years are also presented. We also introduce prominent groups and governing bodies responsible for preparation, inspection and regulation of these standards. The endeavours of numerous international projects instigated for the formulation of both research ventures and standardization is also discussed. Several industrial groups and telecom operators play a vital role in the PLC ecosystem, hence their contribution is also included.

7.2.2 Chapter 2

We have provided a brief introduction of the physical inhome PLC network. Major modeling methodologies for the indoor PLC channels are briefly discussed. Various prominent categories of the inhome PLC noises are also discussed.

7.2.3 Chapter 3

In this chapter we propose a broadband frequency-domain model for practical indoor power-line communication (PLC) channels. We consider a top-down strategy where the channel is regarded as a multipath propagation environment with frequency-selective fading. The model is based on the physical signal propagation effects of numerous PLC architectures which comprise unknown number of branches and load conditions. We further consider the attenuation of a typical power-line to be increasing with length as well as frequency. The applicability of the model is verified with measurements from real channels from our laboratories and offices within the band 1-30 MHz. The generated channel frequency response (CFR) has a good agreement with measurements results from real PLC channels. Furthermore, to improve the generality of the model application, we study the dispersive nature of these channels through their impulse responses (IR), and then compare our results with findings from elsewhere. The comparison is made in terms of the maximum excess delay, mean excess delay and root mean square (rms) delay spread. The chapter continues to present an alternative approach to model the transfer characteristics of power lines for broadband power line communications (PLC). The model is developed by considering the power line to be a two-wire transmission line and the theory of transverse electromagnetic (TEM) wave propagation applied. The characteristic impedance and attenuation constant of the power line are determined through measurements. These parameters are used in model simplification and determination of other model parameters for typical indoor multi-tapped transmission line system. The transfer function of the PLC channel is determined by considering the branching sections as parallel resonant circuits attached to the main line. The model is evaluated through comparison with measured transfer characteristics of known topologies and it is in good agreement with measurements.

7.2.4 Chapter 4

The transmission of high frequency signals over power lines, known as powerline communications (PLC), plays an important role in contributing towards global goals for broadband services inside the home and office. In this chapter, we aim to contribute to this ideal by presenting a powerline channel modeling approach which describes a powerline network as a lattice structure. In a lattice structure, a signal propagates from one end into a net-

work of boundaries (branches) through numerous paths characterized by different reflection/transmission properties. Due to theoretically infinite number of reflections likely to be experienced by a propagating wave, we determine the optimum number of paths required for meaningful contribution towards the overall signal level at the receiver. The propagation parameters are obtained through measurements and other model parameters are derived from deterministic powerline networks. It is observed that the notch positions in the transfer characteristics are associated with the branch lengths in the network. Short branches will result in fewer notches in a fixed bandwidth as compared to longer branches. Generally, the channel attenuation increase with network size in terms of number of branches. The proposed model compares well with experimental data.

7.2.5 Chapter 5

The chapter further discusses the estimation of powerline communication (PLC) asynchronous impulsive noise volatility by studying the conditional variance of the noise time series residuals. In this approach, we use the Generalized Autoregressive Conditional Heteroskedastic (GARCH) models on the basis that in our observations, the noise time series residuals indicates heteroskedasticity. By performing an ordinary least squares (OLS) regression of the noise data, the empirical results show that the conditional variance process is highly persistent in the residuals. The variance of the error terms are not uniform, in fact, the error terms are larger at some portions of the data than at other time instances. Thus, PLC impulsive noise often exhibit volatility clustering where the noise time series is comprised of periods of high volatility followed by periods of high volatility and periods of low volatility followed by periods of low volatility. The burstiness of PLC impulsive noise is therefore not spread randomly across the time period, but instead has a degree of autocorrelation. This provides evidence of time-varying conditional second order moment of the noise time series. Based on these properties, the noise time series data is said to suffer from heteroskedasticity. Numerical results provide evidence that the proposed model is capable of providing an accurate stochastic representation of the impulsive noise in the 1-30 MHz frequency band. The parameter estimates of the model indicates a high degree of persistence in conditional volatility of impulsive noise which is a strong evidence of explosive volatility.

7.2.6 Chapter 6

Parameter estimation of linear regression models usually employs least squares (LS) and maximum likelihood (ML) estimators. While maximum likelihood remains one of the best estimators within the classical statistics paradigm to date, it is highly reliant on the assumption about the joint probability distribution of the data for optimal results. In this paper we use the Generalized Method of Moments (GMM) to address the deficiencies of LS/ML in order to estimate the underlying data generating process (DGP). We use GMM as a statistical technique that incorporate observed noise data with the information in population moment conditions to determine estimates of unknown parameters of the underlying model. Periodic impulsive noise (short-term) has been measured, deseasonalized and modeled using GMM. The numerical results show that the model captures the noise process accurately.

7.3 Possible future prospects

The eventual application of PLC frameworks is inclined towards the progressive smart grid concept, broadband web, and various broadband services. The models and simulation procedures developed during this thesis work are relied upon to form part of the basis towards a fully digitized transmission model that might be utilized to evaluate the performance of the PLC framework. It is necessary to have realistic PLC channel and noise models to properly assess the performance of such systems. In view of smart grid applications, internet and other broadband applications, real-time communications is required. Multiple input multiple output (MIMO) is one of the emerging strategies in PLC which seeks to address these demands. With this regard, some future research possibilities are suggested.

- A lot of work has been done in PLC MIMO channel modeling but there has been very few proposals for physical-deterministic MIMO channel models thus far. In this approach, multi conductor transmission line (MTL) theory can be applied in view of MIMO PLC application. The deterministic models presented in this work can further be extended to accommodate MIMO application. The transmission line equations can be adapted in consideration of three-wire transmission lines prevalent in home environments. Obviously parallel channels will pose issues of interference due to lack of shielding, and this phenomena needs to be handled. Parasitic issues between channels

could also be a problem (channel correlation) and thus need to be studied.

- Modeling of noise in MIMO PLC has also received few proposals to date. The autoregressive model developed in this work using method of general moments can be extended to a MIMO application. By using vector autoregressive modeling, the noise characteristics can be captured and parameters such as cross-correlation determined. The noise power spectral density can also be evaluated to affirm similarity with measured data.

- It is common practice in literature to represent impulsive noise in powerline communications in terms of its arrival rate, amplitude, and duration. Classical probability distribution functions are often used to describe the statistics of these parameters. These parameters can be viewed as the inputs to a queueing process, hence the impulsive noise in PLC channels can be modeled as a queueing process.

APPENDIX A

Appendix

Derivation of total reflection/transmission combinations along numerous paths as viewed at branching points. Reflections from a fifth branch are considered in the equations. This is simply to affirm solution consistency at the fourth branch.

TYPE (1) Paths [Direct Paths]

$$\Psi^{(1)}_{br,1} = T_1 \tag{A.1a}$$

$$\Psi^{(1)}_{br,2} = T_1 T_2 \tag{A.1b}$$

$$\Psi^{(1)}_{br,3} = T_1 T_2 T_3 \tag{A.1c}$$

$$\Psi^{(1)}_{br,4} = T_1 T_2 T_3 T_4 \tag{A.1d}$$

TYPE (2) Paths [Single Reflection]

$$\Psi^{(2)}_{br,1} = r_2 T_1^2 + r_3 T_1^2 T_2^2 + r_4 T_1^2 T_2^2 T_3^2 + r_5 T_1^2 T_2^2 T_3^2 T_4^2 \tag{A.2a}$$

$$\Psi^{(2)}_{br,2} = r_3 T_1 T_2^2 + r_4 T_1 T_2^2 T_3^2 + r_5 T_1 T_2^2 T_3^2 T_4^2 \tag{A.2b}$$

$$\Psi^{(2)}_{br,3} = r_4 T_1 T_2 T_3^2 + r_5 T_1 T_2 T_3^2 T_4^2 \tag{A.2c}$$

$$\Psi^{(2)}_{br,4} = r_5 T_1 T_2 T_3 T_4^2 \tag{A.2d}$$

TYPE (3) Paths [Double Reflection]

$$\Psi^{(3)}_{br1} = 0 \tag{A.3a}$$

$$\Psi^{(3)}_{br,2} = r_1 r_2 T_1 T_2 + r_1 r_3 T_1 T_2^3 + r_1 r_4 T_1 T_2 T^3 T_3^2 + r_1 r_5 T_1 T_2^3 T_3^2 T_4^2 \tag{A.3b}$$

$$\begin{aligned}\Psi^{(3)}_{br,3} = {} & r_1 r_2 T_1 T_2 T_3 + r_2 r_3 T_1 T_2 T_3 + r_1 r_3 T_1 T_2^3 T_3 + r_2 r_4 T_1 T_2 T_3^3 \\ & + r_1 r_4 T_1 T_2 T^3 T_3^3 + r_2 r_5 T_1 T_2 T_3^3 T_4^2 + r_1 r_5 T_1 T_2^3 T_3^3 T_4^2\end{aligned} \tag{A.3c}$$

$$\begin{aligned}\Psi^{(3)}_{br,4} = {} & r_1 r_2 T_1 T_2 T_3 T_4 + r_2 r_3 T_1 T_2 T_3 T_4 + r_3 r_4 T_1 T_2 T_3 T_4 \\ & + r_1 r_3 T_1 T_2^3 T_3 T_4 + r_2 r_4 T_1 T_2 T_3^3 T_4 + r_1 r_4 T_1 T_2^3 T_3^3 T_4 \\ & + r_3 r_5 T_1 T_2 T_3 T_4^3 + r_2 r_5 T_1 T_2 T_3^3 T_4^3 + r_1 r_5 T_1 T_2^3 T_3^3 T_4^3\end{aligned} \tag{A.3d}$$

TYPE (4) Paths [Source Reflections]

$$\Psi^{(4)}_{br,1} = r_1 r_s T_1 + r_2 r_s T_1^3 + r_3 r_s T_1^3 T_2^2 + r_4 r_s T_1^3 T_2^2 T_3^2 + r_5 r_s T_1^3 T_2^2 T_3^2 T_4^2 \tag{A.4a}$$

$$\Psi^{(4)}_{br,2} = r_1 r_s T_1 T_2 + r_2 r_s T_1^3 T_2 + r_3 r_s T_1^3 T_2^3 + r_4 r_s T_1^3 T_2^3 T_3^2 + r_5 r_s T_1^3 T_2^3 T_3^2 T_4^2 \tag{A.4b}$$

$$\Psi^{(4)}_{br,3} = r_1 r_s T_1 T_2 T_3 + r_2 r_s T_1^3 T_2 T_3 + r_3 r_s T_1^3 T_2^3 T_3 + r_4 r_s T_1^3 T_2^3 T_3^3 + r_5 r_s T_1^3 T_2^3 T_3^3 T_4^2 \tag{A.4c}$$

$$\Psi^{(4)}_{br,4} = r_1 r_s T_1 T_2 T_3 T_4 + r_2 r_s T_1^3 T_2 T_3 T_4 + r_3 r_s T_1^3 T_2^3 T_3 T_4 + r_4 r_s T_1^3 T_2^3 T_3^3 T_4 + r_5 r_s T_1^3 T_2^3 T_3^3 T_4^3 \tag{A.4d}$$

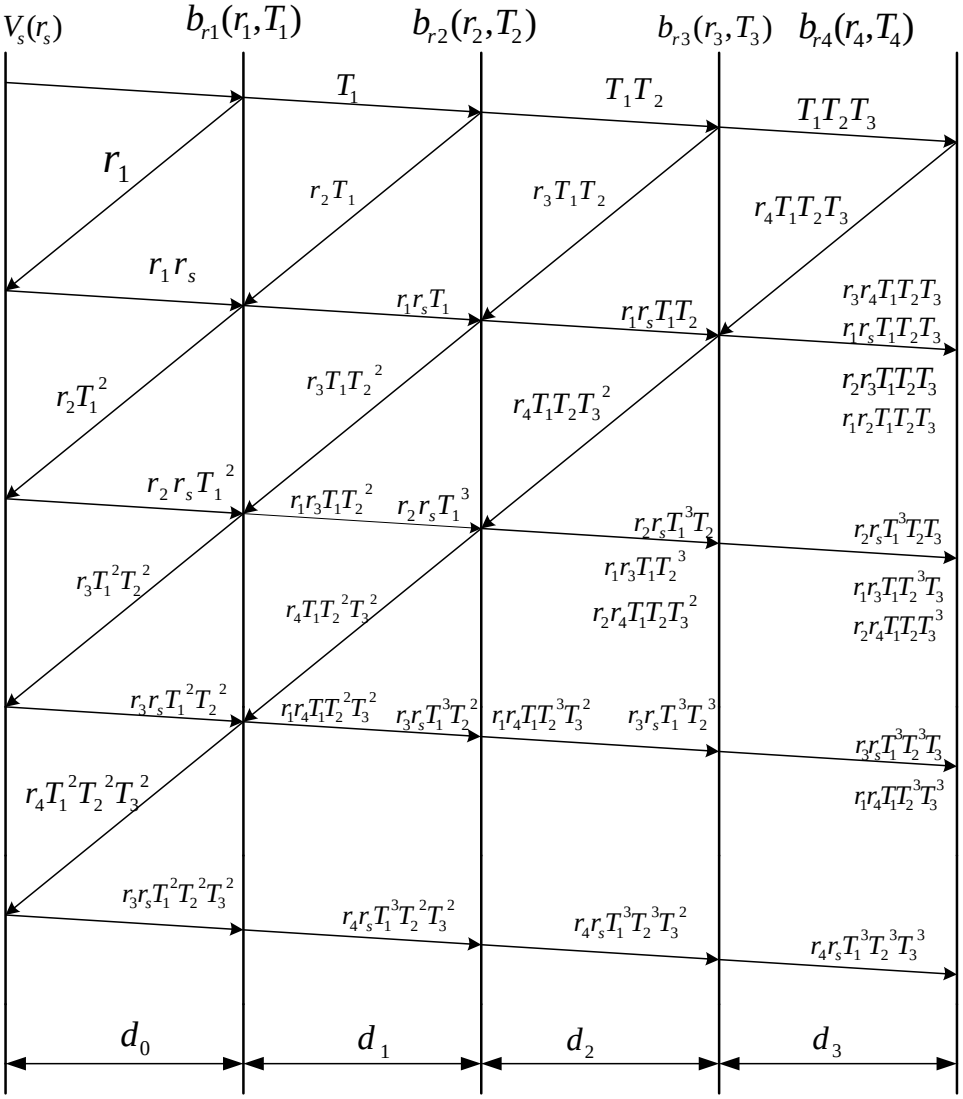

Figure A-1: Bounce Diagram for a Four-Branch Network

References

[1] P. A. Brown, "Power line communications - past, present, and future," in *Proc. of the 3rd Int. Symp. Power Line Commun. Appl.*, Lancaster, UK, March-April 1999, pp. 1–8.

[2] S. Galli and A. Scaglione, "A deterministic frequency-domain model for the indoor power line transfer function," *Proceedings of the IEEE*, vol. 99, no. 6, pp. 998–1027, 2011.

[3] M. S. Yousuf, S. Z. Rizvi, and M. El-Shafei, "Power line communications: an overview - part 2," in *Proc. 3rd Int'l Conf. Info. and Commun.Technologies: From Theory to Applications*, Damascus, Syria, April 2008, pp. 1–6.

[4] OMEGA, "Plc channel characterization and modeling," *Seventh Framework Programme: Theme 3*, vol. ICT-213311, 2008.

[5] [Online], "http://www.etsi.org/website/technologies/powerline."

[6] P. IEEE, "Draft standard for broadband over powerline networks: medium access control and physical layer specifications," 2010.

[7] "http://www.marketwired.com/press-release/atheros-introduces-worlds-first-powerline-solution-support-ieee-1901-homeplug-av-standards-nasdaq-athr-1182935.htm," 2010.

[8] G. ITU-T, "Technical paper: Transmission systems and media, digital systems and networks," 2010.

[9] HPA, "Homeplug power alliance: http://www.homeplug.org."

[10] UPA, "Universal power association: http://www.upaplc.org."

[11] CEPCA, "Consumer electronics powerline communication alliance: http://www.cepca.org."

[12] OMEGA, "Home gigabit access: http://www.ict-omega.org."

[13] POWERNET, "http://www.ist-powernet.org."

[14] OPERA, "http://www.ist-opera.org."

[15] I. C. E. 6.0, "Information technology equipment. radio disturbance characteristics-limits and methods of measurements," 2008-2009.

[16] K. Dostert, *Powerline Communications*. Prentice-Hall, 2001.

[17] G. Held, *Understanding Broadband over Power Line*. Auerbach Publications, 2001.

[18] H. C. Ferreira, L. Lampe, J. Newbury, and T. G. Swart, *Power Line Communications: Theory and applications for narrowband and broadband communications over power lines*. John Wiley & Sons, 2006.

[19] X. Carcelle, *Power Line Communications in Practice*. Artech House, 2006.

[20] M. Yousuf and M. E1-Shafei, "Power line communications: An overview - part i," in *Proc. 4th IEEE International Conference on Innovations in Information Technology*, Dubai, United Arab Emirates, November 2007, pp. 218–222.

[21] M. Zimmermann and K. Dostert, "Analysis and modelling of impulsive noise in broadband powerline communications," *IEEE Trans. Electromagn. Compat.*, vol. 44, no. 1, pp. 249–258, 2002.

[22] M. Gotz, M. Rapp, and K. Dostert, "Power line channel characteristics and their effect on communication systems design," *IEEE Commun. Magazine*, vol. 42, no. 4, pp. 78–86, 2004.

[23] H. Meng, Y. L. Guan, and S. Chen, "Modeling and analysis of noise effects on broadband power-line communications," *IEEE Tranections on Power Delivery*, vol. 20, no. 2, pp. 630–637, 2005.

[24] E. Biglieri and P. Torino, "Coding and modulation for a horrible channel," *IEEE Commun. Magazine*, vol. 41, no. 5, pp. 92–98, 2003.

[25] T. Banwell and S. Galli, "A novel approach to the modeling of the indoor power line channel part 1: circuit analysis and companion model," *IEEE Trans. Power Delivery*, vol. 20, no. 2, pp. 655–663, 2005.

[26] M. Zimmermann and K. Dostert, "A multipath model for the power line channel," *IEEE Trans. Commun.*, vol. 50, no. 4, pp. 553–559, 2002.

[27] H. Philipps, "Modelling of powerline communication channels," in *Proc. of the 3rd Int. Symp. Power Line Commun. Appl.*, Lancaster, UK, April 1999, pp. 14–21.

[28] S. Meng, S. Chen, Y. Guan, C. Law, P. So, E. Gunawan, and T. Lie, "A transmission line model for high-frequency power line communication channel," in *Proc. of Int'l Conf. Power Sys. Tech. (PowerCon)*, Kunming, China, October 2002, pp. 1290–1295.

[29] O. Hooijen, *Aspects of Residential Power Line Communications*. Shaker Verlag, 1998.

[30] M. Zimmermann and K. Dostert, "A multi-path signal propagation model for the power line channel in the high frequency range," in *Proc. of the 3rd Int. Symp. Power Line Commun. Appl.*, Lancaster, UK, March 1999, pp. 45–51.

[31] P. Amirshahi and M. Kavehrad, "High-frequency characteristics of overhead multiconductor power lines for broadband communications," *IEEE J. Sel. Areas Commun.*, vol. 24, no. 7, pp. 1327–1338, 2006.

[32] M. H. Chan and R. W. Donaldson, "Amplitude, width and interarrival distributions for noise impulses on intrabuilding power line communication networks," *IEEE Trans. Electromagn. Compat.*, vol. 31, no. 3, pp. 320–323, 1989.

[33] L. T. Tang, P. L. So, E. Gunawan, S. Chen, T. T. Lie, and Y. L. Guan, "Characterization of power distribution lines for high-speed data transmission," in *Proc. of Int'l. Conf. Power Sys. Tech. (PowerCon 2000)*, Perth, Australia, August 2000, pp. 445–450.

[34] D. Middleton, "Statistical-physical models of electromagnetic interference," *IEEE Trans. Electromagn. Compat.*, vol. 19, no. 3, pp. 106–127, 1977.

[35] A. Spaulding and D. Middleton, "Optimum reception in an impulsive interference environment-part i: Coherent detection," *IEEE Trans. Commun.*, vol. 25, no. 9, pp. 910–923, 1977.

[36] D. Middleton, "Procedures for determining the parameters of the first-order. canonical models of class a and class b electromagnetic interference," *IEEE Trans. Electromagn. Compat.*, vol. 21, no. 3, pp. 190–208, 1979.

[37] N. Andreadou and F. Pavlidou, "Plc channel: Impulsive noise modelling and its performance evaluation under different array coding schemes," *IEEE Trans. Commun.*, vol. 24, no. 2, pp. 585–595, 2009.

[38] H. Matsuo, D. Umehara, M. Kawai, and Y. Morihiro, "An iterative detection for ofdm over impulsive noise channel," in *Proc. of the 6th Int. Symp. Power Line Commun. Appl.*, Athens, Greece, March 2002, pp. 213–217.

[39] R. Pighi, M. Fraceschini, G. Ferrari, and R. Raheli, "Fundamental performance limits for plc systems impaired by impulsive noise," in *Proc. of the 10th Int. Symp. Power Line Commun. Appl.*, Florida, USA, March 2006, pp. 277–282.

[40] ——, "Fundamental performance limits of communications systems impaired by impulsive noise," *IEEE Trans. Commun.*, vol. 57, no. 1, pp. 171–182, 2009.

[41] M. Ghosh, "Analysis of the effect of impulsive noise on multicarrier and single carrier qam systems," *IEEE Trans. Commun.*, vol. 44, no. 2, pp. 145–147, 1996.

[42] Y. H. Ma, P. L. So, and E. Gunawan, "Performance analysis of ofdm systems for broadband power line communications under impulsive noise and multipath," *IEEE Trans. Power Delivery*, vol. 20, no. 2, pp. 674–681, 2005.

[43] S. Zhidkov, "Analysis and comparison of several simple impulsive noise mitigation schemes for ofdm receivers," *IEEE Trans. Commun.*, vol. 56, no. 1, pp. 5–9, 2008.

[44] ——, "Performance analysis and optimization of ofdm receivers with blanking nonlinearity in impulsive noise environment," *IEEE Trans. Vehicular Technology*, vol. 55, no. 1, pp. 234–238, 2006.

[45] S. V. Vaseghi, *Advanced digital signal processing and noise reduction*, 3rd ed. John & Wiley Sons, 2006.

[46] C. F. J. Canete, J. A. Cortes, L. Diez, and J. T. Entrambasaguas, "Analysis of the cyclic short-term variation of indoor power line channels," *IEEE J. Sel. Areas Commun.*, vol. 24, no. 7, pp. 1327–1338, 2006.

[47] S. Sancha, F. J. Canete, L. Diez, and J. T. Entrambasaguas, "A channel simulator for indoor power-line communications," in *Proc. of the 11th Int. Symp. Power Line Commun. Appl.*, Pisa, Italy, March 2007, pp. 104–109.

[48] M. Tlich, H. Chaouche, A. Zeddam, and P. Pagani, "Novel approach for plc impulse noise modeling," in *IEEE Int. Symp. Power Line Commun. Appl.*, Dresden, Germany, March-April 2009, pp. 20–25.

[49] J. A. Cortes, L. Diez, F. J. Canete, and J. Lopez, "Analysis of the periodic impulsive noise asynchronous with the mains in indoor plc channels," in *Proc. IEEE Int. Symp. Power Line Commun. Appl.*, Dresden, Germany, March-April 2009, pp. 26–30.

[50] N. Andreadou and F. N. Pavlidou, "Modeling the noise on the ofdm power-line communications system," *IEEE Trans. Power Del.*, vol. 25, no. 1, pp. 150–157, 2010.

[51] J. A. Cortes, L. Diez, F. J. Canete, and J. J. Sanchez-Matinez, "Analysis of the indoor broadband power-line noise scenario," *IEEE transections on Electromagnetic Compatibility*, vol. 52, no. 4, pp. 849–858, 2010.

[52] K. S. Al-Mawali, F. S. Al-Qahtani, and Z. M. Hussain, "Adaptive power loading for ofdm-based power line communications impaired by impulsive noise," in *Proc. IEEE Int. Symp. Power Line Commun. Appl.*, Rio de Janeiro, Brazil, March 2010, pp. 178–182.

[53] F. Gianaroli, F. Pancaldi, E. Seroni, M. Vigilante, G. M. Vitetta, and A. Barbieri, "Statistical modeling of periodic impulsive noise in indoor power-line channels," *IEEE Trans. Power Del.*, vol. 27, no. 3, pp. 1276–1283, 2012.

[54] K. W. Hipel and A. I. McLeod, *Time Series Modeling of Water Resources and Environmental Systems*. Elsevier, 1994.

[55] P. J. Brockwell and R. A. Davis, *Time Series: Theory and Methods*, second edition ed. Springer, 2006.

[56] Y. Chakhchoukh, "A new robust estimation method for arma models," *IEEE Trans. Signal Process.*, vol. 58, no. 7, pp. 3512–3522, 2010.

[57] S. A. Fattah and W. P. Z. amd M. O. Ahmad, "A novel technique for the identification of arma systems under very low levels of snr," *IEEE Trans. Circuits Syst. I, Reg. Papers*, vol. 55, no. 7, pp. 1988–2001, 2008.

[58] [Online], "http://www.mathworks.com/help/toolbox/ident/ ref/armax.html."

[59] L. Ljung, *System Identification: Theory for the user*. Prentice-Hall, 1999.

[60] C. R. Loubery, "Einrichtung zur elektrischen zeichengebung an die teilnehmereines starkstromnetzes," *Kaiserliches Patenamt*, 1901.

[61] J. A. C. Arrabal, "Modulation and multiple access techniques for indoor broadband power-line communications," 2007.

[62] F. J. Canete, J. A. Cortes, L. Diez, and J. T. Entrambasaguas, "Modeling and evaluation of the indoor power line channel," *IEEE Communications Magazine*, vol. 41, no. 4, pp. 41–47, 2003.

[63] A. Benaissa, A. Abdelmalek, and M. Feham, "Reliability and performance improvement of MIMO-PLC system under alpha-stable noise," *International Journal on Communications Antenna and Propagation*, vol. 6, no. 3, pp. 182–187, 2016.

[64] J. T. E.-M. F. J. Canete-Corripio, L. Diez-del Rio, "Indoor power-line communications: Channel modelling and measurements," in *Proc. of the 4th Int. Symp. Power Line Commun. Appl.*, Limerick, Ireland, April 2000, pp. 117–122.

[65] B. Tan and J. S. Thompson, "Power line communications channel modeling methodology based on statistical features," *Proceedings of the IEEE Trans. Power Del.*, 2012.

[66] L. Tang, P. So, E. Gunawan, Y. Guan, S. Chen, and T. Lie, "Characterization and modeling of in-building power lines for high-speed data transmission," *IEEE Transactions on Power Delivery*, vol. 18, no. 1, pp. 69–77, 2003.

[67] D. Anastasiadou and T. Antonakopoulos, "Multipath characterization of indoor power-line networks," *IEEE Transactions on Power Delivery*, vol. 20, no. 1, pp. 90–99, 2005.

[68] S. Mazer, M. Fattah, M. E. Bekkali, and R. Ouremchi, "Modeling the transfer function of the automotive plc by using the s-parameters," *International Journal on Engineering Applications*, vol. 1, no. 4, pp. 259–262, 2013.

[69] R. Nizigiyimana, J. L. Bunetel, Y. Raingeaud, P. Ravier, G. Lamarque, and A. Achouri, "Analysis and comparison of deterministic power line channel modeling methods," *International Journal on Communications Antenna and Propagation*, vol. 3, no. 6, pp. 273–281, 2013.

[70] S. Galli and T. Banwell, "A novel approach to the modeling of the indoor power line channel-part ii: Power line transmission medium," *IEEE Trans. Power Del.*, vol. 20, no. 3, pp. 1869–1878, 2005.

[71] H. Meng, Y. Guan, C. Law, P. So, E. Gunawan, and T. Lie, "Modeling of transfer characteristics for the broadband power line communications channel," *IEEE Tran on Power Delivery*, vol. 19, no. 3, pp. 1057–1064, 2004.

[72] [Online], "http://www.tesequipmentdepot.com/rhodeschwartz/networkanalyzer/zvl13.htm."

[73] G. Marrocco, D. Statovci, and S. Trautmann, "A plc broadband channel simulator for indoor communications," in *Proc. of IEEE Int. Symp. Power Line Commun. Appl.*, Johannesburg, South Africa, March 2013, pp. 321–326.

[74] A. Z. M. Tlich, G. Avril, "Coherence bandwidth and its relationship with the rms delay spread for plc channels using measurements up to 100 MHz," in *1st International Home Networking Conference*, Paris-France, December 2007, pp. 129–142.

[75] H. Philipps, "Performance measurements of powerline channels at high frequencies," in *Proc. of the 2nd Int. Symp. Power Line Commun. Appl.*, Tokyo, Japan, March 1998, pp. 229–237.

[76] V. Degardin, M. Lienard, A. Zeddam, F. Gauthier, and P. Degauque, "Classification and characterization of impulse noise on indoor power lines and for data communications," *IEEE Transactions on Consumer Electronics*, vol. 48, no. 4, pp. 913–918, 2002.

[77] T. Esmalian, F. R. Kschischang, and P. G. Gulak, "In-building power lines as high speed communication channels: Channel characterization and a test channel ensemble," *Int. J. Comm. Sys*, vol. 16, pp. 381–400, 2003.

[78] T. V. Pasad, S. Srikanth, C. N. Krishnan, and P. V. Ramakrishna, "Wideband characterization of low voltage outdoor powerline communication channels in india," in

Proc. of the 4th Int. Symp. Power Line Commun. Appl., Malmo, Sweden, April 2001, pp. 359–364.

[79] H. Philipps, "Development of a statistical model for power line communications channels," in *Proc. of the 4th Int. Symp. Power Line Commun. Appl.*, Limerick, Ireland, April 2000, pp. 153–162.

[80] M. Mosalaosi and T. J. O. Afullo, "Dispersive characteristics for broadband indoor power-line communication channels," in *Southern Africa Telecommunication Networks and Applications Conference*, Port Elizabeth, South Africa, September 2014, pp. 313–317.

[81] T. K. Sarkav, Z. Ji, K. Kim, A. Medouri, and M. Salazar-Palma, "A survey of various propagation models for mobile communication," *IEEE Antenna and Propagation Magazine*, vol. 45, no. 3, pp. 51–82, 2003.

[82] M. Tlich, A. Zeddam, F. Moulin, and F. Gauthier, "Indoor powerline communications channel characterisation up to 100 mhz-part II: Time-fequency analysis," *IEEE Transections on Power Delivery*, vol. 23, no. 3, pp. 1402–1409, 2008.

[83] H. R. Anderson and J. P. McGeehan, "Direct calculation of coherence bandwidth in urban microcells using a ray-tracing propagation model," in *IEEE Int. Symp. On Wireless Networks*, September 1994, pp. 20–24.

[84] H. Lutz, J. Lampe, and J. B. Huber, "Bandwidth efficient power line communications based on ofdm," *AEU Int. J. Electr. Commun.*, vol. 54, no. 1, pp. 2–12, 1999.

[85] K. S. A. Mawali, "Techniques for broadband power line communications: Impulse noise mitigation and adaptive modulation," 2011.

[86] L. D. Bert, P. Caldera, D. Schwingshack, and A. M. Tonello, "On noise modeling for power line communications," in *IEEE Int. Symp. Power Line Commun. Appl.*, Udine, Italy, April 2011, pp. 283–288.

[87] G. Moreno-Rodriguez, "An iir-filter approach to time variant plc channel modeling," in *Proc. of the 11th Int. Symp. Power Line Commun. Appl.*, Jeju Island, Korea, April 2008, pp. 87–92.

[88] C. Konate, M. Machmoum, and J. F. Diouris, "Multipath model for powerline communication channel in the frequency range of 1mhz -30mhz," in *in Proc. of The International Conference on Computer as a Tool*, Warsaw, Poland, September 2007, pp. 984–989.

[89] G. Jinbo, W. Zanji, L. Haifeng, Z. Yumming, and W. Qiaochen, "Transmission characteristics of low voltage distribution networks in china and its model," *IEEE Transections on Power Delivery*, vol. 20, no. 2, pp. 1341–1348, 2005.

[90] G. Andreou, "Electrical parameters of low-voltage power distribution cables used for power-line communications," *IEEE Trans. Power Del.*, vol. 22, no. 2, pp. 879–886, 2007.

[91] C. R. Paul, *Analysis of Multiconductor Transmission Lines.* John Wiley & Sons, 1994.

[92] D. M. Pozar, *Microwave Engineering*, fourth edition ed. John Wiley & Sons, 2012.

[93] J. K. Oppong, "Loaded high speed computer data highway: A model to aid designers," *Journal of the Institute of Electronic and Radio Engineers*, vol. 55, pp. 37–41, 1985.

[94] D. Misra, *Radio-Frequency and Microwave Communication Circuits: Analysis and Design*. John Wiley & Sons, 2001.

[95] A. Smith, *Radio Frequency Principles and Applications: The Generation, Propagation, and Reception of Signals and Noise*. Wiley-IEEE Press, 1998.

[96] F. Zwane and T. J. O. Afullo, "An alternative approach in power line communication channel modelling," *Progress in Electromagnetic Research C*, vol. 47, no. 2, pp. 85–93, 2014.

[97] H. Philipps, "Modelling of powerline communication channels," in *Proc. of the 4th Int. Symp. Power Line Commun. Appl.*, Vancouver, Canada, April 2005, pp. 14–21.

[98] K. R. Lee, *Impacts of Information Technology on Society in the New Century*. Route de Chavannes, 2009.

[99] M. M. et al., "Modeling of the transmission of power line communication signal through the power electric transformer," *Ann. Teleccomun.*, vol. 67, no. 9, 2011.

[100] M. C. et al., "Improving the multiple access method of home networks over the electrical wiring," *Ann. Teleccomun.*, vol. 66, no. 11, 2011.

[101] J. Barnes, "A physical multi-path model for power distribution network propagation," in *Proc. of the 2nd Intl. Symp. on Power Line Commun. and Its Appl.*, Tokyo, Japan, March 1998, pp. 24–26.

[102] A. M. Tonelo, "Wideband impulse modulation and receiver algorithms for multi-user power line communications," *EURASIP Journal on Advances in Signal Processing*, vol. 2007, pp. 1–14, 2007.

[103] A. M. Tonello, S. D'Alessandro, and L. Lampe, "Adaptive pulse-shaped ofdm with application to in-home power line communication," *IEEE Trans. Commun.*, vol. 58, no. 11, pp. 3265–3276, 2010.

[104] F. Gianaroli, A. Barbieri, F. Pancaldi, A. Mazzanti, and G. M. Vitetta, "A novel approach to power-line channel modeling," *IEEE Trans. Power Del.*, vol. 25, no. 1, pp. 132–140, 2010.

[105] S. Galli and T. Banwell, "A deterministic frequency-domain model for the indoor power line transfer function," *IEEE J. Sel. Areas Commun.*, vol. 24, no. 7, pp. 1304–1316, 2006.

[106] T. Banwell and S. Galli, "A new approach to the modeling of the transfer function of the power line channel," in *Proc. of the 5th Intl. Symp. on Power Line Commun. and Its Appl.*, Malmo, Sweden, April 2001, pp. 4–6.

[107] T. Sartenaer and P. Delogne, "Powerline cables modeling for broadband communications," in *Proc. of the 5th Intl. Symp. on Power Line Commun. and Its Appl.*, Malmo, Sweden, April 2001, pp. 331–338.

[108] T. Esmailian, F. Kschischang, and G. Gulak, "An in-building power line channel simulator," in *Proc. of the 6th Intl. Symp. on Power Line Commun. and Its Appl.*, Athens, Greece, March 2002, pp. 1–5.

[109] M. Mosalaosi and T. J. O. Afullo, "A deterministic channel model for multi-access broadband powerline communication," in *Proc. IEEE AFRICON*, Addis Ababa, Ethiopia, September 2015, pp. 1–5.

[110] J. Anatory, M. M. Kissaka, and N. H. Mvungi, "Channel model for broadband powerline communication," *IEEE Transactions on Power Delivery*, vol. 22, no. 1, pp. 135–141, 2007.

[111] C. T. Mulangu, T. J. Afullo, and N. M. Ijumba, "Modelling of broadband powerline communication channels," *Southern African Institute of Electrical Engineers*, vol. 102, no. 4, pp. 107–112, 2011.

[112] M. Mosalaosi and T. J. Afullo, "Channel model for high-speed indoor powerline communication systems: The lattice approach," *accepted in Annals of Telecommunications*, 2016.

[113] T. Systems, *PCB Interconnect Characterization from TDR Measurements, Application Note*. Application Note, 1999.

[114] J. M. Jong, V. K. Tripathi, L. A. Hayden, and B. Janko, "Lossy interconnect modeling from tdr/t measurements," *in Proc. IEEE 3rd Tropical Meeting on Electrical Performance of Electronic Packaging*, pp. 133–135, 1994.

[115] F. C. Yao, "Analysis of signal transmission in ultra high speed transistorized digital computers," *IEEE Transections on Electronic Computers*, pp. 372–382, 1963.

[116] D. M. Pozar, *Microwave Engineering*, second edition ed. John Wiley & Sons, 1998.

[117] A. M. Tonello, F. Versolatto, and B. Bejar, "A top-down random generator for the in-home plc channel," in *Proceedings of IEEE GLOBECOM*, Houston, TX, USA, December 2011, pp. 1–5.

[118] Y. Hirayama, H. Okada, and T. Y. amd M. Katayama, "Noise analysis on wide-band plc with high sampling rate and long observation time," in *Proc. of the 7th Int. Symp. Power Line Commun. Appl.*, Kyoto, Japan, March 2003, pp. 142–147.

[119] D. Liu, E. Flint, B. Gaucher, and Y. Kwark, "Wide-band ac power line characterization," *IEEE Trans. Consum. Electron.*, vol. 45, no. 4, pp. 1087–1097, 1999.

[120] M. Mosalaosi and T. J. O. Afullo, "Broadband analysis and characterization of noise for in-door power-line communication channels," in *Progress In Electromagnetics Research Symposium Proceedings*, Guangzhou, China, August 2014, pp. 719–723.

[121] R. F. Eagle, "Autoregressive conditional heteroskedasticity with estimates of variance of uk inflation," *Econometrica*, vol. 50, pp. 987–1008, 1982.

[122] T. Bollerslev, "Generalized autoregressive conditional heteroskedasticity," *Journal of Econometrics*, vol. 31, pp. 307–327, 1986.

[123] F. Rouissi, V. Degardin, A. Ghazel, M. Lienard, and F. Gauthier, "Impulsive noise modelling using markov chains in indoor environment-comparison with stochastic model," in *Proc. IEEE 12th In. Conf. Electron., Circuits Syst.*, Gammarth, Tunisia, December 2005, pp. 1–4.

[124] M. Katayama, T. Yamazato, and H. Okada, "A mathematical model of noise in narrowband power line communication systems," *IEEE J. Sel. Areas Commun.*, vol. 24, no. 7, pp. 1267–1276, 2006.

[125] S. Katar, B. Mashbum, K. Afkhamie, H. Latchman, and R. Newrnan, "Channel adaptation based on cyclo-stationary noise characteristics in plc systems," in *Proc. IEEE Int. Symp. Power Line Commun. Appl.*, Orlando, USA, March 2006, pp. 16–21.

[126] M. Nassar, A. Dabak, I. H. Kim, T. Pande, and B. L. Evans, "Cyclostationary noise modeling in narrowband powerline communication for smart grid applications," in *Proc. IEEE Int. Conf. Acoust., Speech Signal Process.*, Kyoto, Japan, March 2012, pp. 3089–3092.

[127] J. Lin and B. L. Evans, "Cyclostationary noise mitigation in narrowband powerline communications," in *Proc. APSIPA Annual Summit and Conference*, Asia-Pacific, December 2012, pp. 1–4.

[128] V. Guillet and G. Lamarque, "Unified background noise model for power line communications," in *Proc. IEEE Int. Symp. Power Line Commun. Appl.*, Rio de Janeiro, Brazil, March 2010, pp. 131–136.

[129] R. Hashmat, P. Pagani, T. Chonavel, and A. Zeddam, "A time-domain model of background noise for in-home mimo plc networks," *IEEE Trans. Power Del.*, vol. 27, no. 4, pp. 2082–2089, 2012.

[130] T. Guzel, E. Ustunel, H. B. Celebi, H. Delic, and K. Mihcak, "Noise modeling and ofdm receiver design in power-line communication," *IEEE Trans. Power Del.*, vol. 26, no. 4, pp. 2735–2742, 2011.

[131] P. A. C. Lopes, J. M. M. Pinto, and J. B. Gerald, "Dealing with unknown impedance and impulsive noise in the power-line communications channel," *IEEE Trans. Power Del.*, vol. 28, no. 1, pp. 58–66, 2013.

[132] J. Antoni, "Cyclic spectral analysis into practice," *Mechanical Systems and Signal Processing*, vol. 21, no. 2, pp. 597–630, 2007.

[133] W. Gardner, A. Napolitano, and L. Paura, "Cyclostationary: Half a century of research," *Signal Processing*, vol. 86, no. 4, pp. 639–697, 2006.

[134] F. Bonnardot, R. B. Randall, and F. Guillet, "Extraction of second-order cyclostationarity sources - application to vibration analysis," *Mechanical Systems and Signal Processing*, vol. 19, pp. 1230–1244, 2005.

[135] W. Gardner, "Statistical spectral analysis," *Prentice-Hall, Englewood Cliffs*, 1991.

[136] G. Jenkins and D. Watts, "Spectral analysis and its applications," *Emerson-Adams Press*, 1996.

[137] H. Farhangi, "The path of the smart grid," *IEEE Power Energy Mag.*, vol. 8, no. 1, pp. 18–28, 2010.

[138] M. Nassar, J. Lin, Y. Mortazavi, A. Dabak, I. H. Kim, and B. L. Evans, "Local utility power line communications in the 3-500khz band," *IEEE Signal Process. Mag.*, vol. 29, no. 5, pp. 116–127, 2012.

[139] F. Gianaroli, F. Pancaldi, and G. M. Vitetta, "Broadband system models basedon zadeh's representation for indoor powerline channels: An experimental validation," in *Proc. IEEE Int. Conf. Commun.*, Budapest, Hungary, June 2013, pp. 4304–4309.

[140] ——, "Design and implementation of a wideband channel sounder for low-voltage powerlines," *IEEE Trans. Smart Grid.*, vol. 5, no. 1, pp. 210–219, 2014.

[141] F. J. C. Corripio, J. A. C. Arrabal, L. D. del Rio, and J. T. E. Munoz, "Analysis of the cyclic short-term variation of indoor power line channels," *IEEE J. Select. Areas Commun.*, vol. 24, no. 7, pp. 1327–1338, 2006.

[142] A. R. Hall, "General method of moments," 2011.